APR 13 '48

UNITED STATES DEPARTMENT OF COMMERCE

Journal of Research

of the

National Bureau of Standards

Vol. 34, No. 2 February 1945

CONTENTS

RP	TITLE AND AUTHOR	Page
1631.	Application of the Ilkovič equation to quantitative polarography. Floyd Buckley and John Keenan Taylor .....[Price 10 cents]	97
1632.	Comparative liquid-junction potentials of some pH buffer standards and the calibration of pH meters. George G. Manov, Nicholas J. DeLollis, and S. F. Acree.....[Price 5 cents]	115
1633.	Spectrographic determination of sodium, potassium, and lithium in portland cement with the direct-current carbon arc. Armin W. Helz .....[Price 10 cents]	129
1634.	Heats, free energies, and equilibrium constants of some reactions involving O_2, H_2, H_2O, C, CO, CO_2, and CH_4. Donald D. Wagman, John E. Kilpatrick, William J. Taylor, Kenneth S. Pitzer, and Frederick D. Rossini.....[Price 10 cents]	143
1635.	Heats of isomerization of the 18 octanes. Edward J. Prosen and Frederick D. Rossini.....[Price 5 cents]	163
1636.	Region of usable imagery in airplane-camera lenses. Francis E. Washer .....[Price 10 cents]	175
1637.	Relaxation of stresses in annealing glass. Arthur Q. Tool. .....[Price 5 cents]	199

The articles listed may be purchased separately (see cover page II) at the prices stated

A monthly periodical of pure and applied science published by our National Government

Journal of Research
of the
National Bureau of Standards

The January 1945 issue of the JOURNAL OF RESEARCH of the National Bureau of Standards began the thirty-fourth semiannual volume of this periodical. Fundamental researches in progress in the Bureau's laboratories are reported in this JOURNAL. If you are interested in new developments in science and technology, you should receive the JOURNAL. If you are not already a subscriber, you are invited to send in your subscription.

Technical News Bulletin

This is a monthly publication containing short articles reporting progress of work in the Bureau laboratories, abstracts of papers which appear in the JOURNAL OF RESEARCH, accounts of scientific and technical meetings in which the Bureau has taken part, a list of all publications by members of the staff, and other items within the Bureau's fields. The BULLETIN is designed primarily to give a general and timely review of the activities of the Bureau in brief form. It is a prompt and reliable source of official information. If you have not already subscribed for the BULLETIN, you are invited to do so.

ANNUAL SUBSCRIPTION	Price	
	United States, Canada, Cuba, Mexico, Newfoundland, Republic of Panama	Other countries
JOURNAL OF RESEARCH of the National Bureau of Standards:		
12 monthly issues (2 volumes), paper covers	$3.50	$4.50
Bound volume (½ year, 1 volume), blue buckram.	3.00	3.50
Technical News Bulletin, 12 monthly issues	.50	.70

Research Papers, reprinted individual articles appearing in the JOURNAL OF RESEARCH, are available from the Superintendent of Documents shortly after appearance of monthly issue of the JOURNAL.

Address order only to
Superintendent of Documents, U. S. Government Printing Office
Washington 25, D. C.

UNITED STATES DEPARTMENT OF COMMERCE
WAYNE C. TAYLOR, Acting Secretary
NATIONAL BUREAU OF STANDARDS
Lyman J. Briggs, Director

✦

Journal of Research

of the

National Bureau of Standards

✦

Volume 34, Number 2

February 1945

[Published with approval of the Director of the Budget]

UNITED STATES
GOVERNMENT PRINTING OFFICE
WASHINGTON : 1945

For sale by the Superintendent of Documents, U. S. Government Printing Office
Washington 25, D. C. - Price 30 cents, $3.50 per year on subscription

The prices of the separate Research Papers appearing in this JOURNAL are given on the front cover page. If 100 or more copies of any separate are ordered, a discount of 25 percent is allowed. Those who desire copies of separate Research Papers should send their orders and remittances without delay to the Superintendent of Documents, U. S. Government Printing Office, Washington 25, D. C. Research Papers are not printed from electrotypes, and usually no more reprints can be had when the first and only printing is exhausted.

MATHEMATICAL TABLES

A list of the mathematical tables now obtainable from the National Bureau of Standards is printed on pages 3 and 4 of the JOURNAL cover. New tables will be announced from time to time as they become available. An order blank is available on the last page of this issue.

U. S. Department of Commerce National Bureau of Standards

RESEARCH PAPER RP1631

Part of Journal of Research of the National Bureau of Standards, Volume 34, February 1945

APPLICATION OF THE ILKOVIČ EQUATION TO QUANTITATIVE POLAROGRAPHY

By Floyd Buckley and John Keenan Taylor

ABSTRACT

Conditions of applicability of the Ilkovič equation to polarographic analysis were investigated for representative ions singly and in mixtures. Gelatin was used to suppress maxima found in current-voltage curves.

Results obtained with a capillary of usual characteristics showed that a suppresser is necessary to secure agreement with the Ilkovič equation over any considerable drop-time range, and that the need increases with the drop-rate of the electrode and the dilution of reducible ion. A criterion of diffusion control satisfactory for classification of polarograms by visual examination was found. The application of the Ilkovič equation to quantitative analysis was shown to be inadvisable unless it is definitely established that the experimental conditions are well within the range for insuring diffusion control. A logarithmic relation between critical drop-time and suppresser concentration was found.

CONTENTS

	Page
I. Introduction	97
II. Apparatus and method	99
III. Results	101
IV. Conclusions	113
V. References	114

I. INTRODUCTION

The polarographic method of chemical analysis is based upon the interpretation of the current-voltage curves obtained when solutions containing electroreducible or electrooxidizable substances are electrolyzed with electrodes, one of which is very small (usually mercury dropping from a fine-bore capillary) so that it is completely polarized, while the other is practically unpolarizable. From the position and magnitude of certain steps observed in these curves, both qualitative and quantitative information concerning the electrolyzed material can be obtained.

The polarograph, an instrument that automatically obtains and records these current-voltage curves, has numerous applications in chemical analysis. Most of the published procedures make use of the instrument as an interpolating device for comparing known and unknown solutions. If the standard and unknown solutions are sufficiently alike, and the same dropping electrode is employed for each under identical conditions, the analysis resolves into a comparison of the heights of the waves or steps on the current-voltage curves.

The phenomenon of a limiting current which gives rise to the characteristic polarographic waves is determined, under ideal conditions, by the rate of diffusion of the electrolyzable ion from an inexhaustible supply in the surrounding solution to the surface of the electrode at which the concentration is zero because the ions are removed as rapidly as they arrive. The expression relating this diffusion current to the constants of the system under investigation was derived by Ilkovič [1] [1] in the form

$$i_d = knD^{1/2}Cm^{2/3}t^{1/6},$$

where i_d is the diffusion current in microamperes, n is the number of electron equivalents per mole of electrode reaction, D is the diffusion coefficient of the reducible (or oxidizable) substance, C is its concentration in millimoles per liter, m is the mass flow of mercury from the dropping electrode in milligrams per second, t is the drop-time in seconds, and k is a proportionality constant. In this equation the quantity $knD^{1/2}$ is a constant for the particular ion under investigation, whereas the other factor depends upon the concentration of the solution and the physical constants of the apparatus employed. Lingane [2] has accordingly proposed that the quantity $knD^{1/2}$, which is experimentally determined by $i_d/Cm^{2/3}t^{1/6}$, be designated as the "diffusion-current constant." [2] The use of this constant, together with the physical characteristics of the capillary and of the electrical system, would eliminate the need for calibration experiments and put polarography on an absolute basis.

The validity of the above procedure depends on strict agreement with the Ilkovič equation under the experimental conditions of the analysis. However, it is found that the polarographic waves are not determined by the diffusion current alone, but are often complicated by the presence of more or less pronounced maxima, caused by adsorption of the reducible ion on the mercury electrode, stirring of the electrolyte near the electrode, or other factors. Certain surface-active materials added to the electrolyte have been found to suppress these maxima. Although the Ilkovič equation has been tested by several investigators [3] and definite statements have been made as to the conditions for its validity, none of these researches has included a systematic study of the effect of suppressers of maxima on the diffusion current, but there are general statements in the literature which describe variations of wave height caused by the addition of a large excess of suppressing agents [4]. Indeed, no satisfactory criteria for determining when maxima have been suppressed and the electrode current is controlled by a simple diffusion process (hereafter referred to as diffusion control) have been proposed. Observations in this laboratory on the occurrence and nature of maxima have suggested the need of an exploratory investigation to determine the influence of the drop-rate of the capillary and the concentration of the suppresser on the validity of the fundamental Ilkovič equation. This information is necessary before Lingane's proposal can be generally applied to quantitative polarography.

---

[1] Figures in brackets indicate the literature references at the end of this paper.

[2] This diffusion-current constant differs from that previously employed by Kolthoff and Lingane (Chem. Rev. **24**, 1 (1939) by the factor $m^{2/3}t^{1/6}$.

II. APPARATUS AND METHOD

The polarograph used was of the photographic recording type and has been described, together with its auxiliary equipment, in a previous communication from this laboratory [5]. The characteristics of the electrical measuring circuit were determined by the Electrical Division of this Bureau. In addition, the calibration of the galvanometer was checked by substituting a standard resistor for the dropping-electrode cell. Full-scale sensitivity of the galvanometer was 2.22×10^{-9} ampere per millimeter at 1 meter. Nominal sensitivity ratios differed by no more than 1 percent from observed values.

The dropping electrode was constructed from a drawn-out capillary so that a maximum drop-time of about 6 seconds was obtained in the solutions under investigation. This capillary was sealed to a long burette of large cross section so that the driving head was not altered significantly during a 10-minute dropping interval. The burette was fitted with an enlarged funnel top and a stopcock sidearm near the bottom to facilitate adjustment of the driving head to obtain any desired drop-time in the range of 1 to 6 seconds.

The flow of mercury in the capillary was determined as a function of the driving head. The apparatus described by Lingane [6] was particularly suitable for this measurement. The flow is practically independent of the immersion medium (air, water, solution) but the drop-time is, of course, quite sensitive to the composition of the supporting electrolyte. A scale attached to the burette furnished a convenient means of ascertaining the driving head and hence the flow of mercury for each polarogram recorded. The drop-time of the capillary was taken by means of a stopwatch at the half-wave potential of the particular ion under investigation.

Galvanometer sensitivities were selected to produce wave heights of such size that errors in their measurement were reduced to about 1 percent, except for the solutions of extreme dilution, in which case the errors were no more than two or three times this amount.

Characteristic types of polarograms encountered in this investigation and the usual methods of measuring wave heights are shown in figure 1. The segment preceding the wave is extended, as shown in the figure, to compensate for rise in residual current. The method for estimating the current at the completion of a wave depends upon the shape of the wave and the slope of the following segment. In the absence of prominent maxima, three types of waves are observed. The slope of the following segment may be equal to, as in *A*, less than, as in *B*, or greater than, as in *C*, that of the initial segment. In cases *A* and *B*, a line is drawn parallel to the initial portion of the wave and through the maximum of the final portion. Case *C* permits the backward extension of the following segment. In each case the wave height is taken as the vertical distance at the half-wave potential. When sharp maxima are present as in *D* and *E*, the peak is ignored and estimation of wave height is made as in *A* and *B*.

The above-described methods of measuring wave heights are frequently used and are satisfactory for comparative purposes, but it is later shown that they do not provide true measures of diffusion currents except when the form of the polarographic wave is like that

shown in figure 1, *A*, as this is the only type of wave obtained when the electrode current is determined by a simple diffusion process. This fact forms the basis of a criterion for the minimum concentration of suppresser necessary to insure diffusion control of the electrode current.

Nickel, cadmium, bismuth, and thallium were selected as the cations for study. This group provided a bivalent ion (Cd) having a half-wave potential very near that of the electrocapillary maximum, one bivalent (Ni) and one univalent ion (Tl) reduced at potentials on either side of the electrocapillary maximum, and one trivalent ion (Bi). The selection is a reasonable cross section of the type of cation encountered in elementary analysis. The supporting electrolyte was 0.1 *N* in potassium chloride for nickel, cadmium, and thallium and 1 *N* in nitric acid for bismuth.

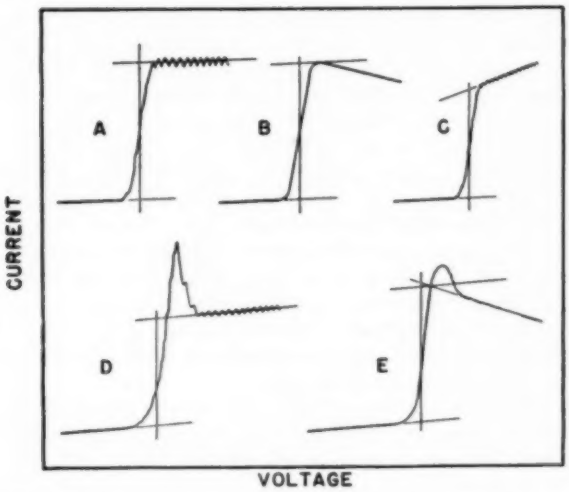

FIGURE 1.—*Methods of measurement for characteristic types of polarographic waves.*

Solutions of nickel, cadmium, and bismuth were prepared by quantitative dilution of standards made from spectrochemically pure metals. The thallium standard was prepared from pure TlCl.

Polarograms for each solution were taken over a drop-time range of 1- to 6-second intervals of approximately 0.5 second for nickel and cadmium and approximately 1 second for thallium and bismuth. The gelatin concentration was increased in increments of 0.002 percent in all cases except for cadmium. The range of gelatin concentration was 0 to 0.008 percent for cadmium, thallium, and bismuth and 0 to 0.020 percent for nickel.

Oxygen was removed by bubbling purified nitrogen through the solution in the cell for 15 minutes preceding the recording of the polarogram, and its reentrance was prevented by a continuous flow of nitrogen over the solution during the measurement.

All measurements were made in a constant-temperature room maintained at 25.5° ±0.3° C.

III. RESULTS

Values of the diffusion-current constant $I_D = i_d/Cm^{2/3}t^{1/6}$ were calculated from the measured wave heights and the characteristics of the apparatus and electrode. The results for various solutions of nickel as a function of drop-time of the electrode and gelatin concentration are given in figure 2. The failure to comply with the law expressed by the equation for I_D is strikingly evident in the absence of a suppresser in that no constant value of I_D over an appreciable range of drop-times is observed. With the small gelatin content of 0.002 percent, however, constant values of I_D are obtained for all drop-times greater than 3 seconds. At a concentration of 0.004 percent of gelatin the critical drop-time is decreased to 2.1 seconds and at 0.006 percent to 1.8 seconds. Solutions containing between 0.008 and 0.020 percent of gelatin give, for fixed gelatin concentrations, constant values of I_D over the entire drop-time range of 1 to 6 seconds.[3]

A representative selection of the polarograms obtained for a solution 0.142×10^{-3} M in nickel is shown in figure 3.[4] For all the polarograms in horizontal alinement, the gelatin content was that indicated at the right side of the figure, and for all those in vertical alinement the drop-time did not differ by more than 0.1 second from the nominal value listed at the top of the figure. Values calculated for the diffusion-current constant are inserted at the base of each polarogram. At first inspection, all the curves with the exception of the last two on the right at 0 percent and the last one on the right at 0.002 percent of gelatin appear regular and "well defined." A study of the figure reveals the danger of gross error incurred from the assumption of diffusion control as determined by the loose criterion of "good definition." A positive criterion that has been found to be sufficient in this and all other cases of this study is the near identity of slope at the beginning and end of a wave.

The effect of gelatin, at least for concentrations less than 0.02 percent, in diminishing the diffusion-current constant, was found to be significant only at high dilution of the reducible ion. The family of curves shown in figure 4 illustrates the magnitude of this effect in solutions of nickel. These curves show that diffusion control exists over the entire drop-time range of 1 to 6 seconds for a concentration of gelatin in the neighborhood of 0.006 percent. An increase in suppresser concentration to 0.014 percent (0.020 percent for solutions 0.568×10^{-3} M and 0.0284×10^{-3} M) gives no further change in I_D for the two higher concentrations of nickel but causes a small continuous decrease at the higher dilutions. The effect is most pronounced at the lowest concentration of nickel.

The results depicted in figure 4 offer an explanation of conflicting statements which have been made regarding the strict proportionality of concentration of the reducible ion and its diffusion current. The curves show that this proportionality depends both upon drop-time

[3] For a given gelatin content, a slight increase in the values for I_D at the higher drop-times is noted, especially for the lowest concentrations of the reducible ion. The magnitude of this increase is small and of the order of the experimental errors involved in its determination. It may be due to some systematic error introduced by the method of measurement of the wave heights. However, the errors incurred on the assumption of a constant value for I_D, when diffusion control is effective, should not exceed ±2 percent.

[4] The conclusions of this paper are based upon the interpretation of approximately 800 current-voltage curves, which obviously can not be published in entirety. The polarograms shown have been selected because they illustrate characteristic behavior.

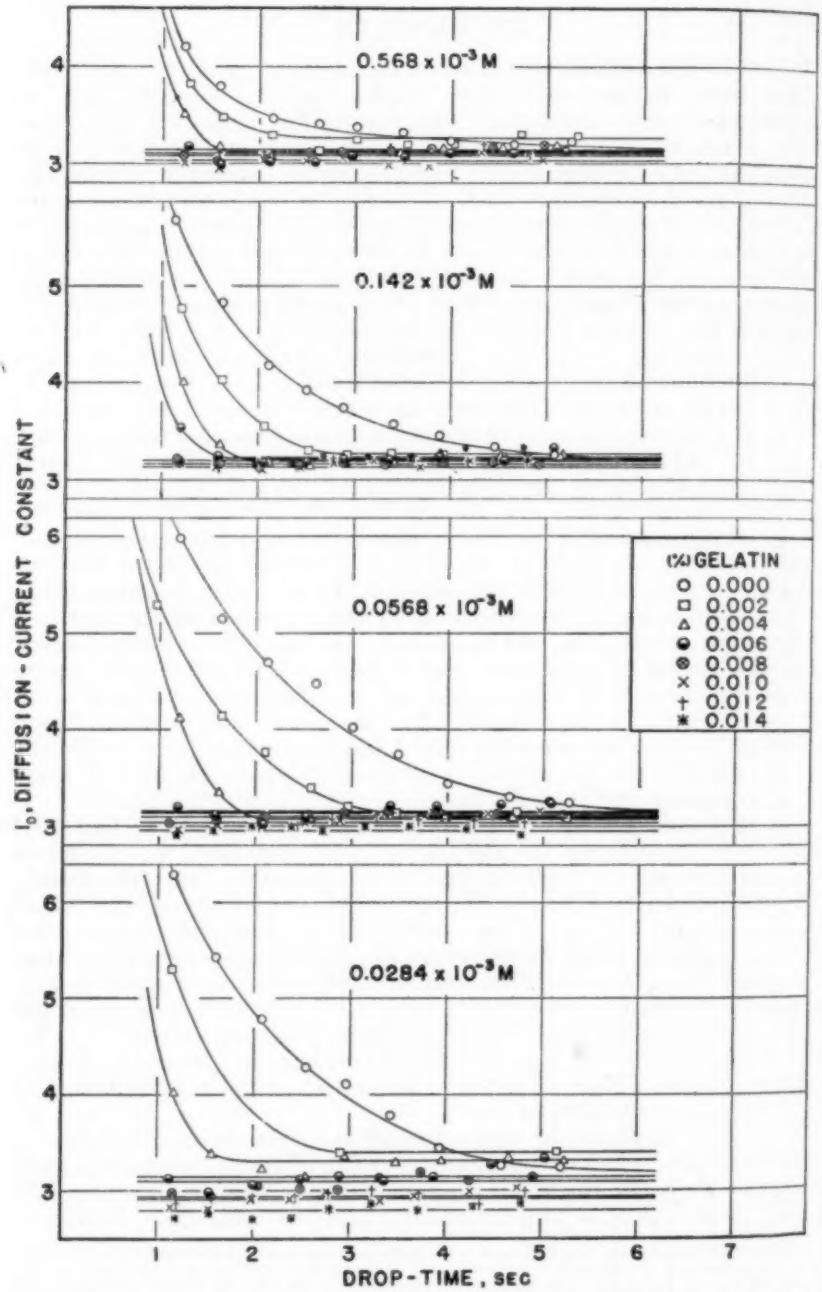

FIGURE 2.—*Effect of gelatin and drop-time on the diffusion-current constant of nickel in a supporting electrolyte of 0.1 N* KCl.

and gelatin content. Thus constant values of I_D are obtained over the entire drop-time range of 1 to 6 seconds only if the gelatin concentration is very near 0.006 percent. At lower gelatin content the proportionality is valid only in a very restricted drop-time range. At high gelatin concentrations, proportionality exists only if the ion concentration is in the vicinity of 0.1×10^{-3} M or higher.

The behavior of cadmium is of special interest as this element is reduced at a potential very close to the electrocapillary maximum. Both the adsorption theory of Heyrovsky [7] and Ilkovič [8], and the electrostatic streaming theory of Antweiler [9] demand that, at this potential, maxima be either absent or of small magnitude. Hence, deviations from the Ilkovič equation might be expected to be very small for this element. Indeed, positive assertions that cadmium shows no maximum in a 0.1-N solution of potassium chloride have been made [10].

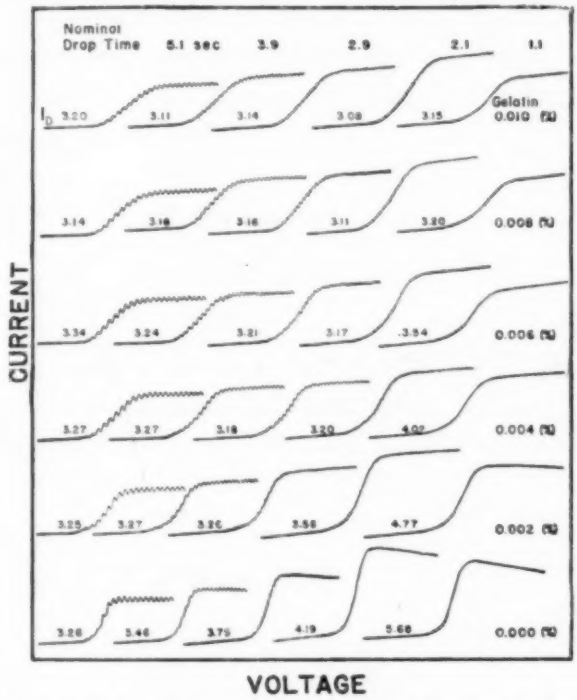

FIGURE 3.—*Characteristic polarographic waves for nickel* (0.142×10^{-3} M) *in a supporting electrolyte of 0.1 N* KCl.

All polarograms were taken at a sensitivity of 1/20, except those at a nominal drop-time of 1.1 seconds, which were taken at 1/40.

Figures 5 and 6 show the results for a solution 0.0148×10^{-3} M in cadmium. The general behavior is similar to that of nickel. Gelatin is required to secure agreement with the Ilkovič equation and deviations at high drop-rates in the presence of insufficient suppresser are shown by the appearance of a decreased slope at the end

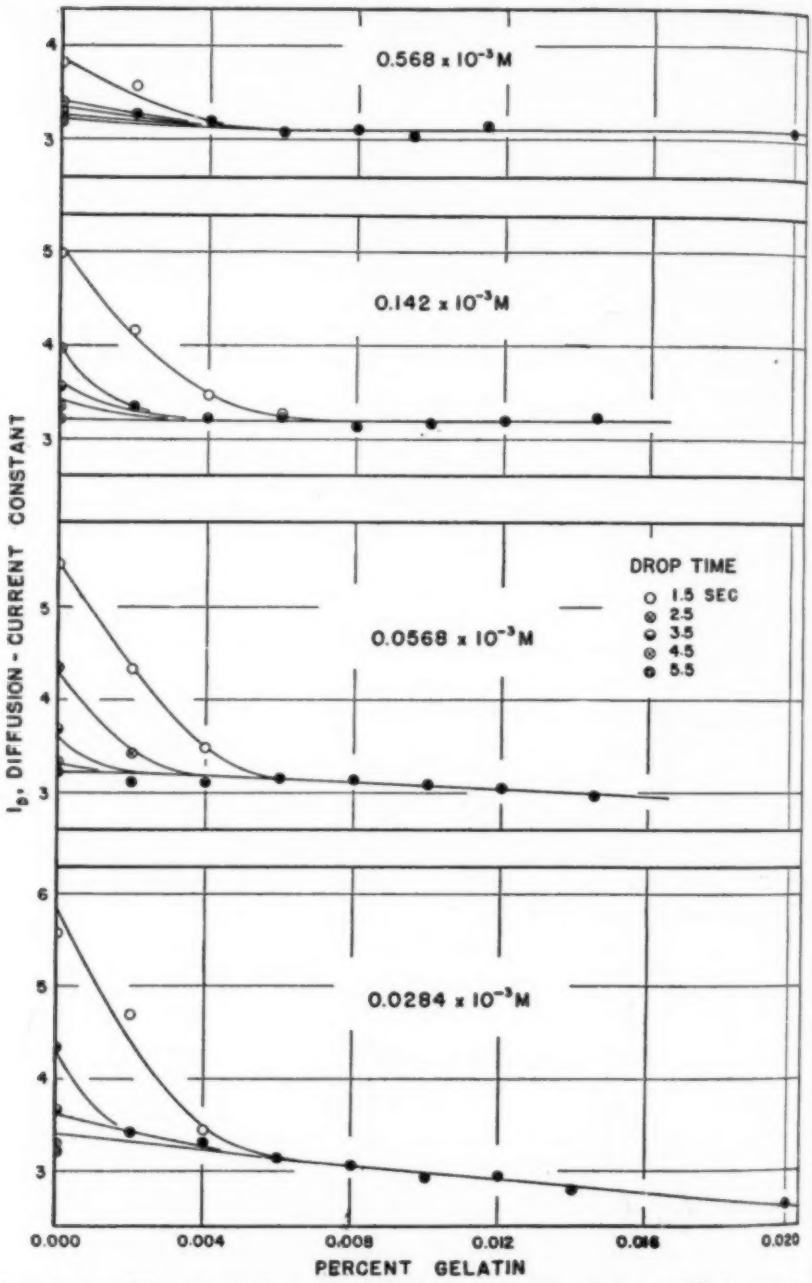

FIGURE 4.—*Effect of gelatin on the diffusion-current constant of nickel for specific drop-times in a supporting electrolyte of 0.1 N* KCl.

The symbol ● denotes the superposition of points corresponding to the different drop-times.

of the wave (figure 6). Sharp maxima are absent and all waves are "well defined." The writers' conclusion that the appearance of well-defined waves is not sufficient evidence for diffusion control is confirmed. The positive criterion found to be valid for nickel, that is, the approximate equality of the slopes preceding and succeeding the wave, was also applicable to all cadmium solutions.

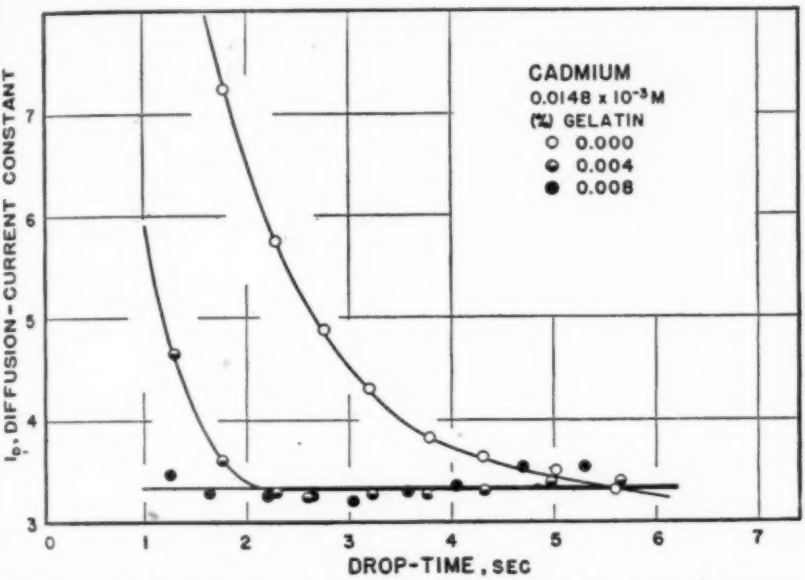

FIGURE 5.—*Effect of gelatin and drop-time on the diffusion-current constant for cadmium in a supporting electrolyte of 0.1 N* KCl.

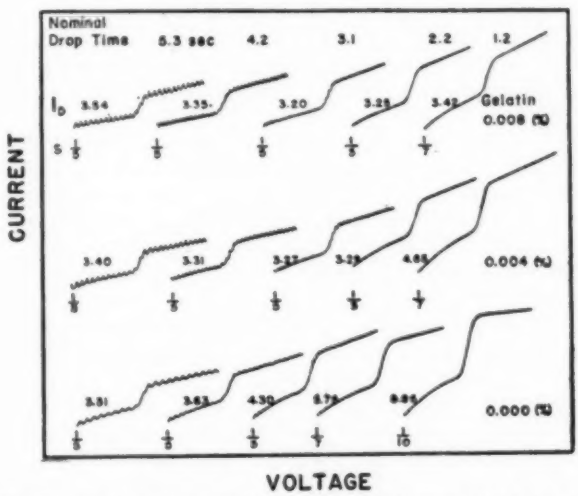

FIGURE 6.—*Characteristic polarographic waves of cadmium* (0.0148×10^{-3} *M*) *in a supporting electrolyte of 0.1 N* KCl.

The fractions under the curves denote sensitivities.

The deviations shown by cadmium when electrolyzed from solutions of potassium chloride of various concentrations and in the absence of gelatin are shown in figure 7. All polarograms are regular, "well defined," and show the characteristic appearance of a decreased slope at the end of the wave for drop-times less than 3 seconds. Constant values of I_D are obtained only for drop-times greater than 3 seconds. The value of I_D found with concentrations of supporting electrolyte less than 1 N is 3.54, which is in excellent agreement with Lingane's value [2] of 3.51 obtained in a solution 0.1 N in potassium chloride.

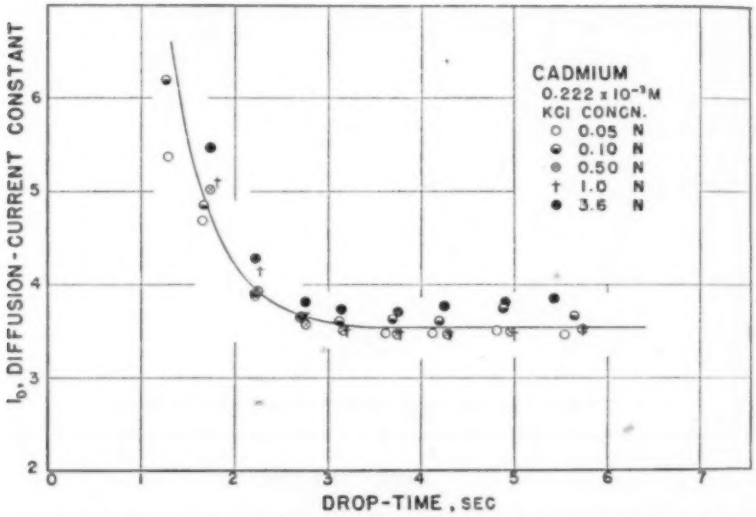

FIGURE 7.—*Influence of drop-time and concentration of supporting electrolyte on the diffusion-current constant of cadmium in solutions of potassium chloride.*

It is interesting to observe from figure 6 that the average value of I_D is 3.35. This low value is in agreement with the results found for nickel where low values of I_D are observed for low concentrations of reducible ion.

Some results for univalent thallium are given in figures 8 and 9. The general behavior of this ion parallels that of nickel in every respect. Both exhibit sharp maxima at high concentrations of reducible ion (polarograms for nickel under these conditions not shown) and deviate from ideal behavior at low concentration in the manner already described. The appearance of the two types of abnormalities is clearly shown in the polarograms given in figure 9. It is observed that there is a sharp (peak) maximum superimposed on the regular type of polarogram that is obtained at low concentrations of reducible ion. With successive additions of gelatin, these sharp maxima gradually decrease and eventually disappear, but additional gelatin is required to destroy the abnormal negative slope and insure diffusion control. The value of I_D for a $1\times10^{-3}M$ solution in the presence of 0.008 percent of gelatin is 2.71, in good agreement with the value of 2.69 reported by Lingane and Kolthoff [3]. The decrease of I_D with extreme dilution of reducible ion previously observed for nickel and cadmium is confirmed in the present instance.

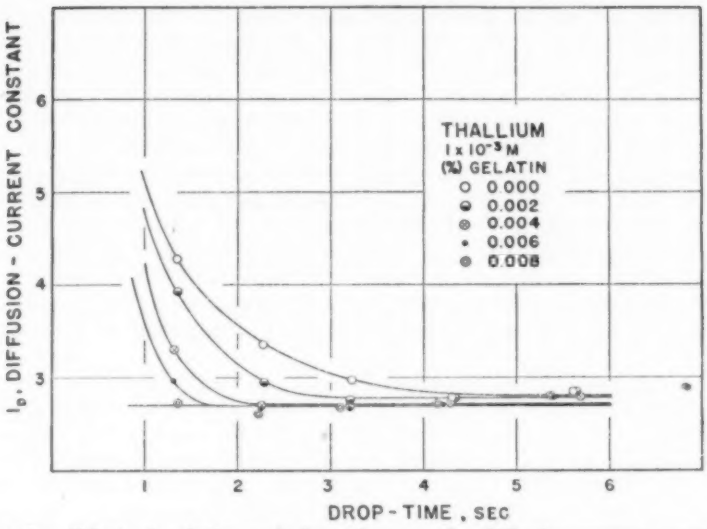

FIGURE 8.—*Effect of gelatin and drop-time on the diffusion-current constant of thallium in a supporting electrolyte of 0.1 N* KCl.

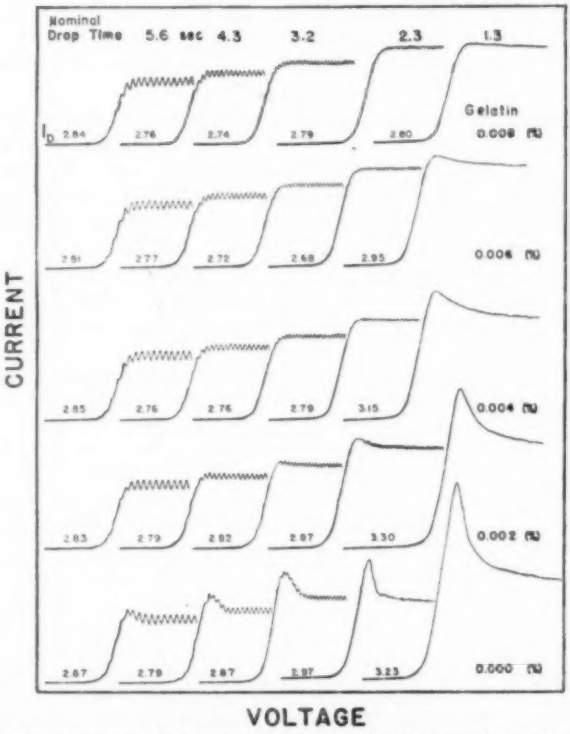

FIGURE 9.—*Characteristic polarographic waves of thallium* ($2 \times 10^{-3} M$) *in a supporting electrolyte of 0.1 N* KCl.

All polarograms were taken at a sensitivity of 1/150, except those at a nominal drop-time of 1.3 seconds for 0.000 and 0.002 percent of gelatin and for 2.3 seconds at 0.000 percent of gelatin, which were taken at a sensitivity of 1/200.

Figures 10 and 11 summarize some results obtained for bismuth in 1 *N* nitric acid. The behavior of this ion differs from that of the preceding in the following ways: (1) Deviations from the Ilkovič equation in the absence of a suppresser are considerably greater than hitherto noted, (2) prominent rounded maxima appear only at the higher drop rates, (3) at concentrations sufficiently large to give very pronounced maxima in the range 1 to 3 seconds, no departure from regular and well-defined waves is noted for drop-times greater than 4 seconds (see fig. 11). In some aspects the behavior of bismuth in an environment of nitric acid is intermediate between that of cadmium, which shows no prominent maxima, and thallium, which exhibits the characteristic peak maximum. The value of I_D for a 1×10^{-3} *M* solution is 4.70, in good agreement with the value of 4.64 reported by Lingane [2].

The applicability of the Ilkovič equation to the analysis of mixtures of reducible ions was studied in the case of *Cd–Ni* (0.297 and 0.568 millimolar, respectively) and *Tl–Cd* (1.00 and 0.897 millimolar, respectively) in a 0.1-*N* solution of potassium chloride. The half-wave potentials differ by 0.5 volt for the first pair and only 0.1 volt for the second. Hence, in accordance with expectation, the analysis of the *Cd–Ni* mixture was very satisfactory and that of *Tl–Cd* quite uncertain. Two series of polarograms over a drop-time range of 1 to 6 seconds at intervals of approximately 1 second were taken for each mixture. One series was without gelatin and the other with 0.010 percent of the suppresser. Typical polarograms are shown in figure 12.

In the series of polarograms for the mixture of cadmium and nickel in the absence of gelatin, the behavior of cadmium is similar to that of the single ion. Nickel differs from its single ion behavior in that the small sharp maxima previously observed at an identical concentration are now absent. At high drop-rates the characteristic decreased slope at the end of the wave remains. Cadmium thus appears to play the role of a suppresser. This is confirmed by the results given in table 1. In the presence of 0.010 percent of gelatin the values of I_D for both ions agree very well with those obtained with single ions.

TABLE 1.—*Diffusion-current constants obtained from electrolysis of a solution 0.568 millimolar in* Ni *and 0.297 millimolar in* Cd

[Supporting electrolyte was 0.1 *N* KCl]

Mercury flow	Cadmium		Nickel	
	0% gelatin	0.01% gelatin	0% gelatin	0.01% gelatin
mg/sec				
1.35	3.47	3.49	3.15	3.18
1.79	3.57	3.46	3.18	3.19
2.40	3.58	3.46	3.20	3.23
3.40	4.09	3.40	3.16	3.19
5.80	6.24	3.35	3.22	3.12

The mixture of cadmium and thallium is of particular interest because of the information it yields regarding the general resolving power of the method of analysis. In the polarograms for this mixture without gelatin, the thallium wave is regular and well defined over the entire drop-time range. The deposition of cadmium immediately

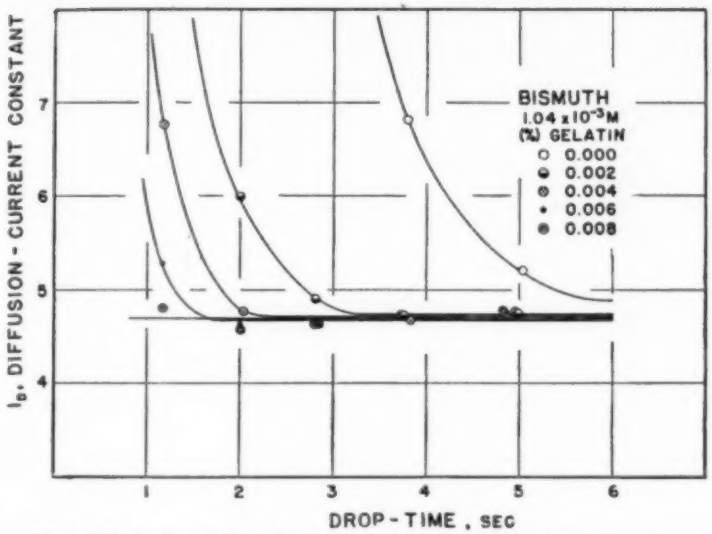

FIGURE 10.—*Effect of gelatin and drop-time on the diffusion-current constant of bismuth in a supporting electrolyte of 1 N* HNO_3.

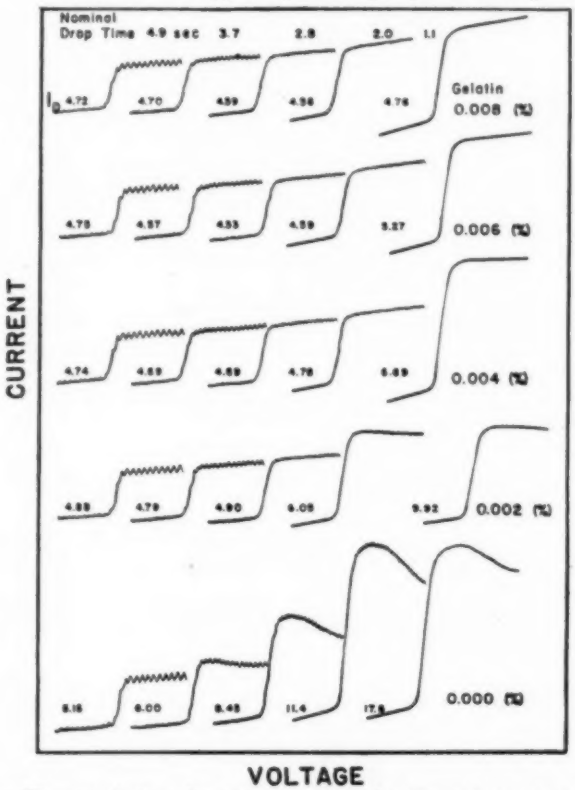

FIGURE 11.—*Characteristic polarographic waves for bismuth* (0.104×10^{-3} *M*) *in a supporting electrolyte of 1 N* HNO_3.

All polarograms were taken at a sensitivity of 1/20, except those at a nominal drop-time of 1.1 seconds for .006 percent and 0.002 percent of gelatin, which were taken at a sensitivity of 1/40.

after that of thallium completely prevents the appearance of the characteristic decreased slope at the end of the wave. In fact, this intermediate portion of the polarogram has an abnormally large positive slope. The shortness of this connecting segment makes it

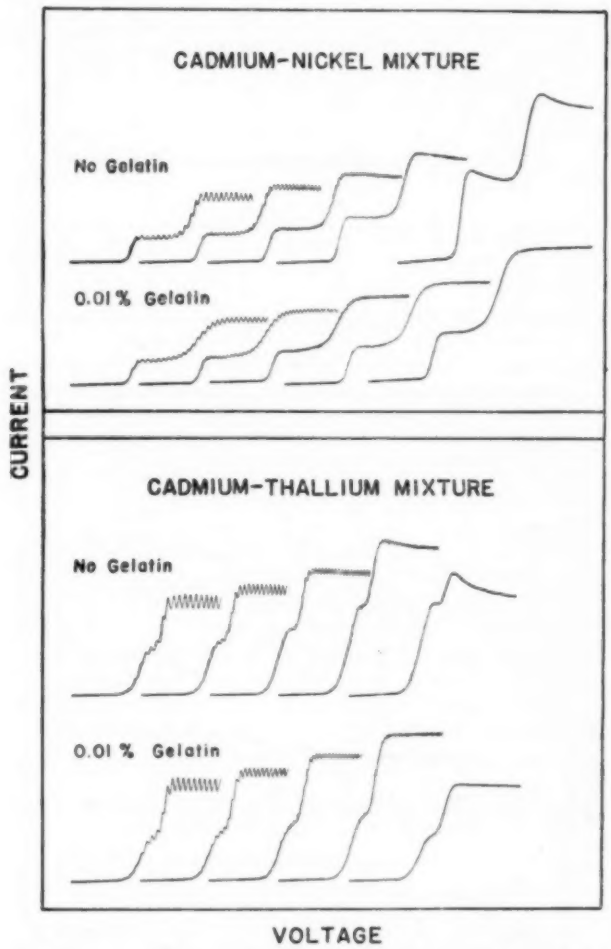

FIGURE 12.—*Polarograms for a cadmium-nickel and a cadmium-thallium mixture taken in the absence and presence of gelatin as a suppresser.*

Polarograms are ordered from left to right with increasing flow of mercury. Those for the cadmium-nickel mixture were taken at a galvanometer sensitivity, $S=1/70$, and those for the cadmium-thallium mixture were taken at $S=1/100$, except the last one in each series for which $S=1/200$. The values for I_D calculated from these curves are given in tables 1 and 2.

very difficult to determine the real wave heights except at the highest drop-rate, where the segment is sensibly parallel to the residual current. The magnitude of the error for thallium as calculated from the Ilkovič equation (which assumes diffusion control) can be seen from table 2.

TABLE 2.—*Diffusion-current constants obtained from electrolysis of a solution 1.0 by 10^{-3} M in thallium and 0.897 by 10^{-3} M in cadmium*

[Supporting electrolyte was 0.1 *N* KCl.]

Mercury flow	Cadmium		Thallium	
	0% gelatin	0.01% gelatin	0% gelatin	0.01% gelatin
mg/sec				
1.35	3.50	3.95	2.82	2.53
1.75	3.17	3.81	2.97	2.51
2.40	3.14	3.73	3.13	2.51
3.40	2.93	3.63	3.53	2.50
5.80	2.09	3.57	5.54	2.65

In this mixture the cadmium wave has the form observed when the ion is alone. However, the series is very abnormal in that the diffusion current for this ion at high drop-rates is much too small. The reason for this is that the total current at the end of the cadmium wave is chiefly limited by the total normal diffusion current of both ions, and therefore thallium, which is characterized by a prominent maximum and is reduced first, assumes a disproportionately large share of the total current. The polarograms clearly show that the fractional reduction of the total current in the presence of 0.010 percent of gelatin is very much less than that for thallium alone. In the presence of a suppresser the cadmium wave becomes normal, and the form of the thallium wave remains unchanged. The difficulty of determining the end of the thallium wave and the beginning of the cadmium wave can be seen from the fact that the values of I_D for thallium are too low and those for cadmium too high. This reflects the difficulty of determining wave-height when the segment connecting two waves is very short and of abnormal slope.

The three types of maxima encountered in this study are illustrated in figures 6, 9, and 11. The sharp maxima characteristic of univalent thallium and nickel (polarograms not shown) and the particularly simple departure from normal behavior exhibited by cadmium (fig. 6) can be taken as extreme types. The rounded maxima appearing at intermediate and high drop-rates in the case of bismuth (fig. 11) can be regarded as a transition type. The change caused in these polarograms by the addition of successive increments of gelatin is instructive. Whereas relatively large concentrations of gelatin are required to suppress maxima of the cadmium type, only small amounts of suppresser are necessary to eliminate sharp or rounded peaks. The resulting polarographic waves, however, show departure from ideal behavior like those of cadmium and exhibit the same response to further additions of suppresser. It is also noted that for the lowest drop-time and at intermediate concentrations of gelatin the waves for thallium appear to be the resultant of a small peak maximum superimposed upon a curve of the cadmium type. At low concentrations of reducible ion (see, for example, fig. 3) only the cadmium type of maximum is found. These observations suggest that sharp maxima may be primarily caused by adsorption and those of the more general and persistent cadmium type chiefly by streaming phenomena.

The appearance of a reduced slope for that segment following the polarographic wave is not caused by a decrease in the value of the

factor $m^{2/3}t^{1/6}$ with increase in applied potential. The results of this study show this quantity is independent of gelatin concentrations as high as 0.012 percent and decreases by only 2.0 percent in the range of voltage from cadmium to nickel. This confirms the earlier work of Lingane and Kolthoff [3] who found a 2.2-percent decrease from −0.5 to −1.1 volts. It is therefore incorrect to attribute the large decrease in slope so frequently observed to the operation of this factor. Greater deviations from parallelism of initial and final portions of a wave must be attributed to lack of diffusion control of the electrode process.

Although there is conclusive evidence of a real deviation from the Ilkovič equation for conditions under which it is generally assumed to be applicable, there might be the objection that the bulk of the discrepancies observed in this investigation are in reality caused by a peculiarity of the dropping electrode. However, if the mass of the drop delivered by a capillary (practically constant over a wide range of flow, gelatin content, and voltage) is considered a satisfactory capillary characteristic, a drop of 7.7 mg mass delivered by the electrode used in this study is well within the range 6 to 9 mg of several electrodes reported in the literature [11]. Moreover, experiments with a special capillary delivering drops of 40.7 mg show the same type of deviations. It was observed, however, that conditions of drop-time, concentration of reducible ion, and gelatin content under which departure from ideality occur were noticeably different.

An examination of all families of curves similar to figure 2 reveals the singular fact that for a fixed gelatin content the critical drop-time at which diffusion control ceases is (within experimental error) independent of the nature of the reducible ion, its concentration, and the supporting electrolyte. This fact suggests that for the simple metal cations diffusion control is primarily determined by characteristics of the dropping electrode and the nature and concentration of the suppressor. Table 3 summarizes the data obtained in this investigation, and figure 13 is the corresponding logarithmic plot for the individual ions.

The results shown in figure 13 are in accord with the simple adsorption theory for the suppression of maxima.[5] From a consideration

TABLE 3.—*Critical drop-times for various reducible ions in the presence of gelatin*

Nickel			Cadmium			Thallium			Bismuth		
Concentration	Gelatin	Critical drop-time	Concentration	Gelatin	Critical drop-time	Concentration	Gelatin	Critical drop-time	Concentration	Gelatin	Critical drop-time
Millimolar	*Percent*	*Seconds*	*Millimolar*	*Percent*	*Seconds*	*Millimolar*	*Percent*	*Seconds*	*Millimolar*	*Percent*	*Seconds*
0.0284	0.002	2.90	0.00593			0.05	0.002	2.90	0.0311	0.002	2.6
	.004	1.80		0.004	2.20		.004	2.20		.004	1.9
	.006						.006			.006	
.0568	.002	3.70	.0148			.10	.002	2.80	.104	.002	3.1
	.004	2.10		.004	2.30		.004	2.20		.004	2.3
	.006						.006	1.80		.006	1.8
.142	.002	2.90				1.0	.002	3.0	1.04	.002	3.3
	.004	2.00					.004	2.2		.004	2.2
	.006	1.80					.006	1.8		.006	1.8
.568	.002	2.40				2.0	.002	3.0			
	.004	1.80					.004	2.3			
	.006						.006	1.8			

[5] It is to be emphasized that the data in figure 13 do not provide information concerning the mechanism for the formation of maxima.

of this theory and the kinetics of the adsorptive process, the concentration of suppresser required to give a minimum coverage of the drop should, for a given size of drop, be an exponential function of the drop-time. The dependence of this function on the size of drops has not been fully investigated. However, preliminary experiments with a capillary producing drops of approximately 41 mg indicate a significant dependence. This behavior is now under study.

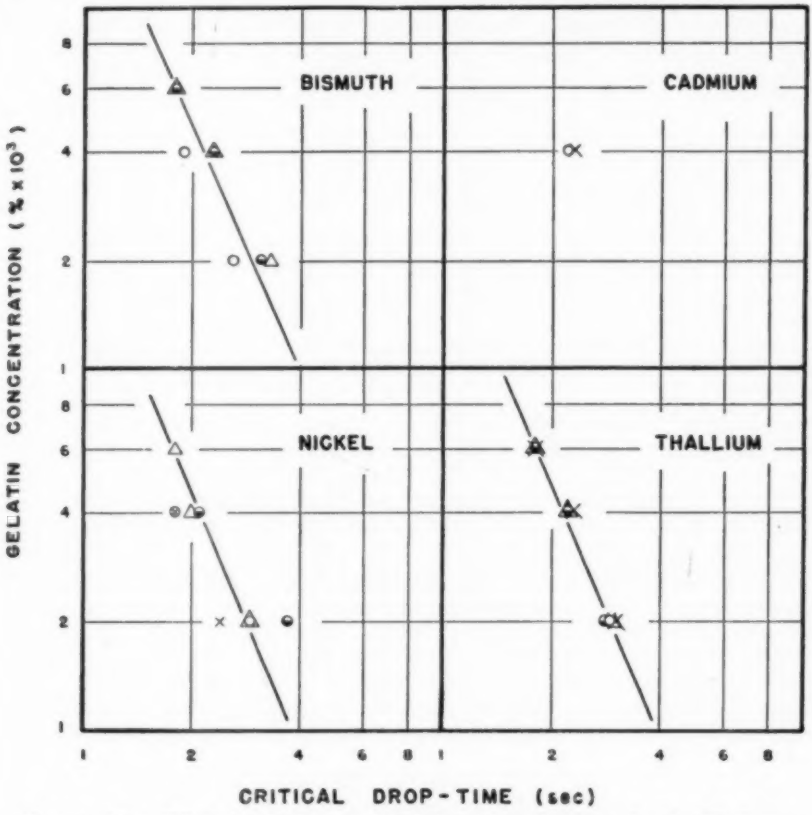

FIGURE 13.—*Effect of gelatin on critical drop-times for several reducible ions.*

Each section of the figure is a logarithmic plot of the corresponding data of table 3. A given symbol in a plot represents a fixed concentration. There is no necessary correspondence between the same symbol used in different plots.

IV. CONCLUSIONS

One of the important conclusions to be drawn from this research is that gelatin (or some other suppresser) is necessary to obtain agreement with the Ilkovič equation over a considerable range of drop-times for capillaries giving drops in the range 6 to 9 mg. The need of a suppresser increases with the dilution of reducible ion and is in all cases most acute for drop-times less than 3 seconds.

The concentration of gelatin required to effect diffusion control over a given drop-time interval is, for a given capillary, practically independent of the nature and concentration of the reducible ion. The effect of an excess of suppresser over that required to insure a con-

stant value of I_D is significant only at high dilutions of the reducible ion.

A linear relation between the logarithm of the critical drop-time and logarithm of the gelatin concentration has been found. This relation has been shown to be independent of the nature of the reducible ion, its concentration, and the supporting electrolyte.

The occurrence of "well-defined" waves so frequently mentioned in the literature has been found unreliable as evidence of diffusion control, unless a critical examination of the polarograms shows that the slopes of the segments preceding and following the wave do not differ by more than a few percent. Waves that conform to this criterion have always shown agreement with the Ilkovič equation, whereas large deviations from this form have resulted in abnormal diffusion currents.

Evidence has been obtained that suggests that at least two factors are operative in causing maxima. One factor gives rise to sharp or rounded peaks, the other to deviation from normal slope of that part of the polarogram following the polarographic wave.

The interpretation of a polarographic wave is complicated by the presence of a maximum, the formation of which is a complex function of the characteristics of the capillary electrode, the concentration of the reducible ion, the presence of simultaneously reducible ions, and concentration of suppressive agents. Consequently, it is not advisable to apply the diffusion-current constant and the Ilkovič equation to quantitative analyses unless it has been established that the experimental conditions are within its range of validity.

Since this paper was written an article by Lingane and Loveridge [13] has appeared, in which the dependence of the diffusion-current constant as a function of $m^{2/3}t^{1/6}$ was studied for several capillaries. Their results, which were for lead in a 1.0–N solution of potassium chloride and in the presence of 0.01 percent of gelatin, when plotted like those in the present paper, give values for critical drop-times in good agreement with those shown in figure 13. The slight increase of diffusion-current constant with decrease in the value of $m^{2/3}t^{1/6}$ (and hence with increasing drop-time) noted by these authors has also been observed and is commented upon in footnote 3 of the present paper.

V. REFERENCES

[1] D. Ilkovič, Collection Czechoslov. Chem. Commun. **6,** 498 (1934).
[2] J. J. Lingane, Ind. Eng. Chem., Anal. Ed. **15,** 583 (1943).
[3] J. Maas, Collection Czechoslov. Chem. Commun. **19,** 42 (1938); I. M. Kolthoff and J. J. Lingane, Chem. Rev. **24,** 1 (1939); J. J. Lingane and I. M. Kolthoff, J. Am. Chem. Soc. **61,** 825 (1939).
[4] I. M. Kolthoff and J. J. Lingane, Polarography, p. 121, (Interscience Publishers, Inc., New York, N. Y. 1941).
[5] H. Matheson, H. S. Isbell, and E. R. Smith, J. Research NBS **28,** 95 (1942) RP1448.
[6] J. J. Lingane, Ind. Eng. Chem., Anal. Ed. **14,** 655 (1942).
[7] J. Heyrovsky, Actualités Scientifiques et Industrielles, No. 90 (Paris, 1934).
[8] D. Ilkovič, Collection Czechoslov. Chem. Commun. **8,** 13 (1936).
[9] H. J. Antweiler, Z. Elektrochem. **43,** 596 (1937); **44,** 719, 831, 888 (1938).
[10] Reference 4, p. 269.
[11] O. H. Müller, J. Am. Chem. Soc. **66,** 1019 (1944); J. Chem. Education **18,** 172 (1941); J. J. Lingane and I. M. Kolthoff, J. Am. Chem. Soc. **61,** 825 (1939); J. J. Lingane, Ind. Eng. Chem., Anal. Ed. **15,** 583 (1943).
[12] Reference 4, p. 68.
[13] J. J. Lingane and B. A. Loveridge, J. Am. Chem. Soc. **66,** 1425 (1944).

WASHINGTON, October 20, 1944.

U. S. DEPARTMENT OF COMMERCE NATIONAL BUREAU OF STANDARDS

RESEARCH PAPER RP1632

Part of Journal of Research of the National Bureau of Standards, Volume 34, February 1945

COMPARATIVE LIQUID-JUNCTION POTENTIALS OF SOME pH BUFFER STANDARDS AND THE CALIBRATION OF pH METERS

By George G. Manov, Nicholas J. DeLollis, and S. F. Acree

ABSTRACT

By application of the equation $pH=(E-E_{ref}-E_j)/k$ to solutions whose pH values were known accurately, the sum of the potentials of the reference electrode and of the liquid-junction potential, $E_{ref}+E_j$, was obtained at 25° C by the method of cells with liquid junction for seven solutions suitable for standards of pH. The solutions used were 0.1018–*m* hydrochloric acid, pH 1.081; 0.01–*m* hydrochloric acid+0.09–*m* sodium chloride, pH 2.101; 0.05–*m* potassium acid phthalate +0.02–*m* potassium chloride, pH 3.989; 0.02–*m* potassium dihydrogen phosphate+0.02–*m* disodium hydrogen phosphate+0.02–*m* sodium chloride, pH 6.863; 0.02–*m* potassium phenolsulfonate+0.02–*m* potassium sodium phenolatesulfonate +0.02–*m* sodium chloride, pH 8.795; 0.02–*m* boric acid+0.02–*m* sodium borate (added together as sodium tetraborate)+0.02–*m* sodium chloride, pH 9.155; and 0.01727–*m* calcium hydroxide+0.01819–*m* sodium chloride, pH 12.38. Silver–silver-chloride electrodes immersed in saturated potassium chloride solution were used rather than the calomel electrodes customarily employed.

As E_{ref} remains constant when the buffer is changed, values for the *differences* in the liquid-junction potentials of various buffers in contact with saturated potassium chloride solution were obtained from the data. These differences were then used to calibrate seven Type 015 and three "low-alkali error" glass electrodes of commercial manufacture. The average agreement between the true pH of the buffer-chloride solution (determined from cells without liquid junctions) and that read on various commercial pH meters when corrected for the difference in the liquid-junction potentials and the alkali error of the electrode was ±0.01 pH unit. The data also furnish a critical test of the consistency of the pH values assigned to the various buffer solutions recommended by this Bureau for the calibration of the pH scale and for checking pH meters.

Recommendations are made for checking pH meters.

CONTENTS

	Page
I. Introduction	116
II. Experimental technic	116
1. Method	116
2. Electrodes	118
3. Chemicals	119
4. Equipment	119
III. Measurements of electromotive force	120
IV. Comparative liquid-junction potentials	123
V. Comparison of available buffer standards	124
VI. Recommendations for the calibration of pH meters	125
VII. References	127

I. INTRODUCTION

Recent publications from this Bureau have given provisional pH values for certain standard buffer solutions [1] [1] and detailed information concerning phthalate [2], phosphate [3], phenolsulfonate [4], and borax buffers [5]. The precision of each standard, established by the method of cells without liquid junctions [6], is considered to be 0.002 pH unit.

In the establishment of the pH scale by electrometric methods, it is assumed that any solution in which the emf of a hydrogen electrode differs from that in a second solution by 59.14 mv at 25° C ($2.3026RT/F$ at other temperatures) has a pH value 1 unit higher or lower than that of the first. The establishment of the pH scale therefore involves the use of one or more standard buffer solutions of known pH to obtain reference points and the subdivision of the scale into desired fractions (e.g. 0.1) of the theoretical pH unit.

It is evident that as many independent sets of calibrations of the scale of a pH meter can be made as there are available buffer standards. As the number of reference materials increases, it becomes important to determine how well the corresponding calibrations agree. Because the potential at the junction between the buffer solution and the electrolyte of the reference electrode (the so-called liquid-junction potential) enters into practically all measurements of pH, data on the comparative values for these liquid-junction potentials are needed. One of the purposes of this paper is to present data on the comparative liquid-junction potentials at 25° C for seven standard buffers that range in pH from 1.081 to 12.38. The method is independent of the potential and of the type of reference electrode.

As glass and hydrogen electrodes agree closely over the range of pH values from 1 to 9 [7], it is possible to use glass electrodes in pH meters, together with the values for the comparative liquid-junction potentials, to determine the accuracy with which the scale of the pH meter can be calibrated by the use of different buffers; that is, how closely the theoretical relation of 59.14 mv (at 25° C) for 1 pH unit is followed. Conversely, if it is assumed that the standards are spaced correctly with relation to one another along the pH scale, it is possible to determine accurately the performance of various types of glass electrodes immersed in different buffer solutions.

II. EXPERIMENTAL TECHNIC

1. METHOD

The pH of a buffer or unknown solution can be obtained by measurement of the electromotive force of the cell

$$-\mathrm{H_2(g)}\,|\,\underset{E_1}{\text{buffer or unknown solution}}\,\|\,\underset{E_j}{\text{saturated KCl}}\,|\,\underset{E_{ref}}{\text{reference electrode}}+ \qquad (1)$$

and the equation

$$\mathrm{pH}=(E-E_{ref}-E_j)/k, \qquad (2)$$

in which E is the measured emf, $(E_1+E_j+E_{ref})$ of the cell between the hydrogen and the reference electrodes, E_1 and E_5 in figure 1:

[1] Figures in brackets indicate literature references at the end of this paper.

E_{ref} is the potential of the reference electrode toward the hydrogen electrode in a solution of unit hydrogen ion activity when E_j is zero. E_j is the potential at the liquid junction between the buffer solution and the saturated potassium chloride, and k is the value for $2.3026RT/F$ at the temperature of the measurements [8]. Conversely, if solutions are available whose pH values are known accurately, a measurement of E permits a simple calculation of $E_{ref}+E_j$ for each buffer. Since the value for E_{ref} does not change with the buffer, it is possible to obtain accurate values for the *differences* in E_j for various buffers by a method that is independent of the nature of the reference electrode.

If the data pertaining to two buffers of known pH are designated by the subscripts I and II, the difference in the liquid-junction potentials is given by the expression

$$E_{j_I}-E_{j_{II}}=(E_I-E_{II})-k(\mathrm{pH_I}-\mathrm{pH_{II}}), \tag{3}$$

directly in terms of the measured quantities.

Independently, values for $E_{ref}+E_j$ can be obtained from the emf of two silver–silver-chloride electrodes, E_2 and E_5, immersed, respectively, in solutions of the buffer (I) containing known concentrations of chloride ions and in saturated potassium chloride (III). The emf of such a cell is given by the equation

$$(E_{ref}+E_j-E_2)=k\log(a_{\mathrm{Cl_I}}/a_{\mathrm{Cl_{III}}})+E_j. \tag{4}$$

If the ratios of the activities of the chloride ions in solutions I and III were known, eq 4 would yield directly values for E_j for each buffer. It is not possible to obtain this ratio, however, and the data permit only the calculation of $E_{ref}+E_j$.

The activity of the chloride ion in the two solutions can be expressed by the following equations:

$$k\log a_{\mathrm{Cl_I}}=k\ \mathrm{pH}-(E_1+E_2)+E^\circ \tag{5}$$

and

$$k\log a_{\mathrm{Cl_{III}}}=E^\circ-E_{ref}, \tag{6}$$

where E° is the normal potential of the silver–silver-chloride electrode, 0.22238 v at 25° C [9]. Equations 4, 5, and 6 can be combined to give

$$E_{ref}+E_j=(E_1+E_2)+(E_{ref}+E_j-E_2)-k\ \mathrm{pH}. \tag{7}$$

Comparison of the sum of (E_1+E_2) and $(E_{ref}+E_j-E_2)$ with the values for $(E_1+E_j+E_{ref})$ obtained by direct measurement indicate a consistency of 0.07 mv (0.001 pH unit) in the two sets of data for each buffer. This comparison is important because the emf between E_2 and E_5 involves electrodes reversible to the same ion, whereas the emf between E_1 and E_2 and between E_1 and E_5 involve electrodes reversible to different ions.

It should be emphasized that it is actually the difference in E_j for various buffers in contact with the saturated potassium chloride which is used in the calibration of pH meters rather than the absolute values for E_j for each buffer. The following example will make this point clear. When a pH meter is calibrated with buffer I and the dial set to read the corresponding pH value, the setting of the "zero

control" knob, E_{zero}, compensates for the liquid-junction potential of the first buffer in contact with the reference electrolyte and for the departure,[2] ΔE_{ref}, of the emf of the reference electrode from its normal value. The emf impressed upon the potentiometer system is then given correctly by the equation

$$E_{obs_I} = E_{ref} + E_{j_I} + E_{g_I} + E_{zero} + \Delta E_{ref}, \tag{8}$$

where E_{g_I} is the potential of the glass (or hydrogen) electrode in contact with buffer I. When buffer I is replaced by buffer II and the setting E_{zero} left unchanged, the observed emf is given by

$$E_{obs_{II}} = E_{ref} + E_{j_{II}} + E_{g_{II}} + E_{zero} + \Delta E_{ref}. \tag{9}$$

The true difference in the pH of the two buffers is given by

$$\mathrm{pH}_{true_{II}} - \mathrm{pH}_{true_I} = (E_{g_{II}} - E_{g_I})/k, \tag{10}$$

whereas the observed difference (as read on the meter) is

$$\begin{aligned} \mathrm{pH}_{obs_{II}} - \mathrm{pH}_{obs_I} &= (E_{obs_{II}} - E_{obs_I})/k \\ &= (E_{g_{II}} - E_{g_I} + E_{j_{II}} - E_{j_I})/k. \end{aligned} \tag{11}$$

Since pH_{obs_I} and pH_{true_I} are equal, the correction to be applied to the reading of the meter is

$$\mathrm{pH}_{true_{II}} = \mathrm{pH}_{obs_{II}} + (E_{j_I} - E_{j_{II}})/k. \tag{12}$$

Because most meters use saturated potassium chloride solution as the reference electrolyte, the measurements reported here were confined to this solution.

2. ELECTRODES

The hydrogen and the silver–silver-chloride electrodes were prepared by methods described previously [5]. Palladinized electrodes were used in solutions of potassium acid phthalate [2]. The silver-silver-chloride electrodes were of greater utiliy than the calomel electrodes generally used, because they were less affected by air and showed considerably smaller thermal hysteresis. When the potassium chloride solution was saturated with silver chloride, successive batches of electrodes agreed in 24 hours to within 0.02 mv (0.0003 pH unit) and remained stable within this limit for several months. If the potassium chloride was not saturated with silver chloride, the emf drifted and became increasingly electropositive with time as the silver chloride dissolved from the surface of the electrode. Drifts as high as 17 mv were observed. It is thus possible to introduce serious errors when microelectrodes are immersed directly in comparatively large volumes of the solution.

[2] This departure can be caused by exposure of the calomel to air [10] or by use of potassium chloride containing traces of bromides [11]. The zero control knob also compensates for the asymmetry potential of the glass electrode, but this is assumed to remain constant when the buffer is changed.

3. CHEMICALS

Potassium chloride of reagent-grade quality stated to contain 0.01 percent bromides was recrystallized twice from conductivity water. The recrystallized material and the corresponding mother liquor were tested by the following method at each stage of the purification process. Two electrodes that previously agreed to within 0.02 mv in a saturated solution of the purest potassium chloride were immersed, respectively, in (a) a solution of the crop of crystals and (b) the corresponding mother liquor, both saturated at 25° C. Oxygen was excluded from the cell system, and the solutions were saturated with silver chloride. The compartments containing the two solutions were connected by a rubber tube with a pinchcock. Measurements were made of the emf of such a cell, the potential of which is due solely to the presence of different quantities of bromide ion in the two solutions. When tested as above, a solution saturated with potassium chloride containing 0.05-mole percent of potassium bromide and 99.95-mole percent of the purest potassium chloride was found to give an emf 1.46 mv higher than the purest potassium chloride alone. From measurements of this type it was concluded that each recrystallization removed approximately 90 percent of the bromides. The final product contained less than 0.0002-mole percent of bromides, which would produce a difference in potential of less than 0.01 mv. The hydrochloric acid used for the preparation of the silver–silver-chloride electrodes was also freed from bromides [5]. Although the values for $E_{j_I}-E_{j_{II}}$ are independent of the emf and of the nature of the reference electrode, the above precautions were employed in order that the values for $E_{ref}+E_j$ for each buffer would not include a systematic error because of the presence of potassium bromide or air in the reference electrolyte.

The solutions were prepared in quantities of 10 liters from weighed amounts of conductivity water and specially purified chemicals. The conductivity water was prepared by C. G. Malmberg and had a specific conductance of 0.2×10^{-6} mho/cm^3 at 25° C. It was stored in an atmosphere of hydrogen until needed. The phosphates and phenolsulfonate were purified by R. G. Bates [4]. Particular care was taken to prevent contamination with atmospheric carbon dioxide. The solutions were transferred when necessary by a vacuum-hydrogen technic [5]. The calcium hydroxide was prepared by carefully washing pure calcium carbonate (low-alkali grade) with distilled water, after which the material was ignited at 1,000° C. The resulting oxide was allowed to react with an excess of water in a stoppered, paraffin-lined bottle and the calcium hydroxide washed several times with conductivity water. The final solution was diluted slightly with water to avoid precipitation at higher temperatures, and the concentration determined by titration with standard hydrochloric acid. This procedure for the preparation of solutions of pure calcium hydroxide was recommended by Flint and Wells [12].

4. EQUIPMENT

The apparatus is shown in figure 1. Reservoir *A* was filled with a solution of potassium chloride and silver chloride saturated at a temperature slightly higher than 25° C and kept free from air by bubbling

hydrogen through the solution. Chamber B contained two silver-silver-chloride electrodes, E_4 and E_5, and was provided with a liquid-junction compartment, C, of the type used previously [13, 14] and a stopcock, D, leading to a waste jar, E. A second chamber, F, served to prevent accidental contamination of the main body of the buffer solution in G by possible diffusion of the saturated potassium chloride solution from the liquid-junction compartment C. Bubbler H was used to saturate the hydrogen gas with water vapor and was filled with the same solution used in F and G. The buffer solution under study was transferred to F and G without exposure to the air. Cell G contained two silver–silver-chloride electrodes, E_2 and E_3, and a double hydrogen electrode, E_1, [14] immersed in the buffer solution. The apparatus was then immersed in a water thermostat, the temperature of which was controlled at 25° C to within 0.01 degree.

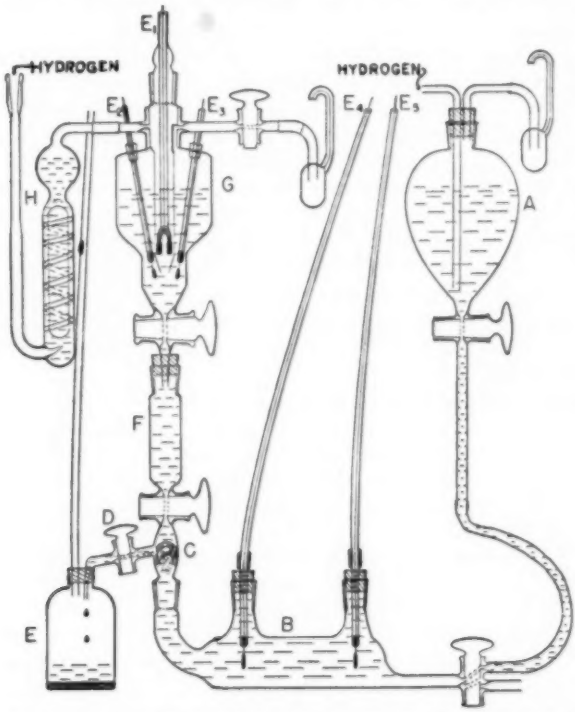

FIGURE 1.—*Apparatus used for the determination of $E_{cell}+E_j$ for buffer-chloride solutions by the method of cells with liquid-junctions.*

A, Reservoir for the saturated potassium-chloride solution; *B*, chamber containing the two silver-silver-chloride electrodes E_4 and E_5; *C*, the liquidjunction compartment with stopcock *D* leading to waste jar *E*; *F*, chamber to prevent contamination of the buffer chloride solution in *G* by accidental mixing of the saturated potassium chloride solution from *B*; *H*, the bubbler which saturates the hydrogen with water vapor before the gas enters the double hydrogen electrode chamber E_1; E_2 and E_3, silver–silver-chloride electrodes immersed in the buffer-chloride solution.

III. MEASUREMENTS OF ELECTROMOTIVE FORCE

The stopcock between F and G was closed, and hydrogen gas was bubbled over the hydrogen electrodes in G. Measurements were made of the emf (E_1+E_2) and of the agreement between the pairs of

electrodes, E_3 and E_2, E_5 and E_4, and of the double hydrogen electrode. The hydrogen electrodes agreed to within 0.01 mv in a number of preliminary trials, and for the balance of the measurements the two hydrogen electrodes were connected by a pool of mercury with a common terminal E_1, as shown in figure 1. Equilibrium was attained in a few hours, after which the emf did not vary by more than 0.05 mv for several days. All values were corrected to 1-atmosphere pressure of hydrogen gas. The values for (E_1+E_2) reported here for hydrochloric acid, hydrochloric acid–sodium chloride, phthalate, phenolsulfonate, and borax agreed within 0.05 mv with data published previously for these buffers; the emf for the phosphate buffer was 0.11 mv (0.0018 pH unit) higher than that subsequently found by Bates in an extension of his work [3], but is within the precision claimed for these measurements. The pH value for the phenolsulfonate buffer was recalculated by a somewhat more detailed method and is 0.006 unit higher than that previously reported [4a]. The pH for the hydrochloric acid-sodium chloride solution was calculated from the data of Harned and Ehlers [9] and differs slightly from that used by Hitchcock and Taylor [15].

After measurements of (E_1+E_2) had been obtained for a buffer solution, cock D was opened, and the liquid junction between the potassium chloride and the buffer solution was made in C. The emf $(E_1+E_j+E_{ref})$ and $(E_{ref}+E_j-E_2)$ were measured at frequent intervals for various combined rates of flow and for various ratios of potassium chloride and buffer solution. The liquid junction for each buffer was quite sharp even at the highest rates of flow and the steadiness of the emf justified measurements to the nearest 0.01 mv. In table 1 is given a portion of the observed data and the calculated value for $E_{ref}+E_j$ for a typical buffer, potassium acid phthalate.

TABLE 1.—*Electromotive force and other data at 25°C for the cell:*

$-$Pt, H_2 | 0.05-*m* KHPhthalate, 0.02-*m* KCl (pH 3.989) || saturated KCl | AgCl, Ag+Ag, AgCl

Rate of flow, drops per minute		Time in minutes after a change in flow rate	Electromotive force in international volts				
Buffer	KCl		$(E_1+E_j+E_{ref})$	$(E_{ref}+E_j-E_2)$	(E_1+E_2)	(E_3+E_2)	(E_3+E_4)
12	0	2	0.43435	−0.13023	0.56443	0.00002	0.00001
		5	.43435	.13021			
12	14	2	.43434	.13021			
		4	.43434	.13021			
12	36	2	.43434	.13021			
		4	.43436	.13019			
48	36	2	.43429	.13023	.56442	.00000	−.00003
		4	.43432	.13021			
72	36	2	.43429	.13024			
		6	.43429	.13026			
8	36	2	.43429	.13026	.56445	.00002	+.00001
		5	.43430	.13026			
Average values:					Values of $E_{ref}+E_j$:		
Flow of buffer > flow of KCl			0.43432	−0.13023	From $E_1+E_j+E_{ref}$		0.19839
Flow of buffer ≃ flow of KCl			.43432	−.13022	From $E_{ref}+E_j-E_2$		.19827
Flow of buffer < flow of KCl			.43432	−.13024			
Grand average			0.43432	−0.13023			0.19833

For comparison with other data in the literature involving calomel electrodes, 0.0455 v should be added to $E_{ref}+E_j$ for each of the buffers given in table 2.

TABLE 2.—*Electromotive force and other data at 25° C for the cell:*

$$-\text{Pt, } H_2 \left| \begin{matrix} \text{Ag, AgCl} \end{matrix} \right| \textit{buffer, NaCl or KCl} \,\|\, \textit{saturated KCl} \left| \begin{matrix} \text{AgCl, Ag} \end{matrix} \right| +$$

Buffer [a]	pH	Electromotive force in international volts			Values of $E_{ref}+E_j$ from	
		(E_1+E_2)	$(E_1+E_j+E_{ref})$	$(E_{ref}+E_j-E_2)$	$(E_1+E_j+E_{ref})$	$(E_{ref}+E_j-E_2)$
Hydrochloric acid	1.081	0.35149	[b] 0.26292 [c] .26296 [d] .26318	[b] −0.08850 [c] .08849 [d] .08829	0.19909	0.19913
		Average	0.26302	−0.08843		
Hydrochloric acid+chloride	2.101	0.41209	[b] 0.32147 [c] .32145 [d] .32155	[b] −0.09065 [c] .09068 [d] .09061	.19724	.19719
		Average	0.32149	−0.09065		
Phthalate+chloride	3.989	0.56443	[b] 0.43432 [c] .43432 [d] .43430	[b] −.013023 .13022 [d] .13024	.19841	.19829
		Average	0.43432	−0.13023		
Phosphate+chloride	6.863	0.73499	[b] 0.60375 [c] .60374 [d] .60373	[b] −0.13124 [c] .13119 [d] .13122	.19786	.19789
		Average	0.60374	−0.13122		
Phenolsulfonate+chloride	8.795	0.84811	[b] 0.71783 [c] .71725 [d] .71726	[b] −0.13080 [c] −.13081 [d] −.13081	.19711	.19716
		Average	0.71725	−0.13081		
Borax+chloride	9.155	0.86919	[b] 0.73976 [c] .73975 [d] .73976	[b] −0.12956 [c] .12954 [d] .12954	.19833	.19822
		Average	0.73976	−0.12954		
Calcium hydroxide+chloride	12.38	1.06350	[b] 0.92900 [c] .92900 [d] .92892	[b] −0.13445 [c] .13447 [d] .13450	.1968	.1969
		Average	0.92897	−0.13447		

[a] Composition of buffer solutions:
0.1018 *m* HCl.
0.01 *m* HCl+0.09 *m* NaCl.
0.05 *m* $KHC_8H_4O_4$+0.02 *m* KCl.
0.02 *m* KH_2PO_4+0.02 *m* Na_2HPO_4+0.02 *m* NaCl.
0.02 *m* KHPs+0.02 *m* KNaPs+0.02 *m* NaCl; (Ps=paraphenolatesulfonate ion).
0.02 *m* H_3BO_3+0.02 *m* $NaBO_2$+0.02 *m* NaCl.
0.01727 *m* $Ca(OH)_2$+0.01819 *m* NaCl.

[b] Flow of buffer > flow of KCl.
[c] Flow of buffer ≅ flow of KCl.
[d] Flow of buffer < flow of KCl.

The data reported here for the emf and the pH of calcium hydroxide–sodium chloride solutions are believed to be the first obtained by the method of cells without liquid junctions. The values 4.5A for a_t and 0.1 for β for this solution were estimated from data for other buffer-chloride mixtures. Reasonable departures therefrom (± 0.5 in a_t and ± 0.05 in β) are unlikely to give rise to uncertainties larger than 0.02 pH unit, a quantity which is negligible in the calibration of the majority of pH meters. A comparison with the available pH

data of other workers is given in table 3. The measurements of Wells [12a] and of Flint and Wells [12b, c] made at 30° C compare favorably with those of Lea and Bessey at 25° C [16] when correction is made for the change in pH with temperature for highly alkaline solutions. Measurements of the emf and the pH at 30° C by the method of cells without liquid junctions indicate that $d\text{pH}/dT = -0.035$ pH unit per degree in this region.

TABLE 3.—pH *values interpolated for 0.01727-m calcium hydroxide solution at 25°C*

Year	Method	pH at 25° C	Investigator
1907	Conductivity	12.45	Noyes and Eastman [17].
1928	Electromotive force, H_2-calomel	12.36	Wells [12a] [a].
1933	do	12.41	Flint and Wells [12b] [a].
1934	do	12.36	Flint and Wells [12c] [a].
1937	do	12.43	Lea and Bessey [16].
1938	do	12.45	Fritsch [19] [b].
1943	do	12.40	Kalousek, Jumper, and Tregoning [18].
1944	Electromotive force, cells without liquid junctions.	12.38	This investigation.

[a] Corrected to 25° C by means of $d\text{pH}/dT = -0.035$ pH/degree at pH 12.4.
[b] Temperature varied from 24° to 27° during the investigation.

IV. COMPARATIVE LIQUID-JUNCTION POTENTIALS

Values of $E_{j_I} - E_{j_{II}}$ can be obtained for various pairs of buffers by application of eq 3 and 7 to the data in table 2. The entries in table 4 represent the average values of $(E_{j_I} - E_{j_{II}})/k$ in terms of pH units. In each case, E_{j_I} designates the buffer listed at the top of columns 2 to 8 and $E_{j_{II}}$ is the corresponding buffer in column 1. The consistency of the data presented in tables 1 and 2 indicates that the values for $(E_{j_I} - E_{j_{II}})/k$ in table 4 have the same degree of precision as claimed for the pH measurements themselves, ± 0.002 unit. In general, the acid and the alkaline buffers have liquid-junction potentials which are, respectively, positive and negative to the saturated potassium chloride solution.

TABLE 4.—*Experimental values for* $(E_{j_I} - E_{j_{II}})/k$ *at 25° C for various pairs of buffers in contact with saturated potassium chloride solution*

Buffer I	Hydrochloric acid	Hydrochloric acid+chloride	Phthalate+chloride	Phosphate+chloride	Phenolsulfonate+chloride	Borax+chloride	Calcium hydroxide+chloride
Buffer II:							
Hydrochloric acid	0.000	−0.032	−0.013	−0.020	−0.033	−0.014	−0.03
Hydrochloric acid+chloride	+.032	+.000	+.019	+.012	−.001	+.018	−.01
Phthalate+chloride	+.013	−.019	+.000	−.007	−.020	−.001	−.02
Phosphate+chloride	+.020	−.012	+.007	+.000	−.013	+.006	−.02
Phenolsulfonate+chloride	+.033	+.001	+.020	+.013	+.000	+.019	−.01
Borax+chloride	+.014	−.018	+.001	−.006	−.019	+.000	−.02
Calcium hydroxide+chloride	+.03	+.01	+.02	+.02	+.01	+.02	+.00

It is beyond the scope of this paper to discuss the actual value of E_{ref} to be used in pH measurements performed with the hydrogen or the glass electrode. It is recommended instead that the meter be calibrated with two or more buffers at the start of the work. In most cases these extra measurements form but a small part of the total

effort expended. More important, however, such a calibration eliminates the errors otherwise present which may be caused by insufficient purification of the potassium chloride, improperly prepared reference electrodes including the effect of air on their potentials, hysteresis, and the possibility of undersaturation of the potassium chloride solution. For purposes of comparison, however, it is of interest to observe the values for $E_{ref}+E_j$, which have been assigned to the saturated calomel electrode by various workers. These data are given in table 5. It should be noted that the value 243.4 $\pm$0.4 mv ($\pm$0.007 pH unit) for the use with average buffers (pH 4 to 9) is identical with that estimated by Hamer [22], 243.4, for buffers of pH 4 to 5. The variations in $E_{ref}+E_j$ given in table 5 are not surprising in view of the possible sources of error. For example, 0.05-mole percent of bromides in the potassium chloride of the reference electrolyte increases the potential by 1.5 mv; an additional increase of 1.5 mv is found if the electrolyte is saturated with air.

TABLE 5.—*Comparison of the potential of the saturated calomel electrode at 25° C obtained by various investigators*

Year	Investigator	$E_{ref}+E_j$ in millivolts		
		Strong acids	Average buffers	Strong bases
1925	Scatchard [20]	245.4	245.4	
1928	Clark [21]	245.8	245.8	
1937	Hamer [22]	245.7	243.4	
1937	Hitchcock and Taylor [15]	245.0	244.1	
1938	MacInnes, Belcher, and Shedlovsky [23]		244.6	
1944	This research [a]	244.6	[b] 243.4	242.4

[a] Corrected for the difference of 45.5 mv in $E_{ref_{HgCl_2}}-E_{ref_{Ag-AgCl}}$.

[b] $\pm$0.4 mv.

V. COMPARISON OF AVAILABLE BUFFER STANDARDS

The buffer solutions in table 2 and the values of $(E_{j_I}-E_{j_{II}})/k$ in table 4 were used to calibrate a total of seven Type 015 and three "low alkali-error" glass electrodes. The apparent pH values at 25° C were measured in a constant-temperature room by means of the Beckman model G, the Coleman model 3C, the Hellige model 7040, and the Leeds & Northrup model 7661–A1 commercial vacuum-tube pH meters.

The results showed that the sum of the dial readings on the meter and the corresponding value of $(E_{j_I}-E_{j_{II}})/k$, together with the alkali-error correction of the glass electrode whenever this was significant, equalled the true pH of the buffer solution to within an average of $\pm$0.01 unit, regardless of the order in which the buffers were selected for use in the initial calibration of the meter. The averages of the data for the Type 015 and for the "low alkali-error" electrodes in which a 0.05-*m* solution of potassium acid phthalate (NBS Standard Sample 84 b) was used for the initial calibration are given in table 6. The correction for the alkali error in 0.01727–*m* calcium hydroxide +0.01819–*m* sodium chloride solution, 0.21 pH unit, was obtained by subtracting the corrected pH reading from the true pH. This

procedure is considered preferable to the use of the value 0.26 obtained by Fritsch [19], because the temperature was not carefully controlled during his experiments.

VI. RECOMMENDATIONS FOR THE CALIBRATION OF pH METERS

The buffer standards listed in table 6 can be used for calibrating pH meters at 25° C when appropriate corrections are made for differences in the liquid-junction potentials and the alkali errors of the glass electrode. The maximum difference found in the calibration of four commerical meters by the use of these buffers was 0.01 unit and is the limit of readability of most of these instruments. In the analysis of unknown solutions, it is recommended that a standardizing buffer be selected that most nearly approximates the unknown in pH and in composition.

TABLE 6.—*Comparison of the calibrations of type 015 and "low-alkali error" glass electrodes in various buffer solutions at 25° C*

[0.05-*m* potassium acid phthalate (pH 4.008) was used for the initial calibration of the pH meters]

Buffer [a]	Known pH value	pH reading observed on meter	$(E_{II}-E_{I})/k$	Correction for alkali error	Corrected value for the observed pH (sum of columns 3, 4, and 5)	$pH_{known}-pH_{obs(corr.)}$
AVERAGE TYPE 015 GLASS ELECTRODE						
Phthalate	4.008	[b] (4.01)	0.00	0.00	4.01	(0.00)
Hydrochloric acid	1.081	1.09	−.01	.00	1.08	.00
Hydrochloric acid+chloride	2.101	2.08	+.02	.00	2.10	.00
Phthalate+chloride	3.989	3.99	.00	.00	3.99	.00
Phosphate+chloride	6.863	6.86	+.01	.00	6.87	−.01
Phenolsulfonate+chloride	8.795	8.77	+.02	.00	8.79	+.01
Borax+chloride	9.155	9.14	.00	.02	9.16	.00
Calcium hydroxide+chloride	[c] 12.38	12.15	+.02	4.21	12.38	.00
					Average difference.	0.00
AVERAGE "LOW-ALKALI ERROR" GLASS ELECTRODE						
Phthalate	4.008	[b] (4.01)	0.00	0.00	4.01	(0.00)
Hydrochloric acid	1.081	1.08	−.01	.00	1.07	+.01
Hydrochloric acid+chloride	2.101	2.09	+.02	.00	2.11	−.01
Phthalate+chloride	3.989	3.99	.00	.00	3.99	.00
Phosphate+chloride	6.863	6.86	+.01	.00	6.87	−.01
Phenolsulfonate+chloride	8.795	8.78	+.02	.00	8.80	.00
Borax+chloride	9.155	9.16	.00	.00	9.16	.00
Calcium hydroxide+chloride	[c] 12.38	12.35	+.02	.00	12.37	+.01
					Average difference.	0.00

[a] Composition of the buffer solutions:
0.05 *m* $KHC_8H_4O_4$.
.1018 *m* HCl.
.01 *m* HCl+0.09 *m* NaCl.
.05 *m* $KHC_8H_4O_4$+0.02 *m* KCl.
.02 *m* KH_2PO_4+0.02 *m* Na_2HPO_4+0.02 *m* NaCl.
.02 *m* $KHPs$+0.02 *m* $KNaPs$+0.02 *m* NaCl.
.02 *m* H_3BO_3+0.02 *m* $NaBO_3$+0.02 *m* NaCl.
.01727 *m* $Ca(OH)_2$+0.01819 *m* NaCl.

[b] The dial of the pH meter was set to read this value, and the instrument was balanced with the "zero control" knob.

[c] Provisional value, ±0.02 pH unit.

[d] Obtained by difference.

The concentrations of the solutions that can be used for the calibration of pH meters are not limited to those given in table 6 but may include others that are either more dilute or more concentrated (references 1 to 5). Since the experimental values for $(E_{j_I}-E_{j_{II}})/k$ in table 4 were determined for buffer-chloride solutions at 25° C, it is of interest to ascertain how much these quantities are changed when chloride-free buffers and other temperatures are employed. From the considerations given below, it can be said that the changes are considerably less than 0.01 pH unit.

Because $(E_1+E_j-E_{ref})$ and $(E_{ref}+E_j-E_2)$ for all buffers studied were affected on the average to less than 0.1 mv by wide variations in the rate of flow and in the ratios of the buffer and saturated potassium chloride solution forming the liquid junction, the differences in $(E_{j_I}-E_{j_{II}})/k$ for the same pairs of buffers with and without chloride are probably less than 0.002 pH unit. A degree of turbulence in the formation of the junction sufficient to cause a mixing of only 4 parts of the saturated potassium chloride solution with 996 parts of the chloride-free buffer would raise the chloride content of the latter to 0.02 *m*. Furthermore, at the concentrations used the difference in the effective mobilities of the positive and the negative ions of a chloride-free buffer is not altered appreciably when the solution is then made 0.02 *m* in sodium or potassium chloride. When the Henderson equation [24] is used to calculate the differences in the potentials of the liquid junction between the reference electrolyte and the buffer solution with and without chloride, the major assumptions made in the initial derivation of this equation are found to cancel; such a procedure should therefore be expected to give reasonably trustworthy values for these differences. The average difference calculated in this manner for the solutions listed in table 4, with and without chloride (hydrochloric acid and hydrochloric acid–sodium chloride excepted), is −0.003 pH unit.[3] Since this average difference is applied to each of the entries for $E_{ref}+E_j$ in table 2, no net change results in the values for $(E_{j_I}-E_{j_{II}})/k$ in table 4.

Likewise, the temperature coefficients for the liquid-junction potentials do not vary greatly. The calculated average liquid-junction potential for the buffers studied here is approximately 0.010 pH unit higher at 35° than at 25° C.[4] Again, the use of this average difference causes no net change in the values in table 4. Until more accurate data for the conductance of mixtures of ions become available, it is recommended that the values in table 4 be used for chloride-free buffers as well as for those that are 0.02 *m* in chloride and for temperatures up to or slightly beyond 35° C. The pH of these solutions varies with the concentration of the chloride ion and the temperature, and the appropriate pH values (references 1 to 5) must be used in addition to the corrections given in table 4.

[3] The individual differences for phthalate, phosphate, phenolsulfonate, borax, and calcium hydroxide buffers are, respectively, −0.004, −0.003, −0.003, −0.005, and −0.002 pH unit. The mobilities of HPr^- and of Pr^{--} were estimated from data on other sulfonic acids.

[4] The individual differences for the buffers listed in table 4 are, respectively, 0.002, 0.006, 0.008, 0.009, 0.009, 0.013, and 0.008 pH unit.

VII. REFERENCES

[1] R. G. Bates, W. J. Hamer, G. G. Manov, and S. F. Acree, J. Research NBS **29,** 183 (1942) RP1495.
[2] W. J. Hamer, G. D. Pinching, and S. F. Acree, J. Research NBS **32,** 215 (1944) RP1586.
[3] R. G. Bates and S. F. Acree, J. Research NBS **30,** 129 (1943) RP1524.
[4a] R. G. Bates, G. L. Siegel, and S. F. Acree, J. Research NBS **31,** 205 (1943) RP1559.
[4b] R. G. Bates and S. F. Acree, J. Research, NBS **32,** 131 (1944) RP1580.
[5] G. G. Manov, N. J. DeLollis, and S. F. Acree, J. Research NBS **33,** 287 (1944) RP1609.
[6] W. J. Hamer and S. F. Acree, J. Research NBS **23,** 647 (1939) RP1261.
[7] M. Dole, The Glass Electrode (John Wiley & Sons, New York, N. Y., 1941).
[8] G. G. Manov, R. G. Bates, W. J. Hamer, and S. F. Acree, J. Am. Chem. Soc. **65,** 1765 (1943).
[9] H. S. Harned and R. W. Ehlers, J. Am. Chem. Soc. **55,** 2179 (1933).
[10] M. Randall and L. E. Young, J. Am. Chem. Soc. **50,** 989 (1928).
[11] F. L. Hahn, J. Am. Chem. Soc. **57,** 2537 (1935).
[12a] L. S. Wells, BS J. Research **1,** 951 (1928) RP34.
[12b] E. P. Flint and L. S. Wells, BS J. Research **11,** 163 (1933) RP584.
[12c] E. P. Flint and L. S. Wells, BS J. Research **12,** 751 (1934) RP687.
[13] G. G. Manov, N. J. DeLollis, and S. F. Acree, J. Research NBS **33,** 273 (1944) RP1608.
[14] C. N. Murray and S. F. Acree, BS J. Research **7,** 713 (1931) RP369.
[15] D. L. Hitchcock and A. C. Taylor, J. Am. Chem. Soc. **59,** 1812 (1937).
[16] F. M. Lea and G. E. Bessey, J. Chem. Soc. 1612 (1937).
[17] A. A. Noyes and G. W. Eastman, Carnegie Inst. Wash. Pub. No. 63 (1907).
[18] G. L. Kalousek, C. H. Jumper, and J. J. Tregoning, J. Research NBS **30,** 215 (1943) RP1530.
[19] A. Fritsch, J. Am. Leather Chem. Assoc. **33,** 592 (1938).
[20] G. Scatchard, J. Am. Chem. Soc. **47,** 696 (1925).
[21] W. M. Clark, The Determination of Hydrogen Ions, (Williams & Wilkins Co., Baltimore, Md., 1928).
[22] W. J. Hamer, Trans. Electrochem. Soc. **72,** 45 (1937).
[23] D. A. MacInnes, D. Belcher, and T. Shedlovsky, J. Am. Chem. Soc. **60,** 1094 (1938).
[24] P. Henderson, Z. physik. Chem. **63,** 325 (1908).

WASHINGTON, November 24, 1944.

627528—45——3

U. S. DEPARTMENT OF COMMERCE NATIONAL BUREAU OF STANDARDS

RESEARCH PAPER RP1633

Part of Journal of Research of the National Bureau of Standards, Volume 34, February 1945

SPECTROGRAPHIC DETERMINATION OF SODIUM, POTASSIUM, AND LITHIUM IN PORTLAND CEMENT WITH THE DIRECT-CURRENT CARBON ARC

By Armin W. Helz*

ABSTRACT

Spectrographic methods, which are much less time-consuming than the usual chemical methods, are described for the determination of sodium, potassium, and lithium in portland cement. For the determination of sodium and potassium the sample is mixed with a mineral base containing silver for the internal standard. For lithium a standard mixture of graphite and strontium carbonate is added to the cement sample. In either case a fixed amount of the resultant mixture is placed in the crater of a graphite electrode, which is made the lower positive element of a direct-current arc. The Na 8194.81 A, *K* 7698.98 A, and Li 3232.61 A lines are used for the quantitative calculations. A discussion of the development of the method is given, followed by details of the adopted analytical procedure. The spectrographic analyses of 41 cements for sodium and potassium are given for comparison with the chemical values.

CONTENTS

	Page
I. Introduction	129
II. Method of analysis for sodium and potassium	130
1. Choice of method	130
2. Choice of spectral region	131
3. Development of the method	132
III. Analytical procedure for sodium and potassium	133
1. Standard mixture	133
2. Sample preparation and electrodes	133
3. Making the spectrogram	133
4. Photometry and analytical curves	134
5. Procedure for high K_2O content	134
6. Time required	135
IV. Results of analysis for sodium and potassium	135
V. Determination of lithium	139
VI. Summary	140
VII. References	141

I. INTRODUCTION

Spectrographic analysis depends upon the fact that elements of a substance can be made to radiate light, a spectrum of which has many lines characteristic of the elements in the source. The relative intensities of these lines for different elements bear a definite relation to the relative quantities, kind, and number of elements in the source, but

*Research Associate at the National Bureau of Standards, representing the Portland Cement Association.

with the present state of knowledge of spectroscopy, this relation is too complicated to predict. It has been found that by controlling the excitation used for the source and dividing analytical problems into type cases, empirical data may be obtained that will give a rapid analytical method. This method of analysis is ideally suited to problems in which (1) a rapid determination is required, (2) the size of the sample is necessarily small, (3) the concentrations of the elements in question are small, or (4) the chemical method is difficult or uncertain. Many examples may be found in the literature on the subject where the accuracy of the results is as good as that of the best chemical methods, and the time for the analysis is a matter of minutes for the spectrographic method as compared to hours for the chemical method.

The percentage error of spectrographic analysis tends to remain constant regardless of the concentration, whereas, in chemical analysis, the absolute error tends to be constant. Thus, for high concentration, chemical methods are preferable to spectrographic methods, whereas for low concentrations the reverse is true. In general, spectrographic analysis has proved advantageous for the determination of concentrations of elements below about 5 percent.

The interest in spectrographic methods by the cement industry arises from the presence in portland cement of small quantities of metallic elements, the specific effects of which it is important to study. Of particular significance at this time are the alkali elements, which are under critical observation by various laboratories in connection with questions on the durability of concrete [1].[1] In the present paper, the elements considered are potassium, sodium, and lithium. The spectrographic method does not require the difficult separations that are involved in the chemical determinations of the alkali elements, and it is much less time-consuming. This advantage of speed will be even greater if the method is extended to include other minor elements, such as magnesium, manganese, and titanium.

No general method of spectrographic analysis has proved entirely satisfactory. It is necessary to make a study of the type of substance to be analyzed, because the intensities of the lines of the minor elements depend not only on their concentrations but also in various degrees upon the major elements and the physical and chemical states of all the elements present. Portland cement, with its limited variability of the major components, may be treated as a single type of material for spectrographic analysis. Primary considerations for this application are the preparation of the sample and excitation of the spectrum. Subsequent details of spectroscopy and photography are readily decided according to established principles. The spectrographic procedure is outlined in detail for the benefit of those in the ceramic industry who are not familiar with this field.

II. METHOD OF ANALYSIS FOR SODIUM AND POTASSIUM

1. CHOICE OF METHOD

In this study, the widely used internal-standard principle of Gerlach and the rotating-stepped-sector method of plate calibration were adopted. For discussions of these matters, papers by Duffendack

[1] Figures in brackets indicate the literature references at the end of the paper.

Wolfe, and Smith [2], Twyman [3], Pierce and Nachtrieb [4], Scribner [5], and Owens [6] may be consulted. But the problems involved in the treatment of the sample, the excitation of the spectrum, and the choice of the spectral region best suited to the present conditions could be settled only by a planned program of experimental tests.

Characteristics of portland cement, of immediate significance in its spectrographic analysis, are its low electrical conductivity, and its ability to sinter and melt at the temperature of the electric arc. Procedures suitable for use with this type of material may be found in the literature relative to the analysis of minerals and inorganic chemicals [6 to 15], ceramic materials [16, 17], and ignited biological materials [6, 7, 9, 18, 19, 24]. A common treatment is to place a small quantity of the sample in the crater of a graphite electrode [7, 16, 20]. The sample is often mixed with graphite [11, 14, 17, 23] or a base material free from the elements sought [13, 19] and bearing with it an internal standard [2] [2, 4] and a spectroscopic buffer [2] [24].

The sample mixture may be compressed into pellets and placed on a graphite electrode [7] or used as the electrode alone [21, 22]. A method designed to use a solution may also be considered because the alkalies in portland cement are readily brought into solution by treatment with dilute hydrochloric acid. The solution may be injected into a flame [9] or a small amount dried on a graphite electrode [8, 10, 12, 20] for arc or spark excitation.

The kind of excitation to use for best results is interrelated to a considerable extent with the condition of the sample. In the references given for the sample treatments discussed in the preceding paragraph, four kinds of excitation are noted: (1) flame, (2) direct-current arc, (3) alternating-current arc (stabilized by the use of a high-voltage, current-limited circuit), and (4) condensed spark.

Several methods and a great many variations in procedure for the determination of the alkalies in portland cement were explored, but for one reason or another were rejected in favor of the direct-current arc procedure. An alternating-current arc [8] with the sample mixed with a powdered metal or graphite and compressed into pellets [21, 22] indicated good possibilities except for requirements of rigidly controlled operating conditions. A solution of the cement sample dried on a graphite electrode for use in an alternating-current arc [8, 12] proved to be impractical because of low intensity of the alkali lines. In the method finally adopted, a fixed quantity of the sample was placed in a cupped graphite electrode and used in a direct-current arc. The preliminary survey indicated good possibilities and at the same time the simplest solution of the problem.

2. CHOICE OF SPECTRAL REGION

It was desired to determine the alkali elements in concentrations between about 0.05 percent and 1.5 percent, the latter value being

[1] Because of unequal vaporization and excitation conditions from sample to sample and variations in photographic properties from plate to plate, the intensity of a spectral line of the "unknown" element is measured relative to that of a line of an element either in the sample in a constant concentration or added to the sample. This is the "internal standard," which should possess the following properties: (1) The reference line should be in the same wavelength region as the analysis line, (2) the excitation characteristics of both lines should be similar, (3) the two elements should have similar vaporization rates, (4) the intensities of the two lines should be similar, and (5) a uniform dispersion of the reference material throughout the sample should be obtained. For practical considerations the internal standard may not have all of the above properties, and variations in the results may be noted from sample to sample due to the presence of extraneous elements and variations in the excitation. These differences may be diminished by the addition of a "spectroscopic buffer"—an element (usually having a relatively high vapor pressure and a low ionization potential) which tends to maintain uniform excitation in the arc.

about the upper limit of concentration of any one alkali element in commercial cements. With the direct-current carbon arc the following lines have intensities convenient for quantitative work (expressed in wavelength in angstroms):[3] Na, 3302.32, 8194.81 and *K*, 4044.14, 7698.98. Lines in the 3,200 to 4,500 region have the advantage over lines in the 7,300 to 8,600 region in that they may be photographed on plates much more suitable for quantitative work. The *K* 4044.14 line, however, occurs in a region of strong cyanogen bands, which interfere with measurements of intensity; but this background may be effectively reduced by a special exposure procedure or by the use of a nitrogen-free atmosphere [18, 19] for the arc. The 7,300 to 8,600 region has much less background interference, but here a difficulty is encountered with the *K* 7698.98 line, which exhibits self-reversal for the higher potassium concentrations.[4] (See fig. 1, *B*.) However, certain refinements and improvements in the procedure made it possible to use that line. Therefore the red region was chosen for the analytical procedure. This is illustrated in figure 1. Spectra *D*1 and *D*2 are in the 8,500 A to 7,600 A region. Each spectrum is divided into five strips of known relative intensity for photometric purposes, explained later in the text.

3. DEVELOPMENT OF THE METHOD

The self-reversal of the potassium lines noted in the powder method was observed only for cements having the higher potassium concentrations and was found to be subject to a partial control by an adjustment of the flow of air around the arc and of the concentration of the sample. Powdered graphite and alumina made the condition more acute, but silica improved the spectrum, forming, however, a refractory melt that gave the arc erratic burning characteristics. A mixture of silica, alumina, and calcium carbonate, which when mixed with the cement sample produces in the arc a fluid low-temperature melt, effectively reduced the self-reversal of the potassium lines. Under these conditions the potassium in the sample evaporated at a steady rate for a period of about 1 minute. The addition of lithium carbonate to the mixture, for buffer action, further improved the behavior of the melt, but erratic results were still obtained, owing to the large volume of gas liberated in the arc. This sudden release of carbon dioxide in some instances forced drops of the sample mixture to flow over the rim of the crater, but it was found that this could be prevented by prefusion of the mixture or the use of a larger-diameter electrode having a conical-drilled crater. Furthermore, the use of this new electrode also decreased the rate of evaporation of the alkali elements by requiring a longer time to reach the maximum temperature.

Silver, introduced as the oxide, was selected for the internal standard because of the similarity in rate of evaporation of silver and the alkalies and the favorable supply of reference lines for sodium and potassium. This internal standard is not ideal but is a practical compromise. For this reason, particular precision was required with such details in the procedure as the weight of the sample in the electrode, the time of exposure, the arc current, the arc gap and its position in relation to the spectrograph.

[3] An angstrom is equal to 10^{-8} cm.

[4] "Self-reversal" is a decrease in the intensity of a spectral line caused by the absorption of radiation from atoms in the central part of the source by atoms of the same kind in the outer part of the source. Such lines appear very broad, blurred, and often completely transparent in the center.

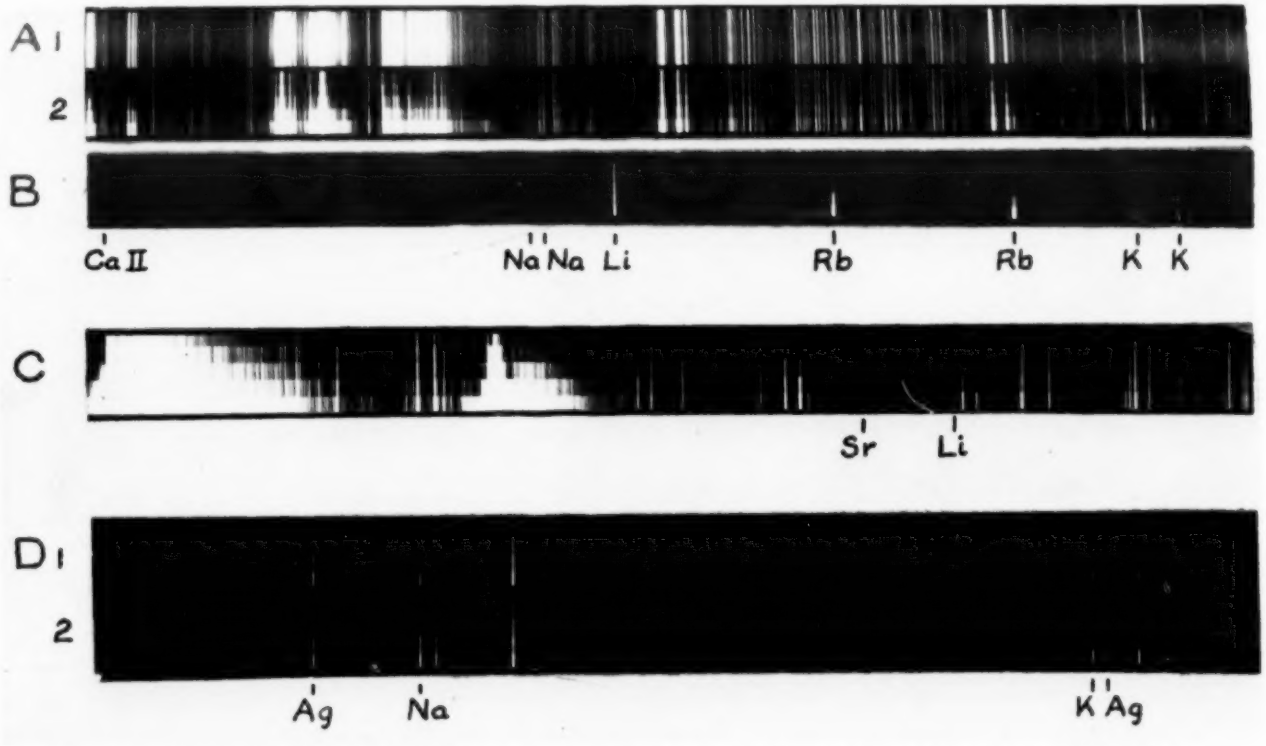

Figure 1.—Illustrations of the intensity pattern, self-reversal, and typical spectra for the determination of the alkalies.

A, spectrum in the 4,000 to 3,000 A region. 1, uniform illumination, 2, pattern produced by the rotating-stepped sector.
B, spectrum in the 8,500 to 7,600 A region showing the alkali lines. The Rb lines are self-reversed.
C, spectrum for the lithium determination of a cement sample containing 0.15 of percent Li_2O. The lithium and strontium (internal standard) lines used for the determination are indicated.
D, spectrum for the sodium and potassium determinations showing the sodium, potassium, and silver (internal standard) lines used in the determination. Sample 1 contains 0.08 percent of Na_2O and 0.35 percent of K_2O. Sample 2 contains 0.74 percent of Na_2O and 0.69 percent of K_2O.
Spectra *A* and *B* were made with a spectrograph having slightly less dispersion than that for spectra *C* and *D*. All spectra in the plate are shown with

III. ANALYTICAL PROCEDURE FOR SODIUM AND POTASSIUM

1. STANDARD MIXTURE

The standard mixture used in the preparation of the sample for analysis of potassium and sodium is made by thoroughly mixing 60 percent (by weight) of SiO_2, 14 percent of Al_2O_3, 20 percent of $CaCO_3$, and 6 percent of Li_2CO_3. Highest purity powdered chemicals are used. The mixture is fused in a platinum boat by heating in an electric furnace to 1,300° C, cooled and crushed to pass a No. 100 sieve. An amount of finely divided silver oxide (alkali free) is added equal in weight to one-tenth of the weight of the fused and ground product just described. Thorough mixing by alternately grinding in an agate mortar and sifting through a No. 100 sieve completes the preparation of the standard mixture. Thirty grams of this mixture is a sufficient quantity for use in analyzing 100 cement samples.

2. SAMPLE PREPARATION AND ELECTRODES

For the determination of sodium and potassium, 0.300 g of the CaO-Al_2O_3-SiO_2-Li_2O mixture is mixed with 0.100 g of the portland cement sample. Small glass vials are convenient for weighing, mixing, and storing the samples. Time is saved if a number of vials are filled in advance with the required amount of the standard mixture. After the addition of the cement sample, mixing is accomplished with the use of an agate mortar and pestle and by sifting through a small No. 100 sieve. Thirty milligrams of the mixture is placed in each of two graphite electrodes prepared for duplicate results.

The electrodes are cut from second grade, spectroscopic carbons, which are suitable for the determination of the alkalies in concentrations above 0.1 percent. The upper electrode consists of a 1-inch length of ⅛-inch-diameter stock with a tapered "pencil" point. The lower electrode similar to the design of Scribner and Corliss [25] consists of two parts, (1) a base and pedestal cut from ¼- or ⅜-inch-diameter stock, which is clamped to the arc stand and acts as a support for (2) the cap which carries the sample. With this design the sample-bearing area of the electrode obtains a more uniform and higher temperature than with the usual one-piece design. The base may be used several times, but the cap and cathode are good for only a single exposure. The cap consists of a 15-mm length of ⅜-inch-diameter-stock graphite with a hole in each end, one to fit the pedestal, which may be cylindrical, but preferably the shape of a truncated cone, and the other to receive the sample. The sample hole has conical sides starting at the top with a diameter of 8 mm and tapering down to 4-mm diameter at a depth of 4 mm. For a depth of 3 mm beyond this point, the hole continues with a cylindrical shape 4 mm in diameter. Special lathe tools make the cutting of these caps a simple and rapid operation.

3. MAKING THE SPECTROGRAM

A grating spectrograph having a dispersion of about 5 A per millimeter was used. This high dispersion is incidental, however, and not necessary for this procedure. Uniformity of illumination at the slit is aided by placing at the slit a convex lens [5], which produces an image of the arc on the grating of the spectrograph. Because the arc

in this work is an extended source with a large flame, and also because the vertical distribution of intensity of the internal standard lines is different from that of the alkali lines, additional specification of the illumination is necessary. Good illumination is obtained with the arc in such a position that the upper limit of its inverted image, or the rim of the lower electrode, coincides with the upper edge of the grating. The image of the upper electrode then falls well within the grating area. This setting and the readjustment required during the burning of the arc to keep the gap at a specified value may be facilitated by projecting an image of the arc on a screen on the side of the arc opposite the spectrograph. A rotating stepped sector [4, 5] for producing a relative-intensity pattern, and a filter, complete the optics outside the spectrograph. Light from the arc passes in order: filter, sector, lens, and slit. A Corning, Noviol B, G38 filter is needed for the sodium-potassium determination if a grating spectrograph is used. This filter cuts out the light of wavelength shorter than 4500 A.

The electrode holder, or arc stand [20, 25], should be designed to provide rapid vertical adjustment of both electrodes, adjustment of the upper electrode during the exposure to keep the gap constant, and controlled ventilation.

A 220-volt direct-current power supply with the current controlled at 10 amperes is used. The lower sample-bearing electrode is made positive [20] and the gap set at 4 mm. An exposure time of 90 seconds is used, starting with the striking of the arc. The arc is conveniently started by the use of an auxiliary circuit, which momentarily induces a high-frequency, high-voltage, low-current spark across the gap [26]. However, the results are the same as when the simpler starting method is used of shorting with a carbon rod. Eastman IIR spectrographic plates are used. The plates in this study were processed in automatically rocked, temperature-controlled trays.

4. PHOTOMETRY AND ANALYTICAL CURVES

The determination of the relative intensities of the spectral lines and their correlation with the concentration of the elements follow standard procedures, for which many references may be found [4, 5]. Measurements of the blackening of the lines are made with a nonrecording microphotometer. The lines measured are K 7698.98 A, Ag 7687.78 A, Na 8194. 81 A, and Ag 8273.52 A. A graph of blackening versus logarithm of the relative intensity is made for each region of the spectrum and for each plate. The most suitable steps of the alkali and internal-standard lines are measured and calculated to relative intensity with the use of the plate-calibration curve.

The alkali concentration is determined by reference to an analytical curve giving the relation between concentration and relative intensity. This is determined by carrying out the entire spectrographic procedure on cements of known alkali content.

5. PROCEDURE FOR HIGH K_2O CONTENT

It has been stated that the direction of the arc flame, towards or away from the spectrograph, affects the self-reversal of the potassium lines. This has been reduced by the choice of a standard mixture

but was not completely eliminated for high K_2O concentrations. This difficulty may be surmounted in either of two ways.

(1) The ventilation of the arc chamber may be controlled to keep the arc flame on the side of the upper electrode nearest the spectrograph. The draft required is very gentle and should not be strong enough to make the arc burn erratically. If the arc chamber is properly ventilated, the self-reversal is not significant for K_2O concentrations below 1.0 percent. If no draft is used, the limit of applicability of the procedure outlined in the preceding sections is lowered to about 0.6 or 0.7 percent of K_2O.

(2) The procedure to be used here and also for K_2O concentrations above 1.0 percent where controlled ventilation is used is followed exactly as outlined to the point of measuring the intensity of the lines. A visual inspection is made to exclude from measurement those potassium lines obviously self-reversed. An analysis of the rejected samples for potassium is repeated with a more dilute mixture. Instead of taking 0.3 g of the standard mixture and 0.1 g of the cement sample (3 to 1), 0.450 g of the standard mixture and 0.050 g of the cement sample are taken (9 to 1). All other details of the procedure are the same, except of course the requirement of another analytical curve made with the more dilute mixture.

6. TIME REQUIRED

The procedure is rapid, requiring about 4 hours for the determination of sodium and potassium in six samples as compared with 30 hours for the chemical procedure. Increasing the number of samples and the extension of the spectrographic method to include other minor elements would increase the time advantage of the spectrographic method over chemical methods. The 4 hours for the spectrographic method does not include the time required to cut graphite electrodes and to prepare the standard mixture. These may be prepared in large quantities and kept on hand.

IV. RESULTS OF ANALYSIS FOR SODIUM AND POTASSIUM

The analytical, or working curve, when plotted in terms of the logarithm of the relative intensity (alkali line relative to the internal-standard line) and the logarithm of the concentration of the alkali, should be a straight line [4]. This was the case for K_2O, but the Na_2O curve deviated from linearity owing to some sodium contamination either in the electrodes or in the standard mixture. In all the calculations the concentrations of the oxides of the alkali elements are used rather than those of the elements, to conform with the customary procedure for reporting analysis of cements.[5]

The reproducibility of the method is shown in table 1. Results are given for 18 individual determinations of Na_2O and K_2O in the same sample. The deviations of values from the average illustrates the errors due to fluctuations in the arc, inhomogeneity of the sample,

[5] The samples for determining the analytical curves for Na_2O and K_2O were analyzed by J. J. Tregoning of the Clay and Silicate Products Division of this Bureau.

and inconsistencies in photometric measurements. The probable errors shown in the table (4.0 percent for duplicate determinations of Na_2O and 5.8 percent for K_2O) represent the precision of the method, but the accuracy is demonstrated best by a comparison of the analyses of a large number of portland cements as is done in table 2, in which the average of the spectrographic results on each cement is compared with chemical results.[6] The average percentage difference between the chemical and spectrographic results is 0.06 for Na_2O and 0.07 for K_2O. This shows a much greater percentage error relative to the average concentration of Na_2O and K_2O than is indicated by the probable errors reported in table 1. This larger error cannot be ascribed alone to inaccuracies in the spectrographic method as it also includes inaccuracies in the chemical method.

TABLE 1.—*Reproducibility of the method for* Na_2O *and* K_2O *as indicated by 18 determinations on the same sample of cement*

[Sample No. 1]

Na_2O [a]	K_2O [b]
%	%
0.33	0.34
.37	.25
.41	.33
.38	.27
.37	.31
.34	.26
.34	.32
.34	.24
.34	.27
.33	.32
.35	.33
.35	.37
.36	.33
.34	.27
.40	.28
.35	.33
.38	.30
.44	.33
Average... 0.36	0.30

[a] Probable error for Na_2O: 1 determination, 5.7% of the concentration; 2 determinations, 4.0.
[b] Probable error for K_2O: 1 determination, 8.2; 2 determinations, 5.8.

Tables 3 and 4 give more detailed data for the first 21 cements listed in table 2. Two spectrographic "results" are given, a "result" being the average of two determinations. The chemical values are the average of two or more determinations (with the exclusion of widely divergent values) and were obtained by five different laboratories. The roman numerals at the head of columns of chemical results designate the laboratories, and the letters *A* and *B* designate the method (*A*, modified Berk-Roller [27] and *B*, the ASTM [28] method). The average difference between the maximum and minimum chemical results of different laboratories is 0.06 percent, which is the same as the difference between chemical and spectrographic results.

[6] Obtained through the courtesy of the Portland Cement Association; Berk-Roller method used.

Also the average difference between the chemical results I *A* and I *B* is greater than the average difference between single determinations for either I *A* or I *B* (not shown in the table). These observations emphasize that reproducibility alone is not a measure of the

TABLE 2.—*Comparison of the results for* Na_2O *and* K_2O *(in percent) obtained by the spectrographic and the chemical (Berk-Roller) methods*

Cement number	Na_2O			K_2O		
	Spectrographic	Chemical	Difference	Spectrographic	Chemical	Difference
2	0.21	0.24	−0.03	0.43	0.59	−0.16
3	.38	.36	+.02	.40	.45	−.05
4	.04	.03	+.01	.24	.19	+.05
5	.14	.06	+.08	1.55	1.37	+.18
6	.06	.06	0	0.24	0.19	+.05
7	.34	.28	+.06	.42	.49	−.07
8	.10	.07	+.03	.47	.44	+.03
9	.10	.16	−.06	.18	.13	+.05
10	.30	.25	+.05	.46	.44	+.02
11	.31	.26	+.05	.36	.39	−.03
12	.58	.66	−.08	.20	.15	+.05
13	.15	.05	+.10	1.48	1.36	+.12
14	.28	.25	+.03	0.58	0.54	+.04
15	.26	.28	−.02	.27	.26	+.01
16	.28	.27	+.01	.38	.46	−.08
17	.34	.32	+.02	.32	.26	+.06
18	.08	.05	+.03	1.35	1.28	+.07
19	.15	.16	−.01	0.34	0.24	+.10
20	.30	.38	−.08	.06	.04	+.02
21	.96	1.17	−.21	.16	.12	+.04
22	.09	0.08	+.01	.30	.27	+.03
23	.56	.42	+.14	.86	.74	+.12
24	.20	.17	+.03	.16	.18	−.02
25	.30	.24	+.06	.82	1.03	−.21
26	.33	.31	+.02	.40	0.51	−.11
27	.40	.29	+.11	.48	.48	0
28	.25	.22	+.03	.20	.22	−.02
29	.39	.28	+.11	.47	.49	−.02
30	.18	.23	−.05	.52	.41	+.11
31	.38	.39	−.01	.53	.57	−.04
32	.14	.16	−.02	.16	.16	0
33	.15	.08	+.07	.67	.68	−.01
34	.33	.31	+.02	.54	.52	+.02
35	.12	.09	+.03	.56	.44	+.12
36	.14	.12	+.02	.20	.19	+.01
37	1.06	.74	+.32	.52	.69	−.17
38	0.11	.06	+.05	.17	.26	−.09
39	.40	.43	−.03	.36	.33	+.03
40	.18	.08	+.10	.47	.35	+.12
41	.13	.21	−.08	.14	.14	0
42	.17	.10	+.07	.34	.28	+.06
Average (disregarding sign)			0.058			0.066

accuracy of either the spectrographic or the chemical method. The best estimate of the suitability of the spectrographic method for any particular application is to be gained from a study of the data in Table 2 comparing the spectrographic results with chemical results for a large number and large variety of cements.

TABLE 3.—*Comparison of results for* Na_2O *(percent) obtained by the spectrographic method and by different chemical laboratories*

Cement No.	Spectrographic		Chemical					
	1	2	I *A*[1]	I *B*[2]	II	III	IV *A*	V *A*
2	0.22	0.20	0.24	0.21	0.13			
3	.40	.36	.36	.28		0.28		
4	.06	.03	.03	.04		.03	0.04	
5	.15	.14	.06	.06			.07	
6	.08	.04	.06	.08	.03			
7	.34	.33	.28	.23	.29			
8	.11	.10	.07	.08				
9	.12	.09	.16	.12	.08	.10		
10	.31	.28	.25	.22	.16	.17		
11	.34	.28	.26	.24	.18			
12	.61	.55	.66	.59	.56		.70	
13	.17	.13	.05	.06		.02	.05	
14	.31	.26	.25	.21	.12			
15	.29	.22	.28	.23	.18			
16	.31	.26	.27	.21	.14			
17	.37	.30	.32	.28	.23			0.2
18	.08	.08	.05	.06			.05	
19	.14	.16	.16	.16	.12			1
20	.32	.27	.38	.33	.31			3
21	.94	.97	1.17	1.00	1.05	1.05		1.0
22	.10	.08	0.08	0.08	0.02		.08	

[1] *A*, Modified Berk-Roller method [27].
[2] *B*, ASTM method [28].

TABLE 4.—*Comparison of results for* K_2O *(percent) obtained by the spectrographic method and by different chemical laboratories*

Cement No.	Spectrographic		I *A*[1]	Chemical				
	1	2		I *B*[2]	II	III	IV A	V A
2	0.41	0.45	0.59	0.51	0.56			
3	.43	.37	.45	.40	.46	0.39		
4	.25	.24	.19	.19	.21	.14	0.21	
5	[3] 1.50	[3] 1.60	1.37	1.30	1.37		1.40	
6	0.23	0.26	0.19	0.23	0.21			
7	.41	.44	.49	.46	.44			
8	.47	.47	.44	.43	.40			
9	.19	.16	.13	.13	.11	0.08		
10	.44	.48	.44	.40	.45	.38		
11	.37	.36	.39	.37	.39			
12	.20	.20	.15	.14	.10		0.15	
13	[3] 1.45	[3] 1.50	1.36	1.30	1.38	1.31	1.40	
14	0.47	0.69	0.54	0.54	0.57			
15	.29	.25	.26	.23	.30			
16	.40	.35	.46	.44	.48			
17	.33	.31	.26	.28	.25			0.2
18	[3] 1.45	[3] 1.25	1.28	1.19	1.22		1.30	
19	0.33	0.35	0.24	0.26	0.29			.2
20	.05	.06	.04	.01				.0
21	.16	.15	.12	.08	.08	0.05		.0
22	.27	.34	.27	.22	.32		0.27	

[1] *A*, Modified Berk Roller method [27].
[2] *B*, ASTM method [28].
[3] The potassium line with the usual (3 to 1) mixture for these cements showed self-reversal. These values were determined with a 9 to 1 mixture. See page 134.

V. DETERMINATION OF LITHIUM

An extension of the spectrographic method to include all the alkali elements, that is, lithium, cesium, and rubidium was considered. The determination of these elements by chemical methods is so difficult that the development of a spectrographic method would be useful in spite of the possibility of these elements occurring in cement only rarely. It appeared possible that lithium might be found in appreciable amounts in portland cement, and therefore a spectrographic procedure for its determination was developed. The method was designed to determine Li_2O in amounts above 0.05 percent.

In the selection of the lithium line to be employed for the determination, it was noted that Li 3232.61 A had some advantages over other possible lines in being of the desired intensity and located in a spectral region that would permit the simultaneous determination of lithium with a number of the other minor elements in cement. These advantages seemed to outweigh the objection that, in its use, the simultaneous determination of lithium with sodium and potassium would not be possible. The Li 3232.61 A line was therefore selected for this study.

Synthesized standards containing lithium were prepared in two ways. (1) Lithium carbonate was added to a CaO-Al_2O_3-SiO_2 mixture to give a product containing 2.89 percent of Li_2O. (2) Lithium carbonate was added to a low-total-alkali cement to give a product containing 2.00 percent of Li_2O. These mixtures were calcined at 1,300° C, then cooled and ground and a chemical analysis made to check the lithium content. The above mixtures were then diluted with additional amounts of the base material to give a series of samples containing Li_2O between 0.10 and 1.0 percent.

The procedure used for the determination was similar to the one for sodium and potassium. A standard mixture consisting of 70 percent of graphite and 30 percent of $SrCO_3$ (internal standard) was used. The graphite may be obtained from the powdered product of cutting and shaping electrodes. It is sieved to eliminate the size fraction above No. 100 sieve. Two-tenths gram of the graphite $SrCO_3$ mixture is used with 0.2 g of the cement sample. Thirty milligrams of the resultant mixture is placed in a graphite electrode for the arc. A 40-second exposure on an Eastman spectrum analysis No. I plate is used with an arc current of 10 amp and arc gap of 4 mm. A ground-glass screen in the optical path near the arc was used to diminish the intensity of the spectrum in preference to the use of a much shorter exposure time. The Li 3232.61 A and Sr 3301.74 A (or Sr 3322.23 A) lines are measured for the analytical calculations.

No lithium was detected in 30 portland cements analyzed, indicating that Li_2O was not present in concentrations exceeding the limit of sensitivity for which the procedure was designed, about 0.05 percent. To detect lower concentrations was considered of no interest at this time.

There remains the possibility that lithium is present in some form less easily detectable than that in the synthetic samples used for the analytical curve, although the procedure employed (heating of the samples after the addition of lithium carbonate) diminishes the probability of such an error. The reliability of the method was

checked by the use of materials of known lithium content, (1) a clay containing 0.21 percent of Li_2O and (2) a spodumene containing 6.35 percent of Li_2O. The clay as obtained was analyzed spectrographically whereas the spodumene was added to several portland cements of widely varying K_2O and Na_2O contents in such amount as to produce mixtures containing 0.15 percent of Li_2O. The alkali contents and spectrographic results for Li_2O are given in table 5.

TABLE 5.—*Comparison of results for* Li_2O *(in percent)*

Chemical				Spectrographic
Sample *	Na_2O	K_2O	Li_2O	Li_2O
Clay	0.12	0.54	0.21	0.18
Cement No. 3	.36	.45	.15	.16
Cement No. 4	.03	.19	.15	.17
Cement No. 5	.06	1.37	.15	.12
Cement No. 21	1.17	.12	.15	.07
Cement No. 43	.02	.11	.10	.10

* The chemical values for lithium were obtained as follows: Clay, chemical analyses; cements 3, 4, 5, and 21, the addition of spodumine; 43, the addition of lithium carbonate.

It will be noted that in general the agreement between the spectrographic and chemical values for Li_2O is good, the chief exceptions being noted with cements 5 and 21. This illustrates a condition, sometimes experienced, of the effect of one element on the spectral intensity of another element. In cements 5 and 21, where the K_2O content in the first case and the Na_2O content in the second case are high, the Li_2O result is too low. The chief reason for this was found to be an enhancement of the intensity of the strontium line (internal standard) by the extraneous alkali element, with only a minor effect on the intensity of the lithium line. Problems of this character could be solved satisfactorily by further experimentation on technique and buffer agents, but the absence of quantities of Li_2O as high as 0.05 percent in the cements examined made further perfection of the procedure seem unwarranted.

VI. SUMMARY

Procedures are described for the spectrographic determination of sodium, potassium, and lithium in portland cement by means of the direct-current carbon arc. Sodium and potassium are determined simultaneously by mixing the sample with a mineral base, by the use of a fixed amount of the mixture in an arc and recording the red region of the spectrum. For lithium, a mixture of the sample with a graphite base is used and the violet region of the spectrum recorded. Internal standards (silver and strontium) and spectrographic buffers are introduced with the standard mixtures. The Na 8194.81 A, K 7698.98 A, and Li 3232.61 A lines are used for the analytical calculations. The procedures are rapid, requiring about 4 hours for the determination of sodium and potassium in six samples and about the same time for lithium.

The procedure was designed to minimize and control self-reversal, unequal rate of evaporation of the alkali and reference elements,

unequal distribution in the arc of intensity of the spectrum of the alkali and reference elements, and the effect of extraneous elements.

An estimate of the reproducibility of the sodium and potassium determinations in terms of the probable error for the average of duplicate determinations is 4.0 percent of the Na_2O concentration and 5.8 percent of the K_2O concentration. The accuracy of the method cannot be expressed in such simple figures but is illustrated by a comparison of chemical and spectrographic analyses of 41 portland cements where the spectrographic results were found to differ from the chemical results by an average value of 0.06 percent (of the sample). Chemical results obtained in five different laboratories are given in this comparison.

The spectrographic examinations of 30 portland cements for lithium indicated that in no case was Li_2O present in amounts in excess of 0.05 percent. The method was checked by the analysis of several cements to which spodumene of known Li_2O content had been added.

The writer is indebted to the Optics Division of this Bureau for the facilities of the spectroscopic laboratory in which the experimental work of this research was performed, and especially to B. F. Scribner for the results of his preliminary study of this problem and for his continued interest and advice throughout the study reported in this paper.

VII. REFERENCES

[1] Report of Committee C-1 on Cement, *Notes on the effect of alkalies in portland cement on the durability of concrete*, Proc. Am. Soc. Testing Materials **43,** 199 (1943).

[2] O. S. Duffendack, R. A. Wolfe, and R. W. Smith, *Quantitative analysis by spectrographic methods*, Ind. Eng. Chem. Anal. Ed. **5,** 226 (1933).

[3] F. Twyman, The Spectrochemical Analysis of Metals and Alloys, p. 95 (Chemical Publishing Co., Inc., New York, N. Y., 1941).

[4] W. C. Pierce and N. H. Nachtrieb, *Photometry in spectrochemical analysis*, Ind. Eng. Chem. Anal. Ed. **13,** 774 (1941).

[5] B. F. Scribner, *Spark spectrographic analysis of commercial tin*, NBS J. Research **28,** 165 (1942) RP1451.

[6] J. S. Owens, *Spectrochemical methods for trace analysis*, Ind. Eng. Chem. Anal. Ed. **11,** 59 (1939).

[7] M. Milbourn, *The spectrographic analysis of soils and plant materials particularly for minor elements*, J. Soc. Chem. Ind. Trans. **56,** 205 (1937).

[8] O. S. Duffendack and R. A. Wolfe, *Analysis of caustic liquors for trace impurities*, Ind. Eng. Chem. Anal. Ed. **10,** 161 (1938).

[9] V. R. Ells, *The Lundegardh flame method of spectrographic analysis*, J. Opt. Soc. Am. **31,** 534 (1941).

[10] C. C. Nitchie and G. W. Standen, *An improved method of quantitative spectrographic analysis*, Ind. Eng. Chem. Anal. Ed. **4,** 182 (1932).

[11] E. Preuss, *Quantitative spectral analysis in the carbon arc*, Z. angew. Mineral. **1,** 167 (1938).

[12] H. I. Oshry, J. W. Ballard, and H. H. Schrenk, *Spectrochemical determination of lead, cadmium, and zinc in dusts, fumes, and ores*, J. Opt. Soc. Am. **31,** 627 (1941).

[13] H. I. Oshry, J. W. Ballard, and H. H. Schrenk, *Spectrochemical determination with mineral powders*, J. Opt. Soc. Am. **32,** 672 (1942).

[14] G. O. Freeman, *Spectroscopic data concerning the presence of the less common elements in rocks*, Am. Mineral. **27,** 776 (1942).

[15] L. W. Strock, *Blank and background effects on photographed spectral lines*, J. Opt. Soc. Am. **32,** 103 (1942).

[16] M. Slavin, *Spectrochemical analysis of glass sand*, Glass. Ind. **22,** 341 (1941).

[17] A. E. Austin and L. B. Bassett, *Spectrochemical procedure in clay analysis*, J. Am. Ceram. Soc. **26,** 185 (1943).
[18] L. T. Steadman, *Carbon arc in oxygen for the spectrochemical determination of potassium*, Physiol. Revs. **63,** 322 (1943).
[19] I. W. Wander, and W. R. Brode, *The spectrochemical determination of potassium in leaf material*, J. Opt. Soc. Am. **31,** 402 (1941).
[20] W. C. Pierce, O. R. Torres, and W. W. Marshall, *Quantitative spectrographic analysis in the arc with graphite electrodes*, Ind. Eng. Chem. Anal. Ed. **12,** 41 (1940).
[21] H. W. Dietert, *Spectrographic analysis of briquetted tablets*, J. Opt. Soc. Am. **31,** 693 (1941).
[22] C. J. Neuhaus, *A study of the applicability of the pressed pellet electrode method to the spectrographic analysis of nickel alloys*, J. Opt. Soc. Am. **33,** 167 (1943).
[23] A. E. Ruehle and E. K. Jaycox, *Some observations on the use of powders in spectrochemical analysis*, J. Opt. Soc. Am. **33,** 109 (1943).
[24] J. S. Owens, *Analysis of organic materials for trace metallic impurities*, Ind. Eng. Chem. Anal. Ed. **11,** 646 (1939).
[25] B. F. Scribner and C. H. Corliss, *An improved electrode holder for spectrographic analysis*, NBS J. Research **30,** 41 (1943) RP1515.
[26] F. G. Brockman and F. P. Hochgesang, *Electrical ignition of the spectrographic arc*, Ind. Eng. Chem. Anal. Ed. **14,** 796 (1942).
[27] A. A. Berk and P. S. Roller, *Direct determination of alkalis in portland cement*, Concrete **43,** 38 (1935).
[28] ASTM Standards C 114–42 Sections 20, 21.

WASHINGTON, June 17, 1944.

U. S. DEPARTMENT OF COMMERCE NATIONAL BUREAU OF STANDARDS

RESEARCH PAPER RP1634

Part of Journal of Research of the National Bureau of Standards, Volume 34, February 1945

HEATS, FREE ENERGIES, AND EQUILIBRIUM CONSTANTS OF SOME REACTIONS INVOLVING O_2, H_2, H_2O, C, CO, CO_2, AND CH_4 [1]

By Donald D. Wagman, John E. Kilpatrick,[2] William J. Taylor,[2] Kenneth S. Pitzer,[3] and Frederick D. Rossini

ABSTRACT

Values are presented for the following thermodynamic properties: The heat-content function, $(H°-H_0°)/T$, the free-energy function, $(F°-H_0°)/T$, the entropy, $S°$, the heat content, $H°-H_0°$, and the heat capacity, $C_p°$, for O_2 (gas) to 5,000 °K, H_2 (gas) to 5,000 °K, H_2O (gas) to 3,000 °K, N_2 (gas) to 5,000 °K, C (solid, graphite) to 1,500 °K, C (solid, diamond) to 1,200 °K, CO (gas) to 5,000 °K, CO_2 (gas) to 3,500 °K, and CH_4 (gas) to 1,500 °K; the standard entropy, $S°$, for H_2O (liq) at 25 °C; the heat of formation, $\Delta Hf°$, the free energy of formation, $\Delta Ff°$, and the equilibrium constant of formation, Kf, from the elements, for H_2O (liq) at 25 °C, and for H_2O (gas), CO (gas), CO_2 (gas), and CH_4 (gas), to 1,500 °K; the increment in heat content, $\Delta H°$, and the increment in free energy, $\Delta F°$, for the transition of graphite into diamond, to 1,200 °K and to 20,000 atmospheres.

From the foregoing, values were calculated for the increment in heat content, $\Delta H°$, the increment in free energy, $\Delta F°$, and the equilibrium constant, K, for the following reactions, most of which are important in connection with the production of liquid hydrocarbon fuels from natural gas or coal and hydrogen:

$C(\text{solid, graphite}) + CO_2(\text{gas}) = 2CO\ (\text{gas})$.
$C(\text{solid, graphite}) + H_2O\ (\text{gas}) = CO(\text{gas}) + H_2(\text{gas})$.
$CO(\text{gas}) + 1/2O_2(\text{gas}) = CO_2(\text{gas})$.
$CO(\text{gas}) + H_2O\ (\text{gas}) = CO_2(\text{gas}) + H_2(\text{gas})$.
$CH_4(\text{gas}) + 1/2O_2(\text{gas}) = CO(\text{gas}) + 2H_2(\text{gas})$.
$CH_4\ (\text{gas}) + CO_2(\text{gas}) = 2CO(\text{gas}) + 2H_2(\text{gas})$.
$CH_4(\text{gas}) + H_2O(\text{gas}) = CO(\text{gas}) + 3H_2(\text{gas})$.
$CH_4(\text{gas}) + 2H_2O(\text{gas}) = CO_2(\text{gas}) + 4H_2(\text{gas})$.

A table of the fundamental constants used in the calculations is given.

CONTENTS

	Page
I. Introduction	144
II. Unit of energy, molecular weights, constants, etc	144
III. Heat-content function, free-energy function, entropy, heat content, and heat capacity	146
1. Method of calculation	146
2. Data used in the calculations	147
3. Results for O_2, H_2, H_2O, N_2, C, CO, CO_2, and CH_4	148

[1] This investigation was performed at the National Bureau of Standards jointly by the Thermochemical Laboratory and the American Petroleum Institute Research Project 44 on the "Collection and Analysis of Data on the Properties of Hydrocarbons."

[2] Research Associate on the American Petroleum Institute Research Project 44 at the National Bureau of Standards.

[3] Consultant to the American Petroleum Institute Research Project 44 at the National Bureau of Standards; Professor of Chemistry, University of California, Berkeley, Calif.

Page

IV. Heat of formation, free energy of formation, and equilibrium constant of formation 154
1. Method of calculation 154
2. Data used in the calculations 154
3. Results for H_2O, CO, CO_2, and CH_4 155
V. Heat and free energy of the transition of graphite into diamond 156
VI. Heats, free energies, and equilibrium constants of some reactions involving O_2, H_2, H_2O, C, CO, CO_2, and CH_4 158
VII. References 161

I. INTRODUCTION

In connection with the work of the Thermochemical Laboratory and the American Petroleum Institute Research Project 44 at the National Bureau of Standards, values for thermodynamic properties of the simple substances oxygen, hydrogen, water, nitrogen, carbon, carbon monoxide, carbon dioxide, and methane have been recalculated. These data have been used to calculate the heats, free energies, and equilibrium constants of a number of reactions involved in the production of liquid hydrocarbon fuels from natural gas or coal and hydrogen. The results of these calculations are presented in this report.

II. UNIT OF ENERGY, MOLECULAR WEIGHTS, CONSTANTS, ETC.

The unit of energy used in this paper is the conventional thermochemical calorie, defined as follows [1]:[4]

$$1 \text{ calorie} = 4.1833 \text{ international joules (NBS)}. \quad (1)$$

The unit of pressure is the conventional standard atmosphere, defined as follows [2, 7]:

$$1 \text{ atmosphere} = 1{,}013{,}250 \text{ dynes/cm}^2. \quad (2)$$

The constants in eq 1 and 2 are conventional constants, and are not subject to experimental error.

The molecular weights were calculated from the values given in the 1941 table of International Atomic Weights [3].

The value of the PV product for an ideal gas (a real gas at zero pressure) at 0°C, $(PV)_{0°C}^{P=0}$, which is equal to the product of the gas constant per mole and the absolute temperature of the ice point, $(RT)_{0°C}$, is taken from the value calculated by Cragoe [4]:

$$(PV)_{0°C}^{P=0} = (RT)_{0°C} = 2271.16 \text{ absolute joules/mole}. \quad (3)$$

The uncertainty in the foregoing relation is estimated to be ± 0.002 percent.

The relation between the absolute watt and the international watt (NBS) is taken from the value recommended by Crittenden and Curtis [5]:

$$1 \text{ international watt (NBS)} = 1.00017 \text{ absolute watts}. \quad (4)$$

The uncertainty in the foregoing relation is estimated to be ± 0.005 percent.

[4] Figures in brackets indicate the literature references at the end of the paper.

The additional constants used in the present calculations are (1) the absolute temperature of the ice point, $T_{0°C}$; (2) the velocity of light, c; (3) the Avogadro number (chemical scale) N; and (4) the Planck constant, h. The relation between the liter and the cubic centimeter has been utilized to convert several quantities to pressure-volume units, since they are often useful. The values recommended by Birge [6] for these constants have been used.

The foregoing values of the constants lead to the consistent set of fundamental and derived constants that are given in table 1. The uncertainties of the constants have been reestimated in some cases by the present authors.

The values of the constants in table 1 have been used to calculate the constants in the equations for the contributions of translation and of rotation of a rigid molecule to the several thermodynamic functions. The contribution of translation is given by the Sackur-Tetrode equation, and is exact for all molecules. The contribution of a rigid rotator is a useful approximation to the rotational contribution in actual molecules. See references [8, 9].

TABLE 1.—*Values of the constants*

No.	Relation	From
a	1 liter = 1000.028 ±0.004 cm³	[6]
b	1 atm = 1,013,250 dyne/cm²	Definition, [2]
c	1 int. joule (NBS) = 1.00017 ±0.00005 abs. joule	[5]
d	1 cal = 4.1833 int. joule (NBS)	Definition, [1]
e	= 4.18401 ±0.00021 abs. joule	d, c
f	= 41.2930 ±0.0021 cm³ atm	d, c, b
g	= 0.0412918 ±0.0000021 liter atm	d, c, b, a
h	$(PV)_{0°C}^{P=0} = (RT)_{0°C}$ = 2271.16 ±0.04 abs. joule/mole	[4]
i	= 22414.6 ±0.4 cm³ atm/mole	h, b
j	= 22.4140 ±0.0004 liter atm/mole	h, b, a
k	$T_{0°C}$ = 273.160 ±0.010 °K	[6]
l	$R = (RT)_{0°C}/T_{0°C}$ = 8.31439 ±0.00034 abs. joule/deg mole	h, k
m	= 8.31298 ±0.00054 int. joule/deg mole	l, c
n	= 1.98718 ±0.00013 cal/deg mole	l, e
o	= 82.0567 ±0.0034 cm³ atm/deg mole	l, b
p	= 0.0820544 ±0.0000034 liter atm/deg mole	l, b, a
q	$N = (6.02283 \pm 0.0022) \times 10^{23}$/mole	[6]
r	$k = (R/N) = (1.38048 \pm 0.00050) \times 10^{-16}$ erg/deg	l, q
s	$h = (6.6242 \pm 0.0044) \times 10^{-27}$ erg sec	[6]
t	$c = (2.99776 \pm 0.00008) \times 10^{10}$ cm/sec	[6]
u	$Z = Nhc$ = 11.9600 ±0.0036 abs. joule cm/mole	q, s, t
v	= 11.9580 ±0.0036 int. joule cm/mole	u, c
w	= 2.8585 ±0.0009 cal cm/mole	u, e
x	$(Z/R) = (hc/k)$ = 1.43847 ±0.00045 cm deg	u, l

The equations in table 2 yield the values of the thermodynamic functions in units of calories, degrees, and moles. The logarithms are common logarithms, to the base 10. M is the molecular weight in grams, and T is the absolute temperature in degrees Kelvin. I is the value of the two equal moments of inertia, in g-cm², of a linear molecule about axes perpendicular to the axis of the molecule. I_1, I_2, and I_3, are the three principal moments of inertia, in g-cm², not necessarily unequal in value, of a nonlinear molecule. Separate equations are required for the rotational contributions of a diatomic or linear polyatomic molecule, and those of a nonlinear polyatomic molecule. The symmetry number, σ, is the number of ways the molecule may be superimposed upon itself by rotation of the entire molecule. For linear molecules the value of σ is either 1 or 2; the equations for the rotational free energy and entropy of a linear molecule are given explicitly for these two cases.

TABLE 2.—*Summary of equations, with constants, for calculating the values of the thermodynamic functions for translation (of all molecules) and rotation (of rigid molecules)*

[Units: $(H^\circ-H_0^\circ)/T$, C°, $(F^\circ-H_0^\circ)/T$, and S° in cal/deg mole; T in °K; M in g/mole; I, I_1, I_2, and I_3 in g-cm²; σ, a dimensionless integer; logarithms to the base 10.]

TRANSLATION (OF ALL MOLECULES)

$(H^\circ-H_0^\circ)/T=C_v^\circ=4.9680$
$(F^\circ-H_0^\circ)/T=-6.8635 \log M+7.2820-11.4391 \log T$
$S^\circ=6.8635 \log M-2.3141+11.4391 \log T$

ROTATION (OF RIGID MOLECULES)

I. *Diatomic or linear polyatomic molecules.*
$(H^\circ-H_0^\circ)/T=C^\circ=1.9872$
(a) σ (symmetry number) = 1:
$(F^\circ-H_0^\circ)/T=-4.5757 \log (I\times10^{39})+2.7676-4.5757 \log T$
$S^\circ=4.5757 \log (I\times10^{39})-0.7804+4.5757 \log T$
(b) σ (symmetry number) = 2:
$(F^\circ-H_0^\circ)/T=-4.5757 \log (I\times10^{39})+4.1450-4.5757 \log T$
$S^\circ=4.5757 \log (I\times10^{39})-2.1578+4.5757 \log T$
II. *Nonlinear polyatomic molecules.*
$(H^\circ-H_0^\circ)/T=C^\circ=2.9808$
$(F^\circ-H_0^\circ)/T=-2.2878 \log (I_1 I_2 I_3\times10^{117})+4.5757 \log \sigma+3.0140-6.8635 \log T$
$S^\circ=2.2878 \log (I_1 I_2 I_3\times10^{117})-4.5757 \log \sigma-0.0332+6.8635 \log T$

III. HEAT-CONTENT FUNCTION, FREE-ENERGY FUNCTION, ENTROPY, HEAT CONTENT, AND HEAT CAPACITY

1. METHOD OF CALCULATION

Values of the thermodynamic properties of the simple molecules, O_2, H_2, H_2O, N_2, CO, and CO_2, in the ideal gaseous state and to high temperatures, were calculated statistically from spectroscopic and other molecular data by Johnston, et. al. [10, 11, 12, 13], Giauque, et. al. [14, 15, 16], Gordon [17, 18], and Kassel [19]. Since such new spectroscopic data as have become available would not lead to values of the thermodynamic functions significantly different than those obtained in the foregoing calculations, it was not considered necessary or justified to repeat these calculations in detail. The values required for the present investigation were obtained by converting the existing values to new ones based on the new values of the fundamental constants and the unit of energy.

The important corrections required to be made arise from the following: (a) Change in the value of the gas constant R from 1.9869 to 1.98718 cal/deg mole, the ratio being 1.00014; (b) change in the value of the constant of the Sackur-Tetrode equation for entropy of translation from −2.300 to −2.3141 cal/deg mole; (c) change in the value hc/k from 1.43242 to 1.43847 cm deg, the ratio being 1.004224; (d) changes in the atomic weights of hydrogen and carbon from 1.0078 to 1.0080 and from 12.00 to 12.010, respectively; (e) correction for rotational stretching in CO_2 and H_2O.

The foregoing corrections were handled in the following manner:

(a) Each thermodynamic function was increased in value by the factor 1.00014, the ratio of the new to the old value of the gas constant.

(b) A constant amount of +0.014 was subtracted from the value of the entropy for translation and added to the value of the free-energy function for translation, for each molecule.

(c) The values previously calculated for the rotational and vibrational contributions to a given thermodynamic property were taken to be correct for a new, slightly higher temperature T^*, such that $T^*/T=1.004224$, the ratio of the new to the old value of hc/k. This

procedure is possible because the previous calculations involved summations with the partition function, in which hc/k appears as a multiplier of $1/T$, as in the expression

$$Q=\sum_i p_i e^{-(hc/k)(\tilde{\nu}_i/T)} \tag{5}$$

The tabulated functions were interpolated from the temperatures T^* to even temperatures, after subtraction of the temperature-dependent term of the Sackur-Tetrode equation for the translational contribution to the entropy and the free-energy function. On a plot of any function $f(T)$ against T, the temperature for which the calculation was originally made, the corrected value of $f(T)$ for the temperature T is the value of the function at $(1-1/1.004224)T=0.00421T$ degrees below T. In practice, the slope of the function at T was calculated by averaging $\Delta f(T)/\Delta T$ for the intervals above and below T. The correction to $f(T)$ due to the change in hc/k is then $-0.00421T\,df(T)/dT$. The correction varies slowly with the temperature.

(d) The entropy and the free-energy function were increased and decreased, respectively, by $3/2R\ln(1+\Delta M/M)$, where M is the molecular weight and ΔM the change in the molecular weight for the given substance. Since $\Delta M/M$ is very small, this expression reduces to $3/2R\Delta M/M$ or $2.98\Delta M/M$.

(e) A small additive correction for rotational stretching, as given by Wilson [20], was made to each of the thermodynamic functions of H_2O and CO_2.

The complete equations used for the conversion are as follows, with the old values primed:

$$(H^\circ-H_0^\circ)/T=1.00014\{[(H^\circ-H_0^\circ)/T]'-0.00421Td[(H^\circ-H_0^\circ)/T]'/dT\}. \tag{6}$$

$$(F^\circ-H_0^\circ)/T=1.00014\{[(F^\circ-H_0^\circ)/T]'-0.00421[Td[(F^\circ-H_0^\circ)/T]'/dT+5/2R']+0.014\}-2.98\Delta M/M. \tag{7}$$

$$S^\circ=1.00014\{(S^\circ)'-0.00421[Td(S^\circ)'/dT-5/2R']-0.014\}+2.98\Delta M/M. \tag{8}$$

$$C_p^\circ=1.00014\{(C_p^\circ)'-0.00421Td(C_p^\circ)'/dT\}. \tag{9}$$

In the case of methane, the statistical calculations made by one of the authors [21] were extended to include other temperatures.

In the case of carbon (graphite) and carbon (diamond), the existing calorimetric data were subjected to graphical analysis to yield selected "best" values for the heat-content function, free-energy function, entropy, heat content, and heat capacity, to 1,500° K for graphite and to 1,200° K for diamond.

2. DATA USED IN THE CALCULATIONS

The data used in the present calculations, according to the procedure described in the preceding section, were from the following sources:

O_2(*gas*).—Statistical calculations from Johnston and Walker [10, 11], who gave values for the free-energy function, the entropy, the heat

content, and the heat capacity, to 5,000° K. See also Gordon and Barnes [22].

H_2 (*gas*).—Statistical calculations from Davis and Johnston [12], who gave values for the free-energy function, entropy, heat content, and heat capacity to 5,000° K, and from Giauque [14], who gave values for the free-energy function. See also Gordon and Barnes [23] and Libby [24].

H_2O (*gas*).—Statistical calculations from Gordon [17, 18], who gave values for the free-energy function, entropy, and heat capacity, to 3,000° K. See also Libby [24].

N_2 (*gas*).—Statistical calculations from Johnston and Davis [13], who gave values for the entropy, heat content, and heat capacity to 5,000° K, and from Giauque and Clayton [15], who gave values for the free-energy function to 5,000° K.

CO (*gas*).—Statistical calculations from Johnston and Davis [13], who gave values for the entropy, heat content, and heat capacity, to 5,000° K, and from Clayton and Giauque [16], who gave values for the free-energy function to 5,000° K. See also Gordon and Barnes [22], and Kassel [25].

CO_2 (*gas*).—Statistical calculations from Kassel [19], who gave values for the free-energy function, heat content, and heat capacity, to 3,500° K. See also Gordon [26] and Gordon and Barnes [23].

CH_4 (*gas*).—Statistical calculations from Pitzer [21], who gave values for the free-energy function, heat content, entropy, and heat capacity to 1,500° K.

C (*solid, graphite*).—Experimental data on heat capacity and heat content from Nernst [27] from 30° to 85° K, from Worthing [28] (indirect measurements) from 1,170° to 2,400° K, from Magnus [29] from 370° to 1,200° K, from Schläpfer and Debrunner [30] from 370° to 1,400° K, and from Jacobs and Parks [31] from 87° to 300° K. See also Magnus [32].

C (*solid, diamond*).—Experimental data on heat capacity and heat content from Weber [33, 34] from 283° to 600° K, from Magnus and Hodler [35] from 670° to 1,180° K, and from Pitzer [36] from 70° to 288° K. See also Bettendorf and Wüllner [37], Nernst and Lindemann [38], and Robertson, Fox, and Martin [39].

3. RESULTS FOR O_2, H_2, H_2O, N_2, C, CO, CO_2, AND CH_4

The resulting values of the thermodynamic properties for O_2 (gas), H_2 (gas), H_2O (gas), N_2 (gas), C (solid, graphite), C (solid, diamond), CO (gas), CO_2 (gas), and CH_4 (gas) are presented in tables 3, 4, 5, 6, and 7, which give, respectively, values of the heat-content function, $(H°-H°_0)/T$, the free-energy function, $(F°-H°_0)/T$; the entropy, $S°$, the heat content, $H°-H°_0$, and the heat capacity, $C_p°$.

A value for the entropy of liquid water at 25° C may be obtained from the value for gaseous water at 25° C and the standard entropy of vaporization of water, as given by eq 20:

$$H_2O(\text{liq.});\ S°_{298.16}=16.716 \pm 0.016 \text{ cal/deg mole.} \qquad (10)$$

TABLE 3.—*Values of the heat-content function* $(H°-H°_0)/T$ *for* O_2 (gas), H_2 (gas), H_2O (gas), N_2 (gas), C (solid, graphite), C (solid, diamond), CO (gas), CO_2 (gas), *and* CH_4 (gas)

TABLE 3.—*Values of the heat-content function, $(H°-H_0°)/T$, for O_2 (gas), H_2 (gas), H_2O (gas), N_2 (gas), C (solid, graphite), C (solid, diamond), CO (gas), CO_2 (gas), and CH_4 (gas)*

Compound	Formula	State	Temperature in degrees Kelvin													
			0	100	150	200	250	298.16	300	400	500	600	700	800	900	1,000
			Heat-content function, $(H°-H_0°)/T$, in calories per degree mole													
Oxygen	O_2	Gas	0			6.9221	6.9307	6.9418	6.9424	6.9811	7.0484	7.1320	7.2248	7.3176	7.4107	7.4970
Hydrogen	H_2	do	0				6.7771	6.7877	6.7882	6.8275	6.8590	6.8810	6.9022	6.9218	6.9423	6.9658
Water	H_2O	do	0					7.934	7.933	7.975	8.039	8.122	8.222	8.333	8.452	8.580
Nitrogen	N_2	do	0			6.9465	6.9482	6.9502	6.9503	6.9559	6.9701	6.9967	7.0361	7.0857	7.1422	7.2025
Carbon (graphite)	C	Solid	0	0.1445	0.28770	0.45986	0.64987	0.84369	0.85101	1.2565	1.6416	1.9968	2.3171	2.6021	2.8549	3.0746
Carbon (diamond)	C	do	0	.01664	.05920	.14528	.27549	.4297	.4360	0.8125	1.204	1.583	1.936	2.255	2.538	2.782
Carbon monoxide	CO	Gas	0			6.9470	6.9495	6.9514	6.9515	6.9594	6.9799	7.0159	7.0654	7.1247	7.1895	7.2565
Carbon dioxide	CO_2	do	0					7.5064	7.5154	7.9870	8.4455	8.8707	9.2590	9.6117	9.9332	10.222
Methane	CH_4	do	0					8.039	8.042	8.307	8.730	9.249	9.816	10.401	10.985	11.56
			1,100	1,200	1,250	1,300	1,400	1,500	1,750	2,000	2,500	3,000	3,500	4,000	4,500	5,000
			Heat-content function, $(H°-H_0°)/T$, in calories per degree mole													
Oxygen	O_2	Gas	7.5775	7.6533	7.6893	7.7238	7.7893	7.8509	7.9885	8.1094	8.3196	8.5000	8.6595	8.8038	8.9295	9.0440
Hydrogen	H_2	do	6.9927	7.0230	7.0387	7.0563	7.0919	7.1295	7.2307	7.3358	7.5402	7.7286	7.8963	8.0420	8.1733	8.2898
Water	H_2O	do	8.709	8.844	8.912	8.981	9.116	9.251	9.57	9.88	10.42	10.86				
Nitrogen	N_2	do	7.2650	7.3273	7.3580	7.3882	7.4467	7.5024	7.6327	7.7497	7.9356	8.0816	8.1986	8.2944	8.3756	8.4405
Carbon (graphite)	C	Solid	3.269	3.442	3.522	3.600	3.744	3.876								
Carbon (diamond)	C	do	2.990	3.168												
Carbon monoxide	CO	Gas	7.3238	7.3898	7.4221	7.4538	7.5149	7.5725	7.7033	7.8182	8.0028	8.1448	8.2572	8.3487	8.4238	8.4905
Carbon dioxide	CO_2	do	10.487	10.727	10.841	10.949	11.151	11.336	11.74	12.07	12.59	12.98	13.29			
Methane	CH_4	do	12.11	12.65	12.90	13.15	13.63	14.09								

TABLE 4.—*Values of the free-energy function* $(F^\circ - H_0^\circ)/T$, *for* O_2 (*gas*), H_2 (*gas*), H_2O (*gas*), N_2 (*gas*), C (*solid, graphite*), C (*solid, diamond*), CO (*gas*), CO_2 (*gas*), *and* CH_4 (*gas*)

Compound	Formula	State	Temperature, in degrees Kelvin													
			0	100	150	200	250	298.16	300	400	500	600	700	800	900	1,000
			Free-energy function, $(F^\circ - H_0^\circ)/T$, in calories per degree mole													
Oxygen	O_2	Gas	0			−39.297	−40.835	−42.061	−42.106	−44.112	−45.675	−46.968	−48.071	−49.044	−49.911	−50.697
Hydrogen	H_2	do	0				−23.331	−24.423	−24.465	−26.422	−27.950	−29.203	−30.265	−31.186	−32.004	−32.738
Water	H_2O	do	0					−37.172	−37.221	−39.508	−41.295	−42.768	−44.026	−45.131	−46.120	−47.018
Nitrogen	N_2	do	0			−36.044	−37.595	−38.817	−38.859	−40.861	−42.415	−43.688	−44.769	−45.711	−46.550	−47.306
Carbon (graphite)	C	Solid	0	−0.0739	−0.1582	−0.2639	−0.3866	−0.5172	−0.5227	−0.8245	−1.146	−1.477	−1.810	−2.138	−2.459	−2.771
Carbon (diamond)	C	do	0	−0.0055	−0.0186	−0.0462	−0.0919	−0.1532	−0.1558	−0.331	−0.554	−0.808	−1.078	−1.358	−1.640	−1.920
Carbon monoxide	CO	Gas	0			−37.574	−39.124	−40.350	−40.391	−42.393	−43.947	−45.222	−46.308	−47.254	−48.097	−48.860
Carbon dioxide	CO_2	do	0					−43.555	−43.601	−45.828	−47.667	−49.238	−50.636	−51.895	−53.047	−54.109
Methane	CH_4	do	0					−36.46	−36.51	−38.86	−40.75	−42.39	−43.86	−45.21	−46.47	−47.65
			1,100	1,200	1,250	1,300	1,400	1,500	1,750	2,000	2,500	3,000	3,500	4,000	4,500	5,000
			Free-energy function, $(F^\circ - H_0^\circ)/T$, in calories per degree mole													
Oxygen	O_2	Gas	−51.415	−52.077	−52.390	−52.695	−53.272	−53.808	−55.027	−56.103	−57.930	−59.468	−60.798	−61.958	−62.990	−63.947
Hydrogen	H_2	do	−33.402	−34.012	−34.305	−34.576	−35.098	−35.590	−36.696	−37.669	−39.328	−40.719	−41.922	−42.988	−43.942	−44.809
Water	H_2O	do	−47.842	−48.605	−48.968	−49.318	−49.989	−50.622	−52.08	−53.38	−55.65	−57.59				
Nitrogen	N_2	do	−47.994	−48.629	−48.929	−49.218	−49.768	−50.284	−52.449	−52.478	−54.228	−55.687	−56.941	−58.043	−59.025	−59.910
Carbon (graphite)	C	Solid	−3.073	−3.365	−3.509	−3.647	−3.919	−4.181								
Carbon (diamond)	C	do	−2.195	−2.46												
Carbon monoxide	CO	Gas	−49.554	−50.196	−50.497	−50.789	−51.345	−51.884	−53.041	−54.078	−55.842	−57.314	−58.578	−59.688	−60.676	−61.566
Carbon dioxide	CO_2	do	−55.096	−56.019	−56.460	−56.887	−57.706	−58.461	−60.26	−61.85	−64.60	−67.11	−68.98			
Methane	CH_4	do	−48.78	−49.86	−50.38	−50.89	−51.88	−52.84								

TABLE 5.—*Values of the entropy, S°, for O_2 (gas), H_2 (gas), H_2O (gas), N_2 (gas), C (solid, graphite), C (solid, diamond), CO (gas), CO_2 (gas), and CH_4 (gas)*

Compound	Formula	State	Temperature in degrees Kelvin													
			0	100	150	200	250	298.16	300	400	500	600	700	800	900	1,000
			Entropy, S°, calories per degree mole													
Oxygen	O_2	Gas	0			46.219	47.766	49.003	49.048	51.093	52.723	54.100	55.296	56.362	57.322	58.194
Hydrogen	H_2	do	0				30.108	31.211	31.253	33.250	34.809	36.084	37.167	38.108	38.946	39.704
Water	H_2O	do	0					45.106	45.154	47.483	49.334	50.890	52.248	53.464	54.572	55.598
Nitrogen	N_2	do	0			42.990	44.543	45.767	45.809	47.818	49.385	50.685	51.805	52.797	53.692	54.509
Carbon (graphite)	C	Solid	0	0.2184	0.4459	0.7238	1.0365	1.3609	1.3737	2.081	2.788	3.474	4.127	4.740	5.314	5.846
Carbon (diamond)	C	do	0	0.0221	0.0778	0.1915	0.3674	0.5829	0.5918	1.14	1.76	2.39	3.01	3.61	4.18	4.70
Carbon monoxide	CO	Gas	0			44.521	46.074	47.301	47.342	49.352	50.927	52.238	53.373	54.379	55.287	56.116
Carbon dioxide	CO_2	do	0					51.061	51.116	53.815	56.113	58.109	59.895	61.507	62.980	64.331
Methane	CH_4	do	0					44.50	44.55	47.17	49.48	51.64	53.68	55.61	57.45	59.21

Compound	Formula	State	1,100	1,200	1,250	1,300	1,400	1,500	1,750	2,000	2,500	3,000	3,500	4,000	4,500	5,000
			Entropy, S°, in calories per degree mole													
Oxygen	O_2	Gas	58.992	59.730	60.079	60.419	61.061	61.659	63.015	64.212	66.250	67.968	69.458	70.762	71.920	72.991
Hydrogen	H_2	do	40.395	41.035	41.344	41.632	42.190	42.720	43.928	45.005	46.868	48.448	49.818	51.030	52.115	53.099
Water	H_2O	do	56.551	57.449	57.880	58.299	59.105	59.873	61.65	63.26	66.07	68.45				
Nitrogen	N_2	do	55.259	55.955	56.287	56.606	57.215	57.786	59.082	60.228	62.163	63.770	65.141	66.338	67.402	68.351
Carbon (graphite)	C	Solid	6.342	6.807	7.031	7.247	7.663	8.057								
Carbon (diamond)	C	do	5.18	5.63												
Carbon monoxide	CO	Gas	56.878	57.586	57.919	58.243	58.860	59.436	60.744	61.896	63.845	65.459	66.835	68.037	69.100	70.056
Carbon dioxide	CO_2	do	65.583	66.746	67.301	67.836	68.857	69.817	72.00	73.92	77.19	80.09	82.27			
Methane	CH_4	do	60.89	62.50	63.28	64.04	65.51	66.93								

TABLE 6.—*Values of the heat content,* $(H^\circ - H^\circ_0)$, *for* O_2 *(gas),* H_2 *(gas),* H_2O *(gas),* N_2 *(gas),* C *(solid, graphite),* C *(solid, diamond),* CO *(gas),* CO_2 *(gas), and* CH_4 *(gas)*

Compound	Formula	State	Temperature in degrees Kelvin													
			0	100	150	200	250	298.16	300	400	500	600	700	800	900	1,000
			Heat content, $(H^\circ - H^\circ_0)$, in calories per mole													
Oxygen	O_2	Gas	0			1384.42	1732.7	2069.78	2082.72	2792.4	3524.2	4279.2	5057.4	5854.1	6669.6	7497.0
Hydrogen	H_2	do	0				1694.28	2023.81	2036.47	2731.0	3429.5	4128.6	4831.5	5537.4	6248.0	6965.8
Water	H_2O	do	0					2365.1	2379.9	3190.0	4019.5	4873.2	5755.4	6666.4	7606.8	8580.0
Nitrogen	N_2	do	0			1389.30	1737.1	2072.27	2085.09	2782.4	3485.0	4198.0	4925.3	5668.6	6428.0	7202.5
Carbon (graphite)	C	Solid	0	14.451	43.155	91.973	162.468	251.56	255.31	502.6	820.8	1198.1	1622.0	2081.7	2569.4	3074.6
Carbon (diamond)	C	do	0	1.664	8.880	29.058	68.873	128.13	130.81	325	602	950	1355	1804	2284	2782
Carbon monoxide	CO	Gas	0			1389.40	1737.38	2072.63	2085.45	2783.8	3490.0	4209.5	4945.8	5699.8	6470.6	7256.5
Carbon dioxide	CO_2	do	0					2238.11	2254.6	3194.8	4222.8	5322.4	6481.3	7689.4	8939.9	10222
Methane	CH_4	do	0					2397	2413	3323	4365	5549	6871	8321	9887	11560

Compound	Formula	State	1,100	1,200	1,250	1,300	1,400	1,500	1,750	2,000	2,500	3,000	3,500	4,000	4,500	5,000
			Heat content, $(H^\circ - H^\circ_0)$, in calories per mole													
Oxygen	O_2	Gas	8335.2	9183.9	9611.6	10041.0	10905.1	11776.4	13980	16211	20790	25500	30308	35215	40183	45220
Hydrogen	H_2	do	7692.0	8427.5	8798.4	9173.2	9928.7	10694.2	12653.7	14672	18851	23186	27637	32168	36780	41449
Water	H_2O	do	9579.9	10613	11140	11675	12762	13876	16748	19760	26050	32580				
Nitrogen	N_2	do	7991.5	8792.8	9197.5	9604.7	10425.4	11253.6	13357	15499	19839	24245	28695	33178	37690	42202
Carbon (graphite)	C	Solid	3596	4130	4403	4680	5242	5814								
Carbon (diamond)	C	do	3289	3802												
Carbon monoxide	CO	Gas	8056.2	8867.8	9277.6	9689.9	10520.9	11358.8	13481	15636	20007	24434	28900	33395	37907	42452
Carbon dioxide	CO_2	do	11536	12872	13551	14234	15611	17004	20542	24144	31480	38950	46520			
Methane	CH_4	do	13320	15170	16130	17100	19090	21130								

TABLE 7.—*Values of the heat capacity, $C_p°$ for O_2 (gas), H_2 (gas), H_2O (gas), N_2 (gas), C (solid, graphite), C (solid, diamond), CO (gas), CO_2 (gas), and CH_4 (gas)*

Compound	Formula	State	Temperature in degrees Kelvin													
			0	100	150	200	250	298.16	300	400	500	600	700	800	900	1,000
			Heat capacity, $C_p°$, in calories per degree mole													
Oxygen	O_2	Gas	0			6.961	6.979	7.017	7.019	7.194	7.429	7.670	7.885	8.064	8.212	8.335
Hydrogen	H_2	do	0				6.769	6.892	6.895	6.974	6.993	7.008	7.035	7.078	7.139	7.217
Water	H_2O	do	0					8.025	8.026	8.185	8.415	8.677	8.959	9.254	9.559	9.869
Nitrogen	N_2	do	0			6.957	6.959	6.960	6.961	6.991	7.070	7.197	7.351	7.512	7.671	7.816
Carbon (graphite)	C	Solid	0	0.394	0.767	1.190	1.632	2.066	2.083	2.851	3.496	4.03	4.43	4.75	4.98	5.14
Carbon (diamond)	C	do	0	0.0673	0.246	0.587	1.013	1.449	1.466	2.38	3.14	3.79	4.29	4.66	4.90	5.03
Carbon monoxide	CO	Gas	0			6.956	6.958	6.965	6.965	7.013	7.120	7.276	7.451	7.624	7.787	7.932
Carbon dioxide	CO_2	do	0					8.874	8.894	9.871	10.662	11.311	11.849	12.300	12.678	12.995
Methane	CH_4	do	0					8.536	8.552	9.736	11.133	12.546	13.88	15.10	16.21	17.21
			1,100	1,200	1,250	1,300	1,400	1,500	1,750	2,000	2,500	3,000	3,500	4,000	4,500	5,000
			Heat capacity, $C_p°$, in calories per degree mole													
Oxygen	O_2	Gas	8.440	8.530	8.570	8.608	8.676	8.739	8.885	9.024	9.305	9.518	9.711	9.879	10.003	10.105
Hydrogen	H_2	do	7.308	7.404	7.454	7.505	7.610	7.713	7.957	8.175	8.526	8.791	8.993	9.151	9.282	9.389
Water	H_2O	do	10.172	10.467	10.611	10.749	11.015	11.263	11.80	12.24	12.9	13.3				
Nitrogen	N_2	do	7.947	8.063	8.116	8.165	8.253	8.330	8.486	8.602	8.759	8.862	8.934	8.989	9.036	9.076
Carbon (graphite)	C	Solid	5.27	5.42	5.50	5.57	5.67	5.76								
Carbon (diamond)	C	do	5.10	5.16												
Carbon monoxide	CO	Gas	8.058	8.167	8.218	8.265	8.349	8.419	8.561	8.665	8.806	8.899	8.963	9.015	9.059	9.099
Carbon dioxide	CO_2	do	13.26	13.49	13.59	13.68	13.85	13.99	14.3	14.5	14.8	15.0	15.2			
Methane	CH_4	do	18.09	18.88	19.23	19.57	20.18	20.71								

IV. HEAT OF FORMATION, FREE ENERGY OF FORMATION, AND THE EQUILIBRIUM CONSTANT OF FORMATION

1. METHOD OF CALCULATION

Values of ΔH_0°, the increment in heat content for the given reaction, with all the reactants and products in their appropriate standard states at 0° K, were calculated by combining values of $\Delta H_{298.16}^\circ$, the increment in heat content for the given reaction at 25° C, with values of $H_{298.16}^\circ - H_0^\circ$ for the reactants and products, by means of the relation

$$\Delta H_0^\circ = \Delta H_{298.16}^\circ - \Delta(H_{298.16}^\circ - H_0^\circ), \tag{11}$$

where the last term on the right is the sum for the products less the sum for the reactants of $H_{298.16}^\circ - H_0^\circ$, the heat content at 298.16° K (25° C) less that at 0° K.

Values of ΔH° for the given reaction at other temperatures were then calculated by means of the relation

$$\Delta H^\circ = \Delta H_0^\circ + \Delta(H^\circ - H_0^\circ). \tag{12}$$

Values of ΔF°, the increment in free energy for the given reaction, with all the reactants and products in their appropriate standard states at the given temperature, were calculated by combining values of ΔH_0° for the given reaction with appropriate values of $(F^\circ - H_0^\circ)/T$, the free-energy function, by means of the relation:

$$\Delta F^\circ/T = \Delta H_0^\circ/T + \Delta[(F^\circ - H_0^\circ)/T], \tag{13}$$

where the last term on the right is the sum for the products less the sum for the reactants of $(F^\circ - H_0^\circ)/T$, the free-energy function at the given temperature.

Values of the equilibrium constant, and its logarithm, for the given reaction, were calculated from the relation [40]

$$\Delta F^\circ = -RT \ln K. \tag{14}$$

2. DATA USED IN THE CALCULATIONS

The following data were used in calculating the heat and free energy of formation of H_2O(liq) at 25° C and of the formation of H_2O (gas), CO (gas), CO_2 (gas), and CH_4 (gas) at various temperatures to 1,500° K:

For the heat of formation of liquid water,

$$H_2(\text{gas}) + 1/2\ O_2(\text{gas}) = H_2O(\text{liq}), \tag{15}$$

the value previously reported from this laboratory [41] was corrected to the present molecular weight of water, yielding for the formation of liquid water according to eq 15:

$$\Delta H^\circ_{298.16} = -68{,}317.4 \pm 9.6 \text{ cal/mole.} \quad (16)$$

On the basis of the present molecular weight, the values previously reported for the standard heat, free energy, and entropy of vaporization of water at 25° C [41], including a small change resulting from an improved value for the vapor pressure of water at 25° C [42], become

$$H_2O(\text{liq}) = H_2O(\text{gas}). \quad (17)$$

$$\Delta H^\circ_{298.16} = 10{,}519.5 \pm 3.1 \text{ cal/mole.} \quad (18)$$

$$\Delta F^\circ_{298.16} = 2{,}054.8 \pm 1.0 \text{ cal/mole.} \quad (19)$$

$$\Delta S^\circ_{298.16} = 28.390 \pm 0.012 \text{ cal/deg mole.} \quad (20)$$

A new value for the heat of formation of carbon dioxide was recently reported [43]:

$$C(\text{solid, graphite}) + O_2(\text{gas}) = CO_2(\text{gas}). \quad (21)$$

$$\Delta H^\circ_{298.16} = -94{,}051.8 \pm 10.8 \text{ cal/mole.} \quad (22)$$

The value previously reported [41] for the heat of combustion of carbon monoxide to carbon dioxide remains unchanged:

$$CO(\text{gas}) + 1/2\ O_2(\text{gas}) = CO_2(\text{gas}). \quad (23)$$

$$\Delta H^\circ_{298.16} = -67{,}636.1 \pm 28.7 \text{ cal/mole.} \quad (24)$$

Combination of eq 21, 22, 23, and 24 yields a new value for the heat of formation of carbon monoxide:

$$C(\text{solid, graphite}) + 1/2\ O_2(\text{gas}) = CO(\text{gas}). \quad (25)$$

$$\Delta H^\circ_{298.16} = -26{,}415.7 \pm 30.7 \text{ cal/mole.} \quad (26)$$

The value for the heat of formation of methane is taken from reference [44]:

$$C(\text{solid, graphite}) + 2H_2(\text{gas}) = CH_4(\text{gas}). \quad (27)$$

$$\Delta H^\circ_{298.16} = -17{,}889 \pm 75 \text{ cal/mole.} \quad (28)$$

3. RESULTS FOR H_2O, CO, CO_2, AND CH_4

The resulting values of the thermodynamic properties for the formation of H_2O(gas), CO(gas), CO_2(gas), and CH_4(gas), from the elements, O_2(gas), H_2(gas), and C(solid, graphite), are presented in

table 8, which gives values of the heat of formation, $\Delta Hf°$, the free energy of formation, $\Delta Ff°$, the equilibrium constant of formation, Kf, and the logarithm of the equilibrium constant of formation, $\log_{10}Kf$, all to 1,500° K.

For the formation of liquid water from its elements at 25° C, the values of the standard heat, free energy, and entropy of formation are

$$H_2 \text{ (gas)} + 1/2\ O_2 \text{ (gas)} = H_2O \text{ (liq)}. \tag{29}$$

$$\Delta H_{298.16} = -68{,}317.4 \pm 9.6 \text{ cal/mole}. \tag{30}$$

$$\Delta F°_{6298.1} = -56{,}689.9 \pm 11.2 \text{ cal/mole}. \tag{31}$$

$$\Delta S°_{298.16} = -38.997 \pm 0.019 \text{ cal/mole}. \tag{32}$$

V. HEAT AND FREE ENERGY OF TRANSITION OF GRAPHITE INTO DIAMOND

The value for the heat of transition of graphite into diamond at 25° C is taken from reference [43]:

$$\text{C (solid, graphite)} = \text{C (solid, diamond)} \tag{33}$$

$$\Delta H°_{298.16} = 453.2 \pm 20.3 \text{ cal/mole}. \tag{34}$$

From the foregoing value and the values for diamond and graphite given in tables 3, 4, 5, and 6, values were calculated for the change in heat content and free energy for the transition of graphite into diamond at 1 atmosphere, as presented in table 9.

TABLE 9.—*Values of the change in heat content and free energy for the transition of graphite into diamond, at a pressure of 1 atmosphere*

C (solid, graphite) = C (solid, diamond)	Temperature in degrees Kelvin											
	0	298.16	300	400	500	600	700	800	900	1,000	1,100	1,200
Heat of reaction, $\Delta H°$, in cal/mole	576.6	453.2	452.1	399.0	358	328	310	299	291	284	270	249
Free energy of reaction, $\Delta F°$, in cal/mole	576.6	685.0	686.7	774.0	873	978	1,089	1,201	1,314	1,428	1,543	1,663

The expressions for the thermal expansion and compressibility of graphite and diamond have been reported previously [45]. Assuming that $(1/V)\ (\partial V/\partial P)_T$ for graphite and diamond are constants independent of temperature and pressure, these values may be combined with the thermodynamic relation $(\partial \Delta F/\partial P)_T = \Delta V$ to calculate the change in free energy for the transition of graphite to diamond at temperatures up to 1,200° K and pressures up to 20,000 atmospheres:

$$\Delta F^p = \Delta F° + \Delta(F^p - F°). \tag{35}$$

TABLE 8.—*Values of the heat of formation, $\Delta Hf°$, free energy of formation, $\Delta Ff°$, logarithm of the equilibrium constant of formation, $\log_{10}Kf$, and the equilibrium consta*
Kf, of H_2O (gas), CO (gas), CO_2 (gas) and CH_4 (gas), from the elements in their standard states

Reaction	Temperature in degrees Kelvin												
	0	298.16	300	400	500	600	700	800	900	1,000	1,100	1,200	1,300
	Heat of formation, $\Delta Hf°$, in kilocalories per mole												
$H_2(gas)+1/2O_2(gas)=H_2O(gas)$	−57.1043	−57.7979	−57.8022	−58.042	−58.276	−58.499	−58.709	−58.902	−59.080	−59.239	−59.384	−59.511	−59.62
C (solid, graphite)+$1/2O_2$ (gas)=CO (gas)	−27.2019	−26.4157	−26.4131	−26.317	−26.295	−26.330	−26.407	−26.511	−26.635	−26.768	−26.909	−27.056	−27.2
C (solid, graphite)+O_2 (gas)=CO_2 (gas)	−93.9686	−94.0518	−94.0520	−94.069	−94.091	−94.123	−94.167	−94.215	−94.268	−94.318	−94.364	−94.410	−94.4
C (solid, graphite)+$2H_2$ (gas)=CH_4 (gas)	−15.987	−17.889	−17.903	−18.629	−19.302	−19.893	−20.401	−20.823	−21.166	−21.43	−21.65	−21.79	−21.92
	Free energy of formation, $\Delta Ff°$, in kilocalories per mole												
$H_2(gas)+1/2O_2(gas)=H_2O(gas)$	−57.1043	−54.6351	−54.6152	−53.516	−52.358	−51.154	−49.912	−48.643	−47.349	−46.036	−44.710	−43.370	−42.01
C (solid, graphite)+$1/2O_2$ (gas)=CO (gas)	−27.2019	−32.8079	−32.8464	−35.007	−37.184	−39.358	−41.526	−43.677	−45.816	−47.942	−50.053	−52.153	−54.23
C (solid, graphite)+O_2 (gas)=CO_2 (gas)	−93.9686	−94.2598	−94.2603	−94.325	−94.392	−94.444	−94.497	−94.539	−94.578	−94.610	−94.637	−94.661	−94.67
C (solid, graphite)+$2H_2$ (gas)=CH_4 (gas)	−15.987	−12.140	−12.104	−10.048	−7.840	−5.49	−3.05	−0.55	+2.01	4.61	7.22	9.85	12.5
	Logarithm of the equilibrium constant of formation, $\log_{10}Kf$												
$H_2(gas)+1/2O_2(gas)=H_2O(gas)$		40.04695	39.78683	29.23972	22.88551	18.63228	15.58315	13.22846	11.49776	10.06104	8.88300	7.89864	7.06
C (solid, graphite)+$1/2O_2$ (gas)=CO (gas)		24.04790	23.92845	19.12672	16.25283	14.33621	12.96479	11.93193	11.12559	10.47772	9.94448	9.49826	9.11
C (solid, graphite)+O_2 (gas)=CO_2 (gas)		69.09145	68.66801	51.53648	41.25820	34.40107	29.50309	25.82664	22.90647	20.67675	18.80256	17.23998	15.91
C (solid, graphite)+$2H_2$ (gas)=CH_4 (gas)		8.8985	8.8177	5.4899	3.4268	2.0001	0.9526	0.1494	−0.4881	−1.0075	−1.4345	−1.7936	−2.10
	Equilibrium constant of formation, Kf												
$H_2(gas)+1/2O_2(gas)=H_2O(gas)$		1.114×10^{40}	6.121×10^{39}	1.737×10^{29}	7.683×10^{22}	4.288×10^{18}	3.830×10^{15}	1.943×10^{13}	3.146×10^{11}	1.151×10^{10}	7.638×10^{8}	7.918×10^{7}	1.158×10
C (solid, graphite)+$1/2O_2$ (gas)=CO (gas)		1.117×10^{34}	8.481×10^{33}	1.339×10^{19}	1.790×10^{16}	2.169×10^{14}	9.221×10^{12}	8.549×10^{11}	1.335×10^{11}	3.004×10^{10}	8.800×10^{9}	3.150×10^{9}	1.311×10
C (solid, graphite)+O_2 (gas) =CO_2 (gas)		1.234×10^{69}	4.656×10^{68}	3.439×10^{51}	1.812×10^{41}	2.518×10^{34}	3.185×10^{29}	6.709×10^{25}	9.257×10^{23}	4.751×10^{20}	6.347×10^{19}	1.738×10^{17}	8.252×10
C (solid, graphite)+$2H_2$ (gas) =CH_4 (gas)		7.916×10^{9}	6.572×10^{9}	3.090×10^{5}	2.672×10^{3}	100	8.906	1.411	0.3250	9.829×10^{-2}	3.677×10^{-2}	1.608×10^{-2}	7.932×10

TABLE 11.—*Values of the logarithm of the equilibrium constant, $\log_{10}K$, and the equilibrium constant, K, for some reactions involving O_2, H_2, H_2O, C(graphite), CO*

Reaction	Temperature in degrees Kelvin												
	0	298.16	300	400	500	600	700	800	900	1,000	1,100	1,200	1,300
	Logarithm of the equilibrium constant, $\log_{10}K$												
C (solid, graphite)+CO_2(gas)=2CO (gas)		−20.99575	−20.81089	−13.28281	−8.75242	−5.72851	−3.57358	−1.96284	−0.71538	+0.27865	1.08638	1.75658	2.31
C (solid, graphite)+H_2O (gas)=CO (gas)+H_2 (gas)		−15.99896	−15.85786	−10.11277	−6.65217	−4.29593	−2.61852	−1.35664	−.37226	+.41655	1.06373	1.59959	2.05
CO (gas)+$1/2O_2$ (gas)=CO_2 (gas)		+45.04367	44.73973	32.40960	25.00541	20.06491	16.53817	13.89475	11.84070	10.19920	8.85796	7.74189	6.79
CO (gas)+H_2O (gas)=CO_2 (gas)+H_2 (gas)		+ 4.99679	4.95303	3.17004	2.10025	1.43258	0.95506	0.60620	0.34312	0.13790	−0.02484	−0.15699	−0.26
CH_4 (gas)+$1/2O_2$ (gas)=CO (gas)+$2H_2$ (gas)		+15.14943	15.11042	13.62866	12.82615	12.33631	12.01203	11.78248	11.61365	11.48514	11.37881	11.29165	11.21
CH_4 (gas)+CO_2 (gas)=2CO (gas)+$2H_2$ (gas)		−29.89351	−29.62931	−18.78203	−12.17882	−7.72859	−4.52613	−2.11227	−0.22705	+1.28594	2.52066	3.54995	4.41
CH_4 (gas)+H_2O (gas)=CO (gas)+$3H_2$ (gas)		−24.89745	−24.67628	−15.61144	−10.05889	−6.29601	−3.57077	−1.50580	+.11607	1.42428	2.49602	3.39314	4.15
CH_4 (gas)+$2H_2O$ (gas)=CO_2 (gas)+$4H_2$ (gas)		−19.90067	−19.72325	−12.44091	−7.93898	−4.86343	−2.61571	−0.80960	+.45919	1.56218	2.47118	3.23615	3.88
	Equilibrium constant, K												
C (solid, graphite)+CO_2 (gas)=2CO (gas)		1.012×10^{-21}	1.546×10^{-21}	5.214×10^{-14}	1.768×10^{-9}	1.868×10^{-6}	2.669×10^{-4}	1.098×10^{-2}	0.1926	1.900	12.20	57.09	2.083×10
C (solid, graphite)+H_2O (gas)=CO (gas)+H_2 (gas)		1.002×10^{-16}	1.387×10^{-16}	7.713×10^{-11}	2.228×10^{-7}	5.059×10^{-6}	2.407×10^{-3}	4.399×10^{-2}	.4244	2.609	11.58	39.77	1.135×10
CO (gas)+$1/2O_2$ (gas)=CO_2 (gas)		1.106×10^{44}	5.492×10^{44}	2.568×10^{28}	1.013×10^{25}	1.161×10^{20}	3.453×10^{16}	7.848×10^{13}	6.930×10^{11}	1.582×10^{10}	7.210×10^{8}	5.519×10^{7}	6.293×10
CO (gas)+H_2O (gas)=CO_2 (gas)+H_2 (gas)		9.926×10^{4}	8.975×10^{4}	1.479×10^{3}	1.260×10^{2}	27.08	9.017	4.038	2.204	1.374	0.9444	0.6966	0.5435
CH_4 (gas)+$1/2O_2$ (gas)=CO (gas)+$2H_2$ (gas)		1.411×10^{13}	1.290×10^{13}	4.253×10^{13}	6.710×10^{12}	2.169×10^{12}	1.028×10^{12}	6.060×10^{11}	4.108×10^{11}	3.056×10^{11}	2.392×10^{11}	1.957×10^{11}	1.652×10
CH_4 (gas)+CO_2 (gas)=2CO (gas)+$2H_2$ (gas)		1.278×10^{-30}	2.348×10^{-30}	1.652×10^{-19}	6.625×10^{-13}	1.868×10^{-8}	2.978×10^{-5}	7.722×10^{-3}	0.5929	19.32	3.316×10^{2}	3.548×10^{3}	2.626×10
CH_4 (gas)+H_2O (gas)=CO (gas)+$3H_2$ (gas)		1.266×10^{-26}	2.107×10^{-25}	2.447×10^{-16}	8.732×10^{-11}	5.058×10^{-7}	2.687×10^{-4}	3.120×10^{-2}	1.306	26.56	3.133×10^{2}	2.473×10^{3}	1.428×10
CH_4 (gas)+$2H_2O$ (gas)=CO_2 (gas)+$4H_2$ (gas)		1.257×10^{-30}	1.891×10^{-30}	3.623×10^{-13}	1.151×10^{-8}	1.369×10^{-6}	2.423×10^{-3}	0.1260	2.879	36.49	2.959×10^{2}	1.723×10^{3}	7.759×10

ibrium constant of formation, $\log_{10}Kf$, and the equilibrium constant of formation, om the elements in their standard states

Temperature in degrees Kelvin								
700	800	900	1,000	1,100	1,200	1,300	1,400	1,500
f formation, $\Delta Hf°$, in kilocalories per mole								
−58.709	−58.902	−59.080	−59.239	−59.384	−59.511	−59.623	−59.724	−59.811
−26.407	−26.511	−26.635	−26.768	−26.909	−27.056	−27.212	−27.376	−27.545
−94.167	−94.215	−94.268	−94.318	−94.364	−94.410	−94.456	−94.505	−94.555
−20.401	−20.823	−21.166	−21.43	−21.65	−21.79	−21.92	−22.00	−22.06
y of formation, $\Delta Ff°$, in kilocalories per mole								
−49.912	−48.643	−47.349	−46.036	−44.710	−43.370	−42.017	−40.661	−39.296
−41.526	−43.677	−45.816	−47.942	−50.053	−52.153	−54.235	−56.308	−58.370
−94.497	−94.539	−94.578	−94.610	−94.637	−94.661	−94.677	−94.690	−94.707
−3.05	−0.55	+2.01	4.61	7.22	9.85	12.50	15.14	17.80
f the equilibrium constant of formation, $\log_{10}Kf$								
15.58315	13.22846	11.49776	10.06104	8.88300	7.89864	7.06367	6.34747	5.72542
12.96479	11.93193	11.12559	10.47772	9.94448	9.49826	9.11762	8.78999	8.50449
29.50309	25.82664	22.96647	20.67675	18.80256	17.23998	15.91654	14.78159	13.79863
0.9526	0.1494	−0.4881	−1.0075	−1.4345	−1.7936	−2.1006	−2.3638	−2.5927
quilibrium constant of formation, Kf								
830×10^{13}	1.943×10^{13}	3.146×10^{11}	1.151×10^{10}	7.638×10^{8}	7.918×10^{7}	1.158×10^{7}	2.226×10^{6}	5.314×10^{5}
221×10^{13}	8.549×10^{11}	1.335×10^{11}	3.004×10^{10}	8.800×10^{9}	3.150×10^{9}	1.311×10^{9}	6.166×10^{8}	3.195×10^{8}
185×10^{29}	6.709×10^{25}	9.257×10^{22}	4.751×10^{20}	6.347×10^{18}	1.738×10^{17}	8.252×10^{15}	6.040×10^{14}	6.290×10^{13}
966	1.411	0.3250	9.829×10^{-2}	3.677×10^{-2}	1.608×10^{-2}	7.932×10^{-3}	4.327×10^{-3}	2.554×10^{-3}

nt, K, for some reactions involving O_2, H_2, H_2O, C(*graphite*), CO, CO_2, *and* CH_4

Temperature in degrees Kelvin								
700	800	900	1,000	1,100	1,200	1,300	1,400	1,500
rithm of the equilibrium constant, $\log_{10}K$								
−3.57358	−1.96284	−0.71538	+0.27865	1.08638	1.75658	2.31863	2.79835	3.21033
−2.61852	−1.35664	−.37226	+.41655	1.06373	1.59959	2.05385	2.44243	2.77906
16.53817	13.89475	11.84070	10.19920	8.85796	7.74189	6.79887	5.99165	5.29440
0.95506	0.60620	0.34312	0.13790	−0.02484	−0.15699	−0.26478	−0.35592	−0.43127
12.01203	11.78248	11.61365	11.48514	11.37881	11.29165	11.21808	11.15376	11.09715
−4.52613	−2.11227	−0.22705	+1.28594	2.52066	3.54995	4.41921	5.16211	5.80289
−3.87077	−1.50580	+.11607	1.42428	2.49602	3.39314	4.15460	4.80634	5.37177
−2.61571	−0.89960	+.45919	1.56218	2.47118	3.23615	3.88982	4.45042	4.94050
Equilibrium constant, K								
2.660×10^{-4}	1.098×10^{-2}	0.1926	1.900	12.20	57.09	2.083×10^{2}	6.286×10^{2}	1.623×10^{3}
2.407×10^{-6}	4.399×10^{-3}	.4244	2.609	11.58	39.77	1.135×10^{2}	2.770×10^{2}	6.013×10^{2}
3.453×10^{16}	7.848×10^{13}	6.930×10^{11}	1.582×10^{10}	7.210×10^{8}	5.519×10^{7}	6.293×10^{6}	9.810×10^{5}	1.970×10^{5}
9.017	4.038	2.204	1.374	0.9444	0.6966	0.5435	0.4406	0.3704
1.028×10^{12}	6.060×10^{11}	4.108×10^{11}	3.056×10^{11}	2.392×10^{11}	1.957×10^{11}	1.652×10^{11}	1.425×10^{11}	1.251×10^{11}
2.978×10^{-3}	7.722×10^{-3}	0.5929	19.32	3.316×10^{3}	3.548×10^{3}	2.626×10^{4}	1.452×10^{5}	6.352×10^{5}
2.687×10^{-4}	3.120×10^{-2}	1.306	26.56	3.133×10^{2}	2.473×10^{3}	1.428×10^{4}	6.402×10^{4}	2.354×10^{5}
2.423×10^{-3}	0.1260	2.879	36.49	2.959×10^{2}	1.723×10^{3}	7.759×10^{3}	2.821×10^{4}	8.720×10^{4}

627528—45 (Face p. 156)

UNIV. OF MICH.

The first term on the right is given in table 9, and the second term on the right is the increment in free energy from 1 atmosphere to P atmospheres for diamond less that of graphite, at a given temperature. Values of $(F^{\circ}_{P}-F^{\circ})$ and $\Delta(F^{\circ}_{P}-F^{\circ})$ for various pressures and temperatures are given by the relations:

For C (solid, graphite)—

$$(F^{\circ}_{P}-F^{\circ})=[0.12843+7.617\times10^{-7}T+4.848\times10^{-10}T^{2}] \quad (36)$$
$$[(P-1)-1.52\times10^{-6}(P^{2}-1)+1.54\times10^{-12}(P^{3}-1)] \text{ cal/mole},$$

For C (solid, diamond)—

$$(F^{\circ}_{P}-F^{\circ})=[0.082777-1.505\times10^{-7}T+5.631\times10^{-10}T^{2} \quad (37)$$
$$+3.6224\times10^{-13}T^{3}][(P-1)-8.0\times10^{-8}(P^{2}-1)$$
$$+4.0\times10^{-15}(P^{3}-1)] \text{ cal/mole},$$

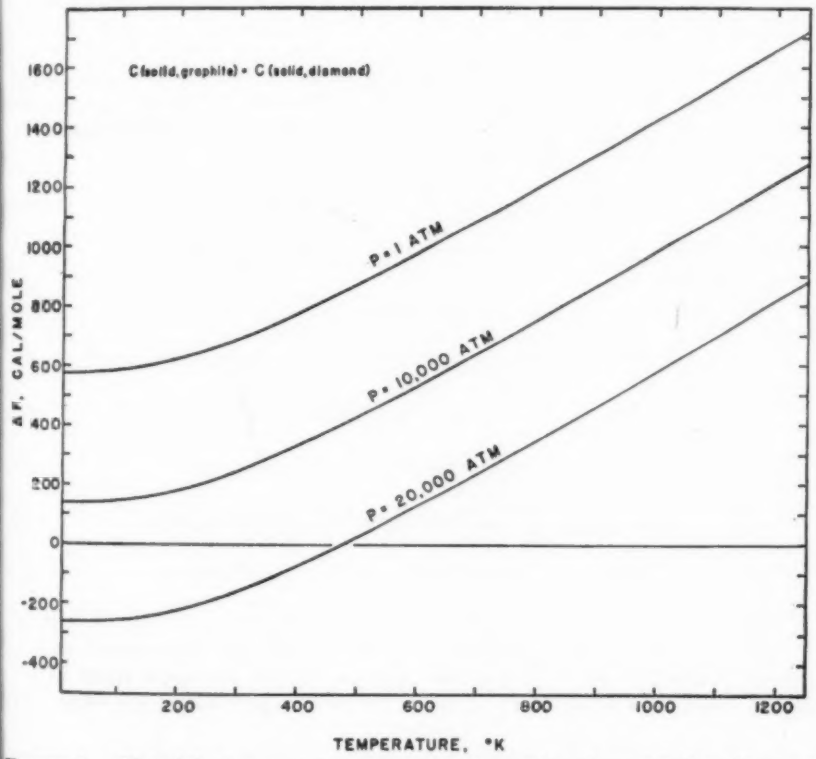

FIGURE 1.—*Plot of the free energy change for the transition of graphite into diamond.*

The scale of ordinates gives the increment in free energy, ΔF°, in cal/mole, for the transition, C (solid, graphite) = C (solid, diamond). The scale of abscissas gives the absolute temperature in degrees Kelvin. As indicated, the three curves are for pressures of 1, 10,000, and 20,000 atmospheres. Values below zero indicate, within the limits of uncertainty, the region in which diamond is thermodynamically more stable than graphite. See text.

For the transition—

$$\text{C (solid, graphite)} = \text{C (solid, diamond)} \tag{38}$$

$$\begin{aligned}\Delta(F^p - F^\circ) = &-[0.045653 + 9.122\times10^{-7}T - 7.83\times10^{-11}T^2 \\ &- 3.6224\times10^{-13}T^3][P-1] + [1.886\times10^{-6} + 1.17\times10^{-12}T \\ &+ 6.92\times10^{-16}T^2 - 2.9\times10^{-20}T^3][P^2-1] - [1.974\times10^{-13} \\ &+ 1.174\times10^{-18}T + 7.44\times10^{-22}T^2 - 1.45\times10^{-27}T^3][P^3-1]\text{cal/mole.}\end{aligned} \tag{39}$$

In eq 36, 37, and 39, P is in atmospheres, and T is in degrees Kelvin.

Values of the change in free energy for the transition of graphite into diamond at various temperatures and pressures are plotted in figure 1.

VI. HEATS, FREE ENERGIES, AND EQUILIBRIUM CONSTANTS OF SOME REACTIONS INVOLVING O_2, H_2, H_2O, C, CO, CO_2, AND CH_4

From the data given in the preceding sections, values were calculated for the increment in heat content, the increment in free energy, the logarithm of the equilibrium constant, and the equilibrium constant, to 1,500° K, for the following reactions:

$$\text{C(solid, graphite)} + \text{CO}_2\text{(gas)} = 2\text{CO(gas)}. \tag{40}$$

$$\text{C(solid, graphite)} + \text{H}_2\text{O(gas)} = \text{CO(gas)} + \text{H}_2\text{(gas)}. \tag{41}$$

$$\text{CO(gas)} + 1/2\text{O}_2\text{(gas)} = \text{CO}_2\text{(gas)}. \tag{42}$$

$$\text{CO(gas)} + \text{H}_2\text{O(gas)} = \text{CO}_2\text{(gas)} + \text{H}_2\text{(gas)}. \tag{43}$$

$$\text{CH}_4\text{(gas)} + 1/2\text{O}_2\text{(gas)} = \text{CO(gas)} + 2\text{H}_2\text{(gas)}. \tag{44}$$

$$\text{CH}_4\text{(gas)} + \text{CO}_2\text{(gas)} = 2\text{CO(gas)} + 2\text{H}_2\text{(gas)}. \tag{45}$$

$$\text{CH}_4\text{(gas)} + \text{H}_2\text{O(gas)} = \text{CO(gas)} + 3\text{H}_2\text{(gas)}. \tag{46}$$

$$\text{CH}_4\text{(gas)} + 2\text{H}_2\text{O(gas)} = \text{CO}_2\text{(gas)} + 4\text{H}_2\text{(gas)}. \tag{47}$$

Values are presented for the above reactions, to 1,500° K, in table 10 for the increment in heat content, ΔH°, and the increment in free energy, ΔF°, and in table 11 (facing p. 156) for the logarithm of the equilibrium constant, $\log_{10}K$, and for the equilibrium constant, K.

TABLE 10.—*Values of the heat, ΔH°, and free energy, ΔF°, for some reactions involving O_2, H_2, H_2O, C (graphite), CO, CO_2, and CH_4*

TABLE 10.—*Values of the heat, $\Delta H°$, and free energy, $\Delta F°$, for some reactions involving O_2, H_2, H_2O, C (graphite), CO, CO_2, and CH_4*

Reaction	Temperature in degrees Kelvin														
	0	298.16	300	400	500	600	700	800	900	1,000	1,100	1,200	1,300	1,400	1,500
	Heat of reaction, $\Delta H°$, in calories per mole														
C (solid, graphite)+CO_2 (gas)=2CO (gas)	39565	41220	41226	41435	41501	41463	41353	41193	40997	40781	40545	40298	40031	39754	39464
C (solid, graphite)+H_2O (gas)=CO (gas)+H_2 (gas)	29902	31382	31389	31725	31981	32169	32302	32391	32445	32470	32474	32454	32411	32348	32265
CO (gas)+1/2O_2 (gas)=CO_2 (gas)	−66767	−67636	−67639	−67752	−67796	−67793	−67760	−67704	−67632	−67550	−67455	−67355	−67243	−67129	−67010
CO (gas)+H_2O (gas)=CO_2 (gas)+H_2 (gas)	−9662	−9838	−9837	−9710	−9520	−9294	−9051	−8802	−8552	−8311	−8071	−7844	−7620	−7406	−7199
CH_4 (gas)+1/2O_2 (gas)=CO (gas)+2H_2 (gas)	−11215	−8527	−8511	−7688	−6993	−6437	−6006	−5689	−5470	−5335	−5262	−5254	−5299	−5379	−5486
CH_4 (gas)+CO_2 (gas)=2 CO (gas)+2H_2 (gas)	55552	59109	59128	60063	60803	61356	61754	62016	62162	62214	62192	62100	61944	61750	61524
CH_4 (gas)+H_2O (gas)=CO (gas)+3H_2 (gas)	45889	49271	49291	50353	51283	52062	52703	53214	53610	53903	54122	54257	54324	54344	54325
CH_4 (gas)+2H_2O (gas)=CO_2 (gas)+4H_2 (gas)	36227	39433	39454	40643	41763	42768	43652	44412	45058	45592	46051	46413	46704	46938	47126
	Free energy of reaction, $\Delta F°$, in calories per mole														
C (solid, graphite)+CO_2 (gas)=2CO (gas)	39565	28644	28567	24311	20024	15727	11446	7185	2946	−1275	−5468	−9645	−13792	−17926	−22034
C (solid, graphite)+H_2O (gas)=CO (gas)+H_2 (gas)	29902	21827	21768	18509	15219	11794	8387	4966	1533	−1906	−5354	−8783	−12217	−15646	−19074
CO (gas)+1/2O_2 (gas)=CO_2 (gas)	−66767	−61452	−61414	−59318	−57208	−55086	−52971	−50862	−48761	−46668	−44584	−42509	−40442	−38382	−36338
CO (gas)+H_2O (gas)=CO_2 (gas)+H_2 (gas)	−9662	−6817	−6799	−5802	−4850	−3933	−3059	−2219	−1413	−631	+125	862	1575	2280	2960
CH_4 (gas)+1/2O_2 (gas)=CO (gas)+2H_2 (gas)	−11215	−20668	−20742	−24944	−29344	−33868	−38474	−43130	−47826	−52552	−57272	−62000	−66729	−71450	−76165
CH_4 (gas)+CO_2 (gas)=2CO (gas)+2H_2 (gas)	55552	40783	40672	34376	27863	21218	14497	7732	935	−5884	−12687	−19492	−26287	−33068	−39828
CH_4 (gas)+H_2O (gas)=CO (gas)+3H_2 (gas)	45889	33967	33873	28573	23013	17285	11437	5512	−478	−6517	−12563	−18631	−24713	−30789	−36869
CH_4 (gas)+2H_2O (gas)=CO_2 (gas)+4H_2 (gas)	36227	27150	27074	22771	18163	13352	8378	3293	−1891	−7148	−12438	−17769	−23138	−28509	−33909

627529—45—5

In figure 2 are plotted the values of the logarithm of the equilibrium constant for these reactions and for reaction (27).

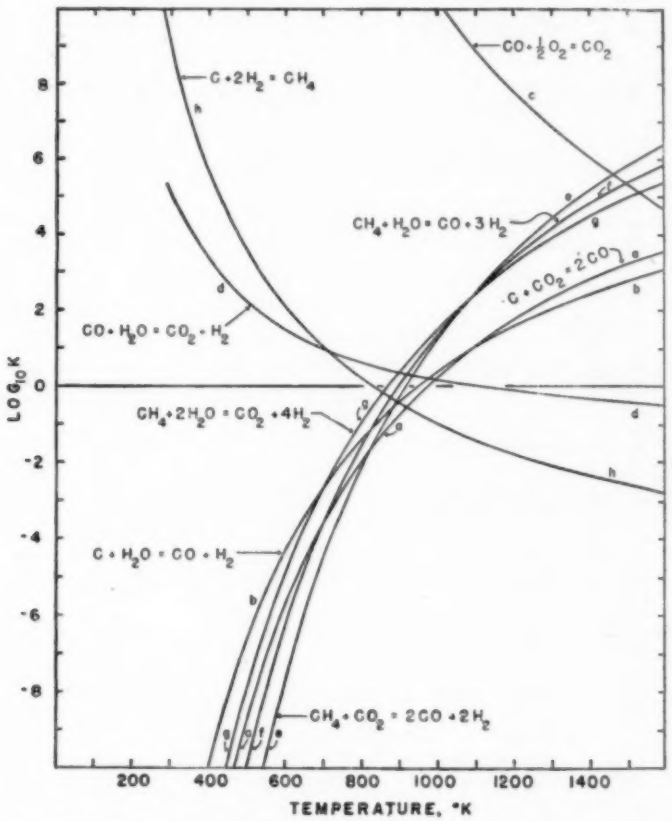

FIGURE 2.—*Plot of the logarithm of the equilibrium constant for eight reaction involving* O_2, H_2, H_2O, C *(graphite)*, CO, CO_2, *and* CH_4.

The scale of ordinates gives the logarithm (to the base 10) of the equilibrium constant, $\log_{10}K$, for the given reaction. The scale of abscissas gives the temperature in degrees Kelvin. The curves apply to the following reactions (see text):

(a) C(solid, graphite)+CO_2(gas)=2CO(gas).
(b) C(solid, graphite)+H_2O(gas)=CO(gas)+H_2(gas).
(c) CO(gas)+1/2O_2(gas)=CO_2(gas).
(d) CO(gas)+H_2O(gas)=CO_2(gas)+H_2(gas).
(e) CH_4(gas)+CO_2(gas)=2CO(gas)+2H_2(gas).
(f) CH_4(gas)+H_2O(gas)=CO(gas)+3H_2(gas).
(g) CH_4(gas)+2H_2O(gas)=CO_2(gas)+4H_2(gas).
(h) C(solid, graphite)+2H_2(gas)=CH_4(gas).

VII. REFERENCES

[1] E. F. Mueller and F. D. Rossini, Am. J. Phys. **12,** 1 (1944).
[2] G. K. Burgess, BS J. Research **1,** 635 (1928) RP22.
[3] G. P. Baxter, M. Guichard, O. Hönigschmid, and R. Whytlaw-Gray, J. Am. Chem. Soc. **63,** 845 (1941).
[4] C. S. Cragoe, J. Research NBS **26,** 495 (1941) RP1393.
[5] E. C. Crittenden, National Bureau of Standards (1943), Private communication; H. L. Curtis, J. Research NBS **33,** 235 (1944) RP1606.
[6] R. T. Birge, Rev. Modern Phys. **13,** 233 (1941).
[7] R. T. Birge, Rev. Modern Phys. **1,** 1(1929).
[8] R. C. Tolman, The Principles of Statistical Mechanics (Oxford University Press, New York, N. Y., 1938.)
[9] J. E. Mayer and M. G. Mayer, Statistical Mechanics (John Wiley & Sons, Inc., New York, N. Y., 1940.)
[10] H. L. Johnston and M. K. Walker, J. Am. Chem. Soc. **55,** 172 (1933).
[11] H. L. Johnston and M. K. Walker, J. Am. Chem. Soc. **57,** 682 (1935).
[12] C. O. Davis and H. L. Johnston, J. Am. Chem. Soc. **56,** 1045 (1934).
[13] H. L. Johnston and C. O. Davis, J. Am. Chem. Soc. **56,** 271 (1934).
[14] W. F. Giauque, J. Am. Chem. Soc. **52,** 4816 (1930).
[15] W. F. Giauque and J. O. Clayton, J. Am. Chem. Soc. **55,** 4875 (1933).
[16] J. O. Clayton and W. F. Giauque, J. Am. Chem. Soc. **55,** 5071 (1933).
[17] A. R. Gordon, J. Chem. Phys. **2,** 65 (1934).
[18] A. R. Gordon, J. Chem. Phys. **2,** 549 (1934).
[19] L. S. Kassel, J. Am. Chem. Soc. **56,** 1838 (1934).
[20] E. B. Wilson, Jr., J. Chem. Phys. **4,** 526 (1936).
[21] K. S. Pitzer, Ind. Eng. Chem. **36,** 829 (1944).
[22] A. R. Gordon and C. Barnes, J. Chem. Phys. **1,** 297 (1933).
[23] A. R. Gordon and C. Barnes, J. Phys. Chem. **36,** 1143 (1932).
[24] W. F. Libby, J. Chem. Phys. **11,** 101 (1943).
[25] L. S. Kassel, J. Chem. Phys. **1,** 576 (1933).
[26] A. R. Gordon, J. Chem. Phys. **1,** 308 (1933).
[27] W. Nernst, Ann. Physik [4] **36,** 395 (1911).
[28] A. G. Worthing, Phys. Rev. **12,** 199 (1918).
[29] A. Magnus, Ann. Physik [4] **70,** 303 (1923).
[30] P. Schläpfer and P. Debrunner, Helv. Chim. Acta **7,** 31 (1924).
[31] C. J. Jacobs and G. S. Parks, J. Am. Chem. Soc. **56,** 1513 (1934).
[32] A. Magnus, Ann. Physik [4] **48,** 983 (1915).
[33] H. F. Weber, Ann. Physik [2] **154,** 367 (1875).
[34] H. F. Weber, Ann. Physik [2] **154,** 553 (1875).
[35] A. Magnus and A. Hodler, Ann. Physik [4] **80,** 808 (1926).
[36] K. S. Pitzer, J. Chem. Phys. **6,** 68 (1938).
[37] A. Bettendorff and A. Wüllner, Ann. Physik [2] **133,** 293 (1868).
[38] W. Nernst and F. A. Lindemann, Z. Elektrochem. **17,** 817 (1911).
[39] R. Robertson, J. J. Fox, and A. E. Martin, Proc. Roy. Soc (London) **A157,** 579 (1936).
[40] G. N. Lewis and M. Randall, Thermodynamics, p. 294 (McGraw-Hill Book Co. Inc., 1923).
[41] F. D. Rossini, J. Research NBS **22,** 407 (1939) RP1192.
[42] C. H. Meyers and C. S. Cragoe, National Bureau of Standards. Unpublished.
[43] E. J. Prosen, R. S. Jessup, and F. D. Rossini, J. Research NBS **33,** 447 (1944) RP1620.
[44] E. J. Prosen and F. D. Rossini, J. Research NBS **34,** 263 (1945) RP1642.
[45] F. D. Rossini and R. S. Jessup, J. Research NBS **21,** 491 (1938) RP1141.

WASHINGTON, October 31, 1944.

U. S. Department of Commerce National Bureau of Standards

RESEARCH PAPER RP1635

Part of Journal of Research of the National Bureau of Standards, Volume 34, February 1945

HEATS OF ISOMERIZATION OF THE 18 OCTANES

By Edward J. Prosen and Frederick D. Rossini

ABSTRACT

The heats of isomerization of all of the 18 octanes were determined by measurement of the ratios of their heats of combustion, in the liquid state for 17 and the solid state for 1, using the procedure previously described for the hexanes and the heptanes.

Values of the heats of isomerization are reported for the condensed (liquid or solid) state at 25° C and for the gaseous state at 25° C and 0° K.

CONTENTS

		Page
I.	Introduction	163
II.	Unit of energy, molecular weights, etc	164
III.	Method and apparatus	164
IV.	Experimental procedures	164
	1. Chemical procedure	164
	2. Calorimetric procedure	167
V.	Results	167
VI.	Data of previous investigations	173
VII.	Discussion	173
VIII.	References	174

I. INTRODUCTION

In continuation of the program of determining the heats of formation and of isomerization of the paraffin hydrocarbons [1, 2, 3, 4][1], calorimetric measurements have been made which yield values for the differences in the heats of combustion of all of the 18 octanes at 25° C. These values for the differences in the heats of combustion, which, for the same state, are also the heats of isomerization at 25° C, have been combined with heats of vaporization (or sublimation for the one solid octane), measured by Osborne and Ginnings [5], to give values for the heats of isomerization in the gaseous state at 25° C. Combination of these with values for the decrease in heat content of the various isomers in the gaseous state from 25° C to 0° K, calculated by Pitzer [6], gives values for the energies of isomerization for the ideal gaseous state at 0° K.

[1] Figures in brackets indicate the literature references at the end of this paper. References to the earlier papers are given in [1].

II. UNIT OF ENERGY, MOLECULAR WEIGHTS, ETC.

The unit of energy upon which the values reported in this paper are based is the international joule. For conversion to the conventional thermochemical calorie, the following relation is used [7]:

4.1833 international joules (NBS)=1 calorie.

The molecular weight of carbon dioxide, the mass of which was used to determine the amount of reaction, was taken as 44.010 from the 1941 table of atomic weights [8].

The uncertainties assigned to the various quantities dealt with in this paper were derived, where possible, by a method previously described [9].

Definitions of all symbols used are given in a previous paper [2].

III. METHOD AND APPARATUS

The same method and apparatus were used in the present investigation as in the work on the hexanes [2] and heptanes [3].

IV. EXPERIMENTAL PROCEDURES

1. CHEMICAL PROCEDURE

The description of the octanes investigated is summarized in table 1, which gives the name of the compound, the normal state (liquid or solid) at 25° C, the source of the material, and, where known, the amount of impurity. For 13 of the octanes, determination of the amount of impurity was made by A. R. Glasgow, Jr., of the American Petroleum Institute Research Project 6 at this Bureau, from time-temperature freezing and melting curves [19]. For the others, estimates of the amount of impurity were made by the authors, considering the method of purification and the purity of related isomers. The octanes used were so prepared and purified that the residual impurities must have consisted largely of isomeric octanes. Further, the impurities would be largely only those isomers having boiling points near that of the given isomer. The values given in table 2 indicate the tolerances with regard to such impurities, and also the actual estimated amounts of impurity. From these data, it appears that the amounts of impurity in the 18 octanes were not sufficient to affect their heats of combustion significantly, with the possible exception of 2,3-dimethylhexane.

The procedures for sealing the liquid hydrocarbons in glass ampoules, purifying the oxygen used for combustion, igniting the hydrocarbon, examining the products of combustion, and determining the amount of reaction have been described previously [2].

TABLE 1.—*Source and purity of the octanes investigated*

Compound	State	Source [a]	Amount of impurity
			Mole fraction
n-Octane (I)	Liquid	A	0.0080±0.0010
n-Octane (II)	do	A	.0035±0.0005
2-Methylheptane	do	A	<.03
3-Methylheptane	do	A	<.03
4-Methylheptane	do	A	<.015
3-Ethylhexane	do	A	[b](<.02)
2,2-Dimethylhexane	do	A, B	<.015
2,3-Dimethylhexane	do	A, B	[b](<.057)
2,4-Dimethylhexane	do	A, B	[b](<.02)
2,5-Dimethylhexane	do	A, B	<.01
3,3-Dimethylhexane	do	A, B	<.005
3,4-Dimethylhexane	do	A, B	[b](<.02)
2-Methyl-3-ethylpentane	do	A	<.01
3-Methyl-3-ethylpentane	do	A, B	<.006
2,2,3-Trimethylpentane	do	A, B	<.005
2,2,4-Trimethylpentane	do	C	<.002
2,3,3-Trimethylpentane	do	A, B	<.01
2,3,4-Trimethylpentane	do	A	<.005
2,2,3,3-Tetramethylbutane	Solid	D	[b](<.02)

[a] The letters in this column have the following significance:
A, Prepared by the American Petroleum Institute Hydrocarbon Research Project at the Ohio State University. These materials were made available by Cecil E. Boord, Supervisor of the Project, and George Calingaert, Chairman of the Subcommittee on Physical Properties.
B, Further purified by the American Petroleum Institute Research Project 6 at the National Bureau of Standards by means of azeotropic distillation in columns of high efficiency (approximately 100 theoretical plates) at a high reflux ratio (100 to 1);
C, purified from relatively pure 2,2,4-trimethylpentane prepared commercially (Rohm and Hass Company, Philadelphia, Pa.) by azeotropic distillation (as under B), by the American Petroleum Institute Research Project 6;
D, purified by crystallization by A. R. Glasgow, Jr., of the American Petroleum Institute Research Project 6, from material prepared by the Chemical Research Laboratory of the Ethyl Corporation, Detroit, Mich. This material was made available by George Calingaert, Director of Chemical Research of the Ethyl Corporation.
[b] Estimated; see text.

For the combustion of the solid 2,2,3,3-tetramethylbutane, glass ampoules could not be used, and, since the sample was required to be inclosed because of its volatility, gelatin capsules were used for the purpose. All the capsules were from one lot of No. 000 gelatin capsules.[2] These were dried by heating in an oven at 100° C, cooled in a desiccator, and weighed in small closed bottles out of contact with the air of the room. A heating time of 6 to 8 hours usually served to bring the capsules to constant weight. For each combustion experiment involving a gelatin capsule as the inclosure for the main combustible material, the mass ("dry") of the gelatin capsule was first determined. Then the solid sample was packed into the capsule and the cover put on. The cover of the capsule was sealed to the body by dipping the entire capsule halfway under water for several seconds.

[2] From Sharp and Dohme, Baltimore, Md.

TABLE 2.—*Tolerances of the amounts of close-boiling isomeric impurities in the octanes*

Compound	Close-boiling isomers	Amount of each such impurity required to change the heat of combustion by five parts in 100,000	Amount of impurity in the material used in the present work
		Mole fraction	*Mole fraction*
n-Octane (I)			0.0080
n-Octane (II)			.0035
2-Methylheptane	3-Methylheptane	0.10	<.03
	4-Methylheptane	.08	
	3-Ethylhexane	.06	
3-Methylheptane	2-Methylheptane	.10	<.03
	4-Methylheptane	.37	
	3-Ethylhexane	.14	
4-Methylheptane	2-Methylheptane	.08	<.015
	3-Methylheptane	.37	
	3-Ethylhexane	.22	
3-Ethylhexane	2-Methylheptane	.06	[a](<.02)
	3-Methylheptane	.14	
	4-Methylheptane	.22	
	3-Methyl-3-ethylpentane	.11	
2,2-Dimethylhexane	2,4-Dimethylhexane	.06	<.015
	2,5-Dimethylhexane	.18	
	2,2,3,3-Tetramethylbutane	.04	
2,3-Dimethylhexane	3,4-Dimethylhexane	.36	[a](0.057)
	2-Methyl-3-ethylpentane	.09	
	2,3,3-Trimethylpentane	.30	
2,4-Dimethylhexane	2,5-Dimethylhexane	.08	[a](<.02)
2,5-Dimethylhexane	2,4-Dimethylhexane	.08	<.01
3,3-Dimethylhexane	2,3,3-Trimethylpentane	.07	<.005
	2,3,4-Trimethylpentane	.11	
3,4-Dimethylhexane	2-Methylheptane	.09	[a](<.02)
	3-Methylheptane	.5	
	4-Methylheptane	>.5	
	3-Ethylhexane	.19	
2-Methyl-3-ethylpentane	2,3-Dimethylhexane	.09	<.01
	3-Methyl-3-ethylpentane	.08	
	2,3,3-Trimethylpentane	.07	
3-Methyl-3-ethylpentane	3-Ethylhexane	.11	<.006
	3,4-Dimethylhexane	.27	
	2-Methyl-3-ethylpentane	.08	
2,2,3-Trimethylpentane	2,4-Dimethylhexane	>.5	<.005
	2,5-Dimethylhexane	.08	
2,2,4-Trimethylpentane			<.002
2,3,3-Trimethylpentane	2,3,4-Trimethylpentane	.18	<.01
	2,3-Dimethylhexane	.30	
2,3,4-Trimethylpentane	3,3-Dimethylhexane	.11	<.005
	2,3,3-Trimethylpentane	.18	
2,2,3,3-Tetramethylbutane	2,2-Dimethylhexane	.04	[a](<.02)
	2,2,4-Trimethylpentane	.03	

[a] Estimated; see text.

For the solid octane, two types of experiments were performed. In the first type were measured the temperature rise of the calorimeter and the mass of carbon dioxide formed in the combustion of a mass (not accurately known) of 2,2,3,3-tetramethylbutane together with a known mass of gelatin capsule. In the second type of experiment were measured in one series, I, the temperature rise of the calorimeter and the mass of carbon dioxide formed in the combustion of a known mass of gelatin capsule, and in another series, II, the temperature rise of the calorimeter and the mass of carbon dioxide formed in the combustion of a known mass of gelatin capsule together with a known mass of pure benzoic acid of known heat of combustion. The second type of experiment served to determine the amount of heat and of carbon dioxide evolved in the combustion of unit mass of gelatin, the I series involving the determination directly on 13 capsules (1 capsule

in experiment No. 1, and 4 capsules each in experiments 2, 3, and 4 of table 4), and the II series involving the determination indirectly, but under conditions simulating more closely the combustion experiments, with two experiments (Nos. 5 and 6 of table 4) involving one capsule and a known standard amount of pure benzoic acid (NBS Standard Sample 39 e).

The average values obtained for the amount of heat evolved and the mass of carbon dioxide formed in the combustion of unit mass of gelatin capsule were combined with the data of the first type of experiment to obtain the temperature rise of the calorimeter and the mass of carbon dioxide formed from the combustion of the 2,2,3,3-tetramethylbutane alone.

2. CALORIMETRIC PROCEDURE

The calorimetric procedure was the same as that in the work on the hexanes [2] and heptanes [3].

V. RESULTS

The experimental results of the present investigation are presented in tables 3, 4, and 5, which give the data yielding values of B in ohms per gram of carbon dioxide, as defined by eq 4 of the paper on the hexanes [2], for 17 of the octanes in the liquid phase, and for the eighteenth octane (2,2,3,3-tetramethylbutane) in the solid phase, at 28° C. The symbols have the same significance as in previous reports [2, 12].

In the experiments on 2-methylheptane, there was a loss of carbon dioxide during the analysis of the products of combustion of the calorimetric combustion experiments. In order to save repeating the latter experiments, a series of four noncalorimetric combustion experiments was performed to determine the ratio of the mass of carbon dioxide formed to that calculated stoichiometrically from the mass of sample. These four experiments yielded the following value for this ratio: Mean, 0.99970; standard deviation of the mean, ± 0.00006. The values of the mass of carbon dioxide formed as given in table 3 are calculated from the foregoing ratio. The uncertainty assigned to the final value for 2-methylheptane was increased by the uncertainty in the stoichiometric ratio.

In table 6 are given, for the 18 octanes, values of the following: The constant B in ohms per gram of carbon dioxide, as given in tables 3 and 5; the ratio of the heat evolved, per mole of hydrocarbon, in the bomb process at 28° C for each isomer to that for *n*-octane; the difference, between *n*-octane and each isomer, in the heat of combustion in the bomb process at 28° C; and the heat of isomerization of *n*-octane into each isomer, at 25° C and 1 atm, for the liquid state for the 17 normally liquid octanes and for the solid state for 2, 2, 3, 3-tetramethylbutane. The value of the heat of isomerization was obtained by means of the relation [2]

$$(-\Delta U_B)_n-(-\Delta U_B)_i=(-\Delta U_B)_n(1-B_i/B_n).$$

For this calculation, the value of $(-\Delta U_B)_n$ at 28° C was taken as 5458.8 int. kj/mole [4].

TABLE 3.—*Results of the calorimetric combustion experiments on the seventeen liquid octanes*

Compound	Number of experiments [a]				Mass of carbon dioxide formed	k	K	U	ΔR_c	Δr_i	Δr_c	B [a]	
	A	B	C	Total								Mean	Standard deviation of the mean
					g	*min*$^{-1}$	*Ohm*	*Ohm*	*Ohm*	*Ohm*	*Ohm*	*Ohm/g* CO_2	*Ohm/g* CO_2
n-Octane		[b] 4	[b] 6	10	2.26440 to 2.87367	0.001937 to .001957	0.000418 to .002160	0.000070 to .000365	0.255416 to .323369	0.000400 to .000421	0.000020 to .000098	0.1125810	±0.0000062
2-Methylheptane	7			7	2.28907 to 2.68633	.001932 to .001939	.000853 to .002061	.000024 to .000072	.258272 to .303029	.000529 to .000542	.000063 to .000088	.1124730	.0000030
3-Methylheptane	3	3		6	2.32827 to 2.61833	.001939 to .001953	.000791 to .001857	.000088 to .000125	.261931 to .301352	.000410 to .000424	.000082 to .000089	.1125282	.0000050
4-Methylheptane		5		5	2.34562 to 2.63248	.001938 to .001947	.000979 to .001838	.000077 to .000166	.263945 to .296124	.000398 to .000423	.000077 to .000089	.1125434	.0000053
3-Ethylhexane			5	5	2.22709 to 2.55087	.001952 to .001971	.001293 to .002293	.000348 to .000376	.251115 to .287541	.000399 to .000409	.000017 to .000021	.1125690	.0000039
2,2-Dimethylhexane			4	4	2.17294 to 2.25164	.001961 to .001973	.002090 to .002518	.000349 to .000406	.244059 to .252910	.000411 to .000421	.000026 to .000030	.1123315	.0000025
2,3-Dimethylhexane			7	7	2.17520 to 3.02957	.001950 to .001974	−.000202 to .002509	.000315 to .000382	.245209 to .341297	.000382 to .000417	.000019 to .000042	.1125232	.0000104
2,4-Dimethylhexane			5	5	2.00103 to 2.52870	.001959 to .001975	.001449 to .003063	.000367 to .000430	.225384 to .284591	.000380 to .000415	.000020 to .000032	.1124320	.0000049
2,5-Dimenthylhexane			5	5	2.15555 to 2.65585	.001956 to .001982	.000986 to .002559	.000365 to .000466	.242613 to .298781	.000392 to .000416	.000018 to .000041	.1123625	.0000104
3,3-Dimethylhexane			5	5	2.08676 to 2.77636	.001952 to .001976	.000687 to .002761	.000317 to .000430	.235016 to .311844	.000381 to .000415	.000030 to .000034	.1124209	.0000036
3,4-Dimethylhexane			5	5	2.19862 to 2.67840	.001957 to .001982	.000901 to .002405	.000302 to .000371	.247923 to .301809	.000392 to .000414	.000020 to .000026	.1125389	.0000110
2-Methyl-3-ethylpentane		5		5	2.52729 to 2.92399	.001934 to .001949	−.000012 to .001064	.000051 to .000141	.284412 to .328979	.000403 to .000414	.000084 to .000094	.1125857	.0000074
3-Methyl-3-ethylpentane			5	5	2.18795 to 2.67840	.001968 to .001982	.001965 to .002405	.000354 to .000371	.246577 to .301809	.000403 to .000414	.000027 to .000026	.1125184	.0000067

3-Methyl-3-ethylpentane			5	5	2.18795 to 2.33820	.001968 to .001971	.001965 to .002452	.000354 to .000429	.246577 to .263508	.000403 to .000419	.000027 to .000033	.1125184	.0000067
2,2,3-Trimethylpentane			5	5	2.16458 to 2.90827	.001951 to .001973	.000254 to .002600	.000306 to .000429	.243840 to .327328	.000402 to .000419	.000029 to .000037	.1124337	.0000102
2,2,4-Trimethylpentane		5	1	6	2.12289 to 2.58952	.001920 to .001956	.001037 to .002599	.000061 to .000421	.238699 to .290815	.000405 to .000423	.000022 to .000085	.1123867	.0000086
2,3,3-Trimethylpentane			5	5	2.34694 to 2.67128	.001948 to .001963	.000989 to .001971	.000330 to .000362	.264472 to .300999	.000409 to .000426	.000030 to .000034	.1125043	.0000091
2,3,4-Trimethylpentane		5		5	2.45424 to 2.56721	.001937 to .001950	.001199 to .001516	.000074 to .000102	.276063 to .289019	.000409 to .000422	.000077 to .000084	.1124729	.0000123

[a] The numbers in columns *A*, *B*, and *C* indicate the number of experiments performed with calorimeter systems *A*, *B*, and *C* (see section V-1 and section VII-1 of reference [4]).
[b] Samples I and II were used in the experiments with calorimeter systems *B* and *C*, respectively.
[c] All the values of *B* were converted to apply to calorimetric system *C* (see section VII-1 of reference [4]).

TABLE 4.—*Results of the calorimetric combustion experiments with gelatin*

Experiment No. [a]	Mass of gelatin	Mass of benzoic acid	k	K	U	ΔR_c	Δr_i	Δr_n	Δr (benzoic acid) [b]	B'	Deviation from mean	Mass CO_2 / Mass gelatin	Deviation from mean
Series I:	*g*	*g*	*min*$^{-1}$	*Ohm*	*Ohm*	*Ohm*	*Ohm*	*Ohm*	*Ohm*	*Ohm/g gelatin*	*Ohm/g gelatin*	*g* CO_2*/g gelatin*	*g* CO_2*/g gelatin*
1	0.19019		0.001886	0.001343	0.000368	0.030331	0.000375	0.000098		0.156994	−0.000289	1.79184	−0.00047
2	.76263		.001923	.000530	.000317	.120500	.000384	.000410		.156977	−.000306	1.78953	−.00278
3	.72279		.001936	.000628	.000298	.114391	.000406	.000365		.157208	−.000075	1.79145	−.00086
4	.77277		.001927	.000532	.000304	.122587	.000418	.000400		.157588	.000305	1.79535	.00304
Series II:													
5	.19597	1.34079	.001957	.001171	.000395	.288651	.000415	.000180	0.257274	.156958	−.000325	[c] 1.79339	.00108
6	.20141	1.34037	.001952	.001192	.000245	.289533	.000304	.000196	.257193	.157971	.000688		
Mean										0.157283		1.79231	
Standard deviation of the mean										±0.000169		±0.00098	

[a] All of these experiments were performed with calorimeter system *C* (see section V–1 and section VII–1 of reference [4]).
[b] Calculated from the mass of benzoic acid, using 26,428.4 int. J/g for the heat of the bomb process under standard conditions [11].
[c] The mass of carbon dioxide arising from the benzoic acid was calculated from the mass of the benzoic acid, using a stoichiometrical value of unity, as determined in other experiments [12].

TABLE 5.—*Results of the calorimetric combustion experiments on 2,2,3,3-Tetramethylbutane*

Experiment No. [a]	Mass of gelatin	Total mass of carbon dioxide formed	Mass of carbon dioxide formed from 2, 2, 3, 3-tetramethylbutane	k	K	U	ΔR_c	Δr_i	Δr_n	Δr (gelatin)	B	Deviation from mean
	g	*g*	*g*	*min*$^{-1}$	*Ohm*	*Ohm*	*Ohm*	*Ohm*	*Ohm*	*Ohm*	*Ohm/g* CO_2	*Ohm/g* CO_2
1	0.17509	3.91090	3.59708	0.001953	−0.002421	0.000211	0.431586	0.000407	0.000187	0.027539	0.1121590	−0.0000274
2	.18258	3.32958	3.00234	.001953	−.000887	.000267	.366063	.000412	.000162	.028717	.1121662	−.0000202
3	.16505	2.24386	1.94804	.001939	.002432	.000307	.245180	.000415	.000177	.025960	.1122241	.0000377
4	.15359	2.59138	2.31610	.001944	.001387	.000277	.284606	.000427	.000152	.024157	.1121964	.0000100
Mean											0.1121864	
Standard deviation of the mean											±0.0000149	

[a] All these experiments were performed with calorimeter system *C* (see section V–1 and section VII–1, of reference [4]).

TABLE 6.—*Heats of isomerization of the octanes in the liquid (or solid) state* [a]

Standard deviation of the mean				±0.0000149		

[a] All these experiments were performed with calorimeter system *C* (see section V–1 and section VII–1, of reference 10).

TABLE 6.—*Heats of isomerization of the octanes in the liquid (or solid) state* [a]

Substance	State	*B* at 28.00° C	Ratio of the heats of combustion in the bomb process B_l/B_s at 28.00° C	Difference in the heats of combustion in the bomb process [b] $(-\Delta U_B)_s - (-\Delta U_B)_l$ at 28° C	Heats of isomerization of the condensed phase $H_l°$ (liq or solid) $-H_s°$ (liq) at 25° C	
		Ohm/g CO_2		*Int. kj/mole*	*Int. kj/mole*	*kcal/mole*
n-Octane	Liquid	0.1125810 ±0.0000124	1.000000	0.00	0.00	0.00
2-Methylheptane	do	.1124730 ±0.0000142	0.999041 ±0.000168	5.23 ±0.92	−5.23 ±0.92	−1.25 ±0.22
3-Methylheptane	do	.1125282 ±0.0000100	.999531 ±0.000142	2.56 ±0.78	−2.56 ±0.78	−0.61 ±0.19
4-Methylheptane	do	.1125434 ±0.0000106	.999666 ±0.000145	1.82 ±0.79	−1.82 ±0.79	−.44 ±0.19
3-Ethylhexane	do	.1125690 ±0.0000078	.999893 ±0.000130	0.58 ±0.71	−0.58 ±0.71	−.14 ±0.17
2, 2-Dimethylhexane	do	.1123315 ±0.0000050	.997784 ±0.000119	12.10 ±0.65	−12.10 ±0.65	−2.89 ±0.16
2, 3-Dimethylhexane [c]	do	.1125232 ±0.0000208	.999487 ±0.000215	2.80 ±1.17	−2.80 ±1.17	−0.67 ±0.28
2, 4-Dimethylhexane	do	.1124320 ±0.0000098	.998677 ±0.000140	7.22 ±0.76	−7.22 ±0.76	−1.73 ±0.18
2, 5-Dimethylhexane	do	.1123625 ±0.0000208	.998059 ±0.000215	10.60 ±1.17	−10.60 ±1.17	−2.53 ±0.28
3, 3-Dimethylhexane	do	.1124209 ±0.0000072	.998578 ±0.000128	7.76 ±0.70	−7.76 ±0.70	−1.85 ±0.17
3, 4-Dimethylhexane	do	.1125389 ±0.0000220	.999626 ±0.000226	2.04 ±1.23	−2.04 ±1.23	−0.49 ±0.29
2-Methyl-3-ethylpentane	do	.1125857 ±0.0000148	1.000042 ±0.000172	−0.23 ±0.94	+0.23 ±0.94	+.05 ±0.22
3-Methyl-3-ethylpentane	do	.1125184 ±0.0000134	0.999444 ±0.000162	3.04 ±0.88	−3.04 ±0.88	−.73 ±0.21
2, 2, 3-Trimethylpentane	do	.1124337 ±0.0000204	.998692 ±0.000212	7.14 ±1.16	−7.10 ±1.16	−1.70 ±0.28
2, 2, 4-Trimethylpentane	do	.1123867 ±0.0000172	.998274 ±0.000189	9.42 ±1.03	−9.38 ±1.03	−2.24 ±0.25
2, 3, 3-Trimethylpentane	do	.1125043 ±0.0000182	.999319 ±0.000196	3.72 ±1.07	−3.72 ±1.07	−0.89 ±0.26
2, 3, 4-Trimethylpentane	do	.1124729 ±0.0000246	.999040 ±0.000245	5.24 ±1.34	−5.25 ±1.34	−1.25 ±0.32
2, 2, 3, 3-Tetramethylbutane	Solid	.1121864 ±0.0000298	.996495 ±0.000287	19.13 ±1.57	−18.84 ±1.57	−4.50 ±0.38

[a] All the uncertainties assigned to the experimental quantities in this table are equal to twice the standard deviation of the mean. The uncertainty to be assigned to the value of the heat of isomerization of any one of the isomers into any other one may conservatively be taken, on the average, as ±0.25 kcal/mole, except that when one of the isomers is 2,2,3,3-tetramethylbutane the uncertainty may be taken as ±0.40 kcal/mole and except for 2,3-dimethylhexane, for which see footnote c below.

[b] Obtained by subtracting the value in column 4 from unity and multiplying with the factor 5,458.8 int. kj/mole (see text).

[c] The values assigned to 2,3-dimethylhexane may be uncertain by several times the amount indicated because of the uncertainty as to purity (see tables 1 and 2).

The values in column 6 differ from those in column 5 because of the difference in the heat capacities of the isomers over the range 25° to 28° C, the Washburn conversion to zero pressure [20], and the conversion of ΔU to $\Delta(U+PV)=\Delta H$. Account was taken of the effect of the gelatin and of benzoic acid on the Washburn correction of the results of the experiments given in tables 4 and 5.

In table 7 are given values for the following: The heat of isomerization, for the condensed phase, of *n*-octane into each isomer, at 25° C and 1 atm, as given in table 6; the difference, between *n*-octane and each isomer, in the heat of vaporization (sublimation for 2, 2, 3, 3-tetramethylbutane), at 25° C, as taken from the work of Osborne and Ginnings [5], reduced to the ideal state [10]; the heat of isomerization, for the ideal gaseous state, of *n*-octane into each isomer at 25° C; the difference, between *n*-octane and each isomer, in the value of $H^\circ_{298.16}-H^\circ_0$, the heat content at 298.16° K (25° C) referred to the absolute zero, for the ideal gaseous state [6]; and, finally, the energy of isomerization, for the ideal gaseous state, of *n*-octane into each isomer at 0° K.

TABLE 7.—*Heats of isomerization of the octanes in the gaseous state* [a]

Substance	Heat of isomerization of the condensed phase [b] H°_i (liq or solid) − H°_n (liq) at 25° C		Difference in the heats of vaporization [c] $(\Delta He^\circ)_n-(\Delta He^\circ)_i$ at 25° C	Heat of isomerization of the gas H°_i (g) − H°_n (g) at 25° C	$(H^\circ_{298.16}-H^\circ_0)_n-(H^\circ_{298.16}-H^\circ_0)_i$	Heat of isomerization of the gas H°_i (g) − H°_n (g) at 0° K
	int. kj/mole	*kcal/mole*	*kcal/mole*	*kcal/mole*	*kcal/mole*	*kcal/mole*
n-Octane	0.00	0.00	0.00	0.00	0.00	0.00
2-Methylheptane	−5.23±0.92	−1.25±0.22	.43±0.01	−1.68±0.22	−.59±0.20	−1.09±0.30
3-Methylheptane	−2.56±0.78	−0.61±0.19	.39±0.01	−1.00±0.19	−.69±0.25	−0.31±0.31
4-Methylheptane	−1.82±0.79	−.44±0.19	.43±0.01	−0.87±0.19	−.77±0.25	−.10±0.31
3-Ethylhexane	−0.58±0.71	−.14±0.17	.44±0.01	−.58±0.17	−1.20±0.40	+.62±0.43
2, 2-Dimethylhexane	−12.10±0.65	−2.89±0.16	1.00±0.01	−3.89±0.16	−0.99±0.35	−2.90±0.39
2, 3-Dimethylhexane [d]	−2.80±1.17	−0.67±0.28	0.64±0.01	−1.31±0.28	−.88±0.30	−0.43±0.41
2, 4-Dimethylhexane	−7.22±0.76	−1.73±0.18	.89±0.01	−2.62±0.18	−1.21±0.40	−1.41±0.44
2, 5-Dimethylhexane	−10.60±1.17	−2.53±0.28	.86±0.01	−3.39±0.28	−1.11±0.35	−2.28±0.45
3, 3-Dimethylhexane	−7.76±0.70	−1.85±0.17	.94±0.01	−2.79±0.17	−1.22±0.40	−1.57±0.43
3, 4-Dimethylhexane	−2.04±1.23	−0.49±0.29	.60±0.01	−1.09±0.29	−0.90±0.30	−0.19±0.42
2-Methyl-3-ethylpentane	+0.23±0.94	+.05±0.22	.71±0.01	−0.66±0.22	−1.03±0.35	+.37±0.41
3-Methyl-3-ethylpentane	−3.04±0.88	−.73±0.21	.81±0.01	−1.56±0.21	−1.21±0.40	−.35±0.45
2, 2, 3-Trimethylpentane	−7.10±1.16	−1.70±0.28	1.09±0.01	−2.79±0.28	−1.35±0.45	−1.44±0.53
2, 2, 4-Trimethylpentane	−9.38±1.03	−2.24±0.25	1.51±0.01	−3.75±0.25	−1.35±0.45	−2.40±0.52
2, 3, 3-Trimethylpentane	−3.72±1.07	−0.89±0.26	1.02±0.01	−1.91±0.26	−1.23±0.40	−0.68±0.48
2, 3, 4-Trimethylpentane	−5.25±1.34	−1.25±0.32	0.90±0.01	−2.15±0.32	−1.36±0.45	−.79±0.55
2, 2, 3, 3-Tetramethylbutane	−18.84±1.57	−4.50±0.38	−.33±0.01	−4.17±0.38	−1.41±0.45	−2.76±0.59

[a] The uncertainty to be assigned to the value of the heat of isomerization of any one of the isomers into any other one may be taken as ±0.25 kcal/mole for the condensed phase at 25° C, ±0.25 kcal/mole for the gas at 25° C, and ±0.50 kcal/mole for the gas at 0° K, except for 2,2,3,3-tetramethylbutane for which the uncertainty is somewhat larger, and except for 2,3-dimethylhexane, for which see footnote "d" below.

[b] All are liquid except 2, 2, 3, 3-tetramethylbutane, which is solid.

[c] For the solid 2, 2, 3, 3-tetramethylbutane, the heat of sublimation is involved.

[d] The values assigned to 2,3-dimethylhexane may be uncertain by several times the amount indicated because of the uncertainty as to purity (see tables 1 and 2).

VI. DATA OF PREVIOUS INVESTIGATIONS

The only published papers describing the determination of the heat of combustion of one or more octanes are the following:

Investigators	Year	Reference	Compounds
Zubow	1898	[14]	*n*-Octane
Richards and Jesse	1910	[15]	*n*-Octane 2-Methylheptane 3-Ethylhexane 2,5-Dimethylhexane 3,4-Dimethylhexane
Jessup	1928	[16]	*n*-Octane 2,2,4-Trimethylpentane 2,2,3,3-Tetramethylbutane
Banse and Parks	1933	[17]	*n*-Octane
Jessup	1937	[18]	*n*-Octane

Of the foregoing data, only those of Richards and Jesse [15] and of Jessup [16] yield values for the heats of isomerization of any of the octanes.

The data of Richards and Jesse [15] yield the following values for the ratio of the heat of combustion of a given isomer to the heat of combustion of *n*-octane: *n*-octane, 1.0000; 2-methylheptane, 1.0010; 3-ethylhexane, 0.9983; 2,5-dimethylhexane, 0.9990; 3,4-dimethylhexane, 0.9993. The corresponding values of heats of isomerization for the four isoparaffins become, for *n*-octane into a given isomer, in the liquid state, $\Delta H = +1.3$, -2.2, -1.3, -0.9 kcal/mole, respectively. The corresponding values from the present investigation are -1.25, -0.14, -2.53, -0.49 kcal/mole, respectively. Since the values from Richards and Jesse may be uncertain by as much as 2 kcal/mole or more, it is seen that their data are substantially in accord with those of the present investigation within the respective limits of uncertainty.

The data of Jessup [16] were obtained in an investigation in which circumstances made it possible to perform only two complete combustion experiments on each of three isomers. His data yield, for the heat of isomerization of liquid *n*-octane into liquid 2,2,4-trimethylpentane and into solid 2,2,3,3-tetramethylbutane, $\Delta H = -1.8$ and -3.2 kcal/mole, respectively. The corresponding values from the present investigation are -2.24 and -4.50 kcal/mole. Because of the then unavoidable limitations placed upon these experiments of Jessup, the values of heats of isomerization deduced from them are arbitrarily assigned an uncertainty of ± 1.0 kcal/mole. It is seen that Jessup's values are in accord with those of the present investigation within the respective limits of uncertainty.

VII. DISCUSSION

As has been previously pointed out, values of the heats of isomerization of the octanes, along with those of the other paraffin hydrocarbons, are needed in calculating, in combination with free-energy functions, values of the free energies of isomerization and in studying

the influence of structure upon the energy content of the molecule.

With regard to the correlation of the energy content with structure, a separate report will be made. It may be pointed out here, however, that the data on the energies of isomerization of the octanes are in accord with the generalization previously made [1, 3] concerning the change with structure of the energy content of hydrocarbons.

The use of these data on energies of isomerization for calculating equilibria and free energies of isomerization of the 18 octanes is discussed in another report [13].

VIII. REFERENCES

[1] F. D. Rossini, Chem. Rev. **27,** 1 (1940).
[2] E. J. Prosen and F. D. Rossini, J. Research NBS **27,** 289 (1941) RP1420.
[3] E. J. Prosen and F. D. Rossini, J. Research NBS **27,** 519 (1941) RP1439.
[4] E. J. Prosen and F. D. Rossini, J. Research NBS **33,** 255 (1944) RP1607.
[5] N. S. Osborne and D. C. Ginnings, National Bureau of Standards. Unpublished data.
[6] K. S. Pitzer, University of California. Unpublished data.
[7] E. F. Mueller and F. D. Rossini, Am. J. Phys. **12,** 1 (1944).
[8] G. P. Baxter, M. Guichard, O. Hönigschmid, and R. Whytlaw-Gray, J. Am. Chem. Soc. **63,** 845 (1941).
[9] F. D. Rossini and W. E. Deming, J. Wash. Acad. Sci. **29,** 416 (1939).
[10] D. D. Wagman, W. J. Taylor, and F. D. Rossini, National Bureau of Standards. Unpublished data.
[11] R. S. Jessup, J. Research NBS **29,** 247 (1942) RP1499.
[12] E. J. Prosen and F. D. Rossini, J. Research NBS **33,** 439 (1944) RP1619.
[13] E. J. Prosen, K. S. Pitzer and F. D. Rossini. J. Research NBS **34,** 255 (1945) RP1641.
[14] P. Zubow, J. Russ. Phys. Chem. Soc. **30,** 926 (1898).
[15] T. W. Richards and R. H. Jesse, Jr., J. Am. Chem. Soc. **32,** 268 (1910).
[16] R. S. Jessup, National Bureau of Standards. Unpublished data. (1928.)
[17] H. Banse and G. S. Parks, J. Am. Chem. Soc. **55,** 3223 (1933).
[18] R. S. Jessup, J. Research NBS **18,** 115 (1937) RP966.
[19] A. R. Glasgow, Jr., and F. D. Rossini, National Bureau of Standards. Unpublished data.
[20] E. W. Washburn, J. Research NBS **10,** 525 (1933) RP546.

WASHINGTON, March 30, 1944.

U. S. DEPARTMENT OF COMMERCE NATIONAL BUREAU OF STANDARDS

RESEARCH PAPER RP1636

Part of Journal of Research of the National Bureau of Standards, Volume 34, February 1945

REGION OF USABLE IMAGERY IN AIRPLANE-CAMERA LENSES

By Francis E. Washer

ABSTRACT

The proper positioning of a lens with respect to the focal plane in a fixed-focus camera, such as an airplane-mapping camera, is governed by several factors that relate to the optical qualities of the lens. These factors are quality of imagery, depth of focus at a given stop opening, and curvature of field. This investigation shows that there is reasonably good agreement between observed depth of focus at a given stop opening and that predicted on the basis of geometric optics. Observed values of the maximum resolving power at various angular separations from the axis are generally lower at the larger stop openings than values predicted on the basis of physical optics. This lowering is doubtless a consequence of residual aberrations, inherent in an actual lens, which are more noticeable at large aperture ratios. A method of presenting the resolving power characteristics throughout the range of useful imagery in the form of sets of master curves has been developed. These curves show at a glance the variation of resolving power with distance from the plane of best axial imagery, the depth of focus for any observed value of the resolving power, the effect of field curvature on imagery in any given image plane, and the differing performance for tangential and radial imagery at various angular separations from the axis. Successive groups of these master curves show how variations in stop opening affect the performance of a lens.

CONTENTS

	Page
I. Introduction	175
II. Method	176
III. Theory	177
1. Maximum resolving power of an ideal lens	177
2. Depth of focus for an ideal lens	178
IV. Results of measurement	180
1. Variation in depth of focus on the axis with stop opening	187
2. Variation in resolving power on the axis with stop opening	191
3. Effect of field curvature	192
4. Change in depth of focus with angular separation from the axis	193
5. Change in maximum resolving power with angular separation from the axis	195
6. Variation of resolving power in a given image plane with stop opening	197

I. INTRODUCTION

In the use of aerial photographs for mapping, the quality of definition is of considerable importance. Since quality of definition in a photograph is directly related to the resolving power of the lens used

in the aerial camera, the factors affecting resolving power throughout the entire area of the image plane are of special interest. These factors are depth of focus, stop opening, and curvature of field. All of these factors are considered in the proper positioning of the lens in the camera. For a lens free from aberration, the image plane of best definition is unique and its position can readily be determined theoretically, but for an actual lens it is necessary to resort to experiment and to compromise upon a position of the lens that yields best average definition throughout the image plane. This is usually done at the maximum stop opening of the lens, and this setting is then held, in the fixed-focus airplane camera, for all smaller stop openings.

Since the position of best average definition for a lens is generally determined with the lens not mounted in a camera, and since the lens may then be mounted in such manner that the distance from rear vertex of lens to image plane (back focal length) is not that prescribed for best average definition, it is of interest to know how great a departure from the prescribed position is allowable before the deterioration of imagery becomes sufficient to impair the usefulness of the camera. These tolerances are best determined from information on the depth of focus and curvature of field of lenses used in practice. The present paper therefore shows the results of measurement on resolving power for several typical airplane camera lenses. This information is presented in such manner that the effect of depth of focus, stop opening, and curvature of field is readily apparent.

II. METHOD

The precision lens testing camera [1] is well suited to the study of the resolving power characteristics of a lens throughout the region of usable imagery. The only modification in procedure from that previously reported [2] is the increasing of the range through which the camera back moves in making a resolving power negative. Fifty-seven steps instead of nineteen are made, and the negative shows the resolving power at definite intervals from 6.5 mm nearer to the lens to 6.5 mm farther from the lens than the plane of best axial focus. The negatives are examined under a microscope and the resolving powers recorded for each image. A pattern is not considered resolved unless all coarser patterns are also resolved and the number of lines in the resolved patterns agree with that of the corresponding patterns in the test chart. In this manner, the values of the resolving power are determined for each of the 57 image planes at every 5° interval from the axis from 0° to the limiting angle set by the lens. By making such a negative for each stop opening, the region of usable imagery is explored throughout the range of aperture selected.

Although a large number of lenses have been studied in this manner the results of only four are here presented, and of these four, two are selected for a more complete description. The lenses selected are representative of a wide range of focal lengths, angular fields, and function in mapping. Lens *A* is a wide angle airplane-mapping lens, nominal focal length is 150 mm, maximum aperture *f*/6, and a useful field of view 45°. Lens *B* is a lens usable in copying cameras or for general photography; it has a nominal focal length of 195 mm, maximum aperture *f*/5.6, and a normally useful field angle between 20°

[1] J. Research NBS **18**, 449 (1937) RP984.
[2] J. Research NBS **23**, 729 (1939) RP1216.

and 25°. Lens C is usable in copying cameras or for general photography; it has a nominal focal length of 210 mm, maximum aperture $f/6.8$ and a normally useful field angle of 25°. Lens D is frequently used in aerial cameras and also in copying cameras; it has a nominal focal length of 125 mm, maximum aperture $f/8$, and a normally useful field angle of 35°. Lenses A and B have been selected for the fuller description of their resolving power characteristics whereas C and D are limited to a partial description.

III. THEORY

A brief discussion of the resolving power characteristics as predicted from theoretical considerations is necessary before proceeding to the results of measurements. This theory has long been established and predictions from it will be used in this article only for the purpose of providing a yardstick against which to compare the performance of the lenses studied. Since the predicted values of resolving power are for an ideal lens, it is not surprising that some apparent contradictions to the theory will be found in the experimental results. These deviations result from aberrations inherent in any actual lens. These departures do not however signify that the theory is without value in the prediction of lens performance. On the contrary, the number of times that the observed data are of the same order of magnitude as the predicted values is sufficiently high that one may feel more confident than ever that the predicted values are sufficiently close to the true values as to render them a valuable aid. This is particularly true when dealing with resolving powers of the same order of magnitude as those of the more commonly used photographic emulsions.

1. MAXIMUM RESOLVING POWER OF AN IDEAL LENS

The smallest separation of two star images theoretically obtainable on the basis of diffraction of light is

$$X=\frac{1.22F\lambda}{d} \tag{1}$$

where X is the separation, F the focal length of the lens, d the diameter of the lens and λ the wavelength of the incident light. For the purpose of the present work, it will be assumed that the same equation is valid where the images are composed of parallel lines instead of points. It is also more convenient to express the maximum resolving power, A_m, in lines per millimeter. It can be shown that the equation,

$$A_m=\frac{1426}{b}\text{lines per millimeter,} \tag{2}$$

where b is the f-number, is equivalent to eq 1. This relation is computed for a wavelength of 575 millimicrons, which is the effective wavelength of the light used in making resolving power negatives with the precision lens-testing camera. This equation is valid only on the axis of the lens. For extra axial points, it is necessary to use the two

additional approximate relations, one for maximum resolving power for tangential lines,

$$A_{t\theta}=\frac{1426}{b}\cdot\cos^3\theta, \tag{3}$$

and another for maximum resolving power for radial lines,

$$A_{r\theta}=\frac{1426}{b}\cdot\cos\theta, \tag{4}$$

where θ is the angular separation from the axis of the point considered Table 1 gives the values computed for the resolving power in both orientations at 5° intervals from 0° to 45° for a series of f-numbers ranging from $f/4$ to $f/64$ in a form convenient for use.

TABLE 1.—*Maximum resolving power for an ideal lens as a function of stop opening in lines per millimeter*

Relative aperture or f-number	Resolving power for tangential lines. Angular distance from axis.									
	0°	5°	10°	15°	20°	25°	30°	35°	40°	45°
4	356	352	340	321	295	265	231	196	160	126
5.6	255	252	244	230	212	190	166	140	115	90
8	178	176	170	160	148	132	116	98	80	63
11	130	128	124	117	108	97	84	71	58	46
16	89	88	85	80	74	66	58	49	40	31
22	65	64	62	58	54	48	42	36	29	23
32	45	44	43	41	37	33	29	25	20	16
45	32	32	31	29	26	24	21	18	14	11
64	22	22	21	20	18	16	14	12	10	8
	Resolving power for radial lines. Angular distance from axis.									
	0°	5°	10°	15°	20°	25°	30°	35°	40°	45°
4	356	355	351	344	334	323	308	292	273	252
5.6	255	254	251	246	240	231	221	209	195	180
8	178	177	175	172	167	161	154	146	136	126
11	130	130	128	126	122	118	113	106	100	92
16	89	89	88	86	84	81	77	73	68	63
22	65	65	64	63	61	59	56	53	50	46
32	45	45	44	43	42	41	39	37	34	32
45	32	32	32	31	30	29	28	26	25	23
64	22	22	22	21	21	20	19	18	17	16

2. DEPTH OF FOCUS FOR AN IDEAL LENS

The term "depth of focus" as used throughout this paper refers to the range measured along the axis in the image space that may be traversed without the resolving power measured in the image plane falling below an arbitrarily selected value. It is not to be confused with "depth of field," which refers to the range in the object space for which all point objects are imaged with a radius of the circle of confusion remaining less than or equal to some arbitrarily selected value.

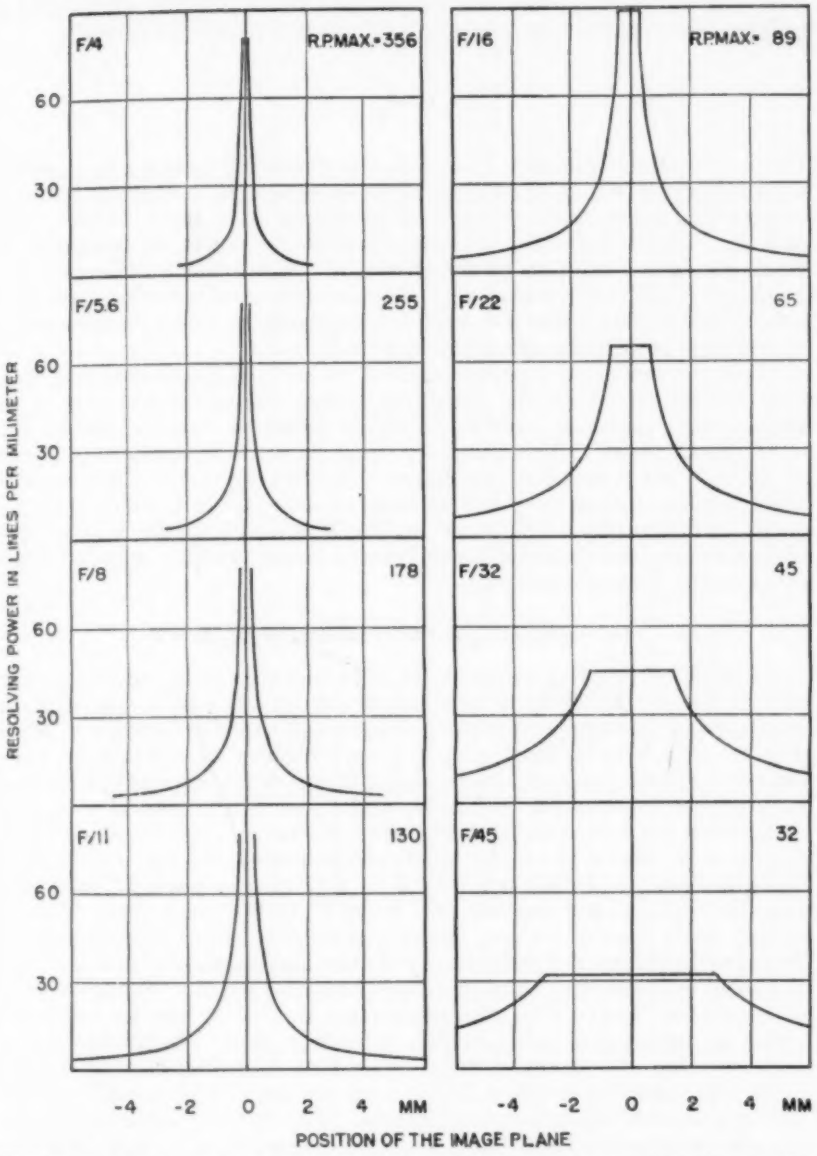

FIGURE 1.—*Axial resolving power versus position of the image plane for an ideal lens at several stop openings.*

Where the maximum value of the resolving power theoretically possible according to physical optics falls within the scale range of the graphs, a straight-line intercept parallel to the axis of abscissas is shown to indicate that it is not significant to extend higher the two curves, asymptotic to the focal plane, that are derived from geometric optics. Where this maximum falls outside the scale range of the graphs the asymptotic curves are left open at the top but are to be assumed to extend beyond the range of the graph to the theoretical maximum value of the resolving power, which is indicated in the upper right-hand corner of the frame for each stop opening. The zero of abscissas marks the position of best axial focus, and positive values of abscissas indicate positions farther from the lens.

It can be shown that the magnitude of the depth of focus d in millimeters can be approximately computed from the relation

$$d=\frac{4b}{a}, \tag{6}$$

where b is the f-number and a is the resolving power, in lines per millimeter, for which the depth of focus is sought. Eq 6 is based on geometric optics and is restricted to values of a lying between zero and A_m, where A_m is the maximum resolving power as computed by eq 2, which is based on physical optics. According to the theory of geometric optics the value of d is independent of angular separation from the axis for a given b, and consequently no additional equations for off-axis conditions are necessary.

With the aid of eq 6 supplemented by eq 2, it is possible to predict the manner in which the resolving power varies on the axis as the image plane assumes various positions along the axis in the vicinity of the focal plane. This has been done, and the results are presented in figure 1 for a series of apertures. It may be noted that values of the resolving power that are considered acceptable for lenses used in aerial photography, such as 20 on the axis and 7 at the wider angles of separation, are obtained throughout a considerable range of settings even at the largest aperture.

IV. RESULTS OF MEASUREMENT

In order to present a comprehensive picture of the performance of actual lenses throughout the entire region of usable imagery, the results of measurements on the two lenses A and B are shown in figures 2 to 8. For lens A, figures 2, 3, 4, and 5 show the resolving power curves for both tangential and radial imagery for all marked aperture ratios from $f/6$ to $f/45$, inclusive, and at each 5° interval of angular separation from the axis from 0° to 45°, inclusive. In a similar manner, figures 6, 7, and 8 show the resolving-power curves for lens B for all marked aperture ratios from $f/5.6$ to $f/32$ and at each 5° interval of angular separation from the axis from 0° to 30°, inclusive. For any one of these master curves, the ordinates give the resolving power in lines per millimeter clearly resolved; the corresponding abscissas give the axial distance from the plane of best axial focus. Negative values of abscissas signify that the points are nearer to the lens than the plane of best axial focus, which reference plane marks the zero of abscissas for all curves shown. The lens identification by symbol, focal length, and f-number is given in the upper-right-hand corner of the uppermost frame for each group. The type of imagery and the angular separation from the axis are indicated in the upper left-hand corner of each frame. Tangential imagery is signified by the letter T and radial imagery by the letter R.

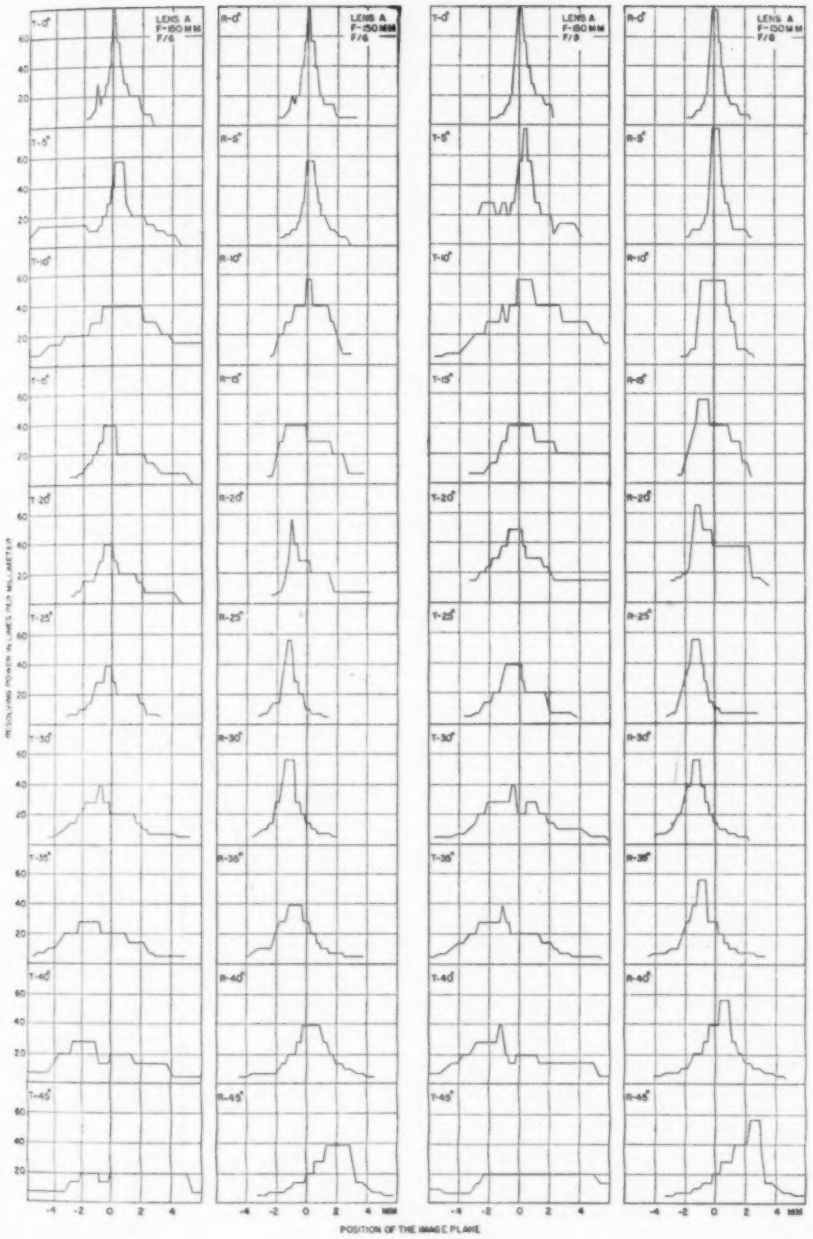

FIGURE 2.—*Resolving power versus position of the image plane for lens A at apertures f/6 and f/8.*

The resolving power throughout the region of useful imagery is shown for tangential (*T*) and radial (*R*) lines at 5° intervals from 0° to 45°. The zero of abscissa marks the position of best visual focus on the axis at /6, and positive values of abscissas indicate positions farther from the lens.

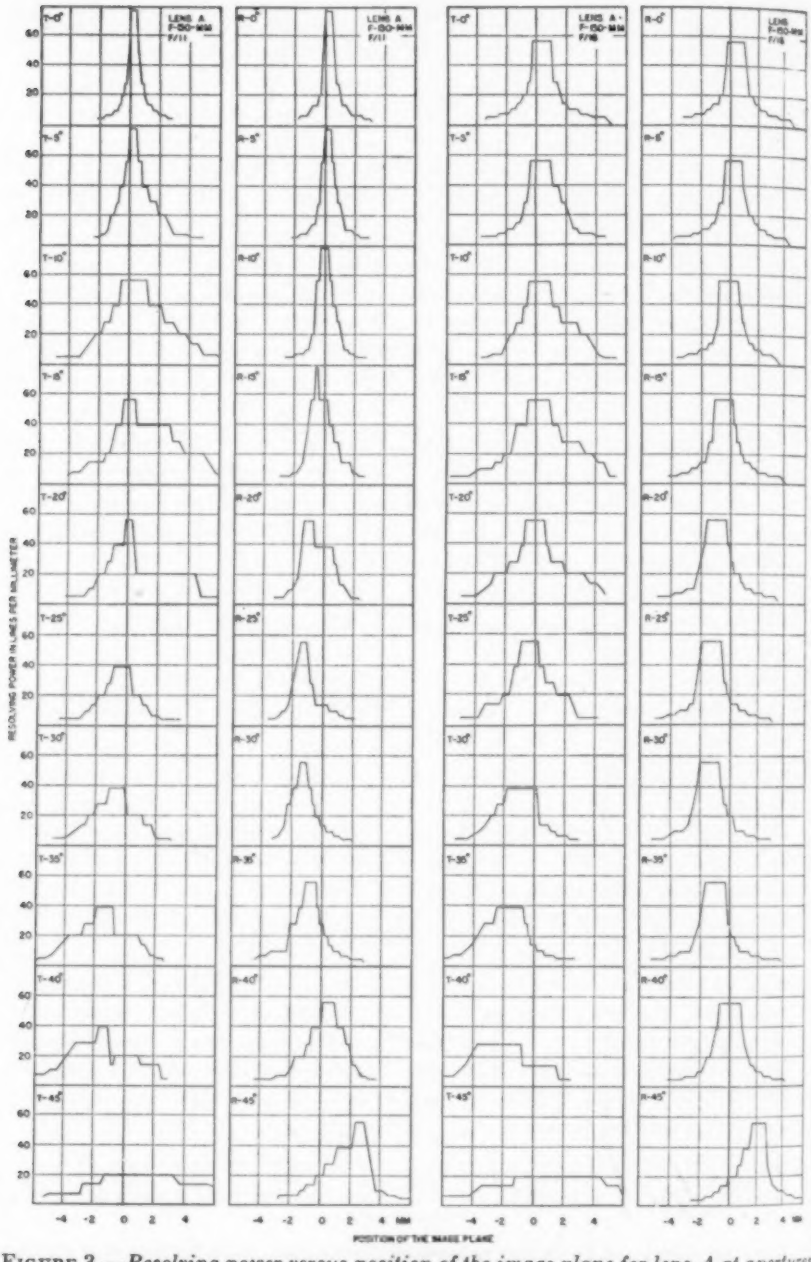

FIGURE 3.—*Resolving power versus position of the image plane for lens A at apertures f/11 and f/16.*

The resolving power throughout the region of useful imagery is shown for tangential (*T*) and radial (*R*) lines at 5° intervals from 0° to 45°. The zero of abscissas marks the position of best visual focus on the axis at *f*/6, and positive values of abscissas indicate positions farther from the lens.

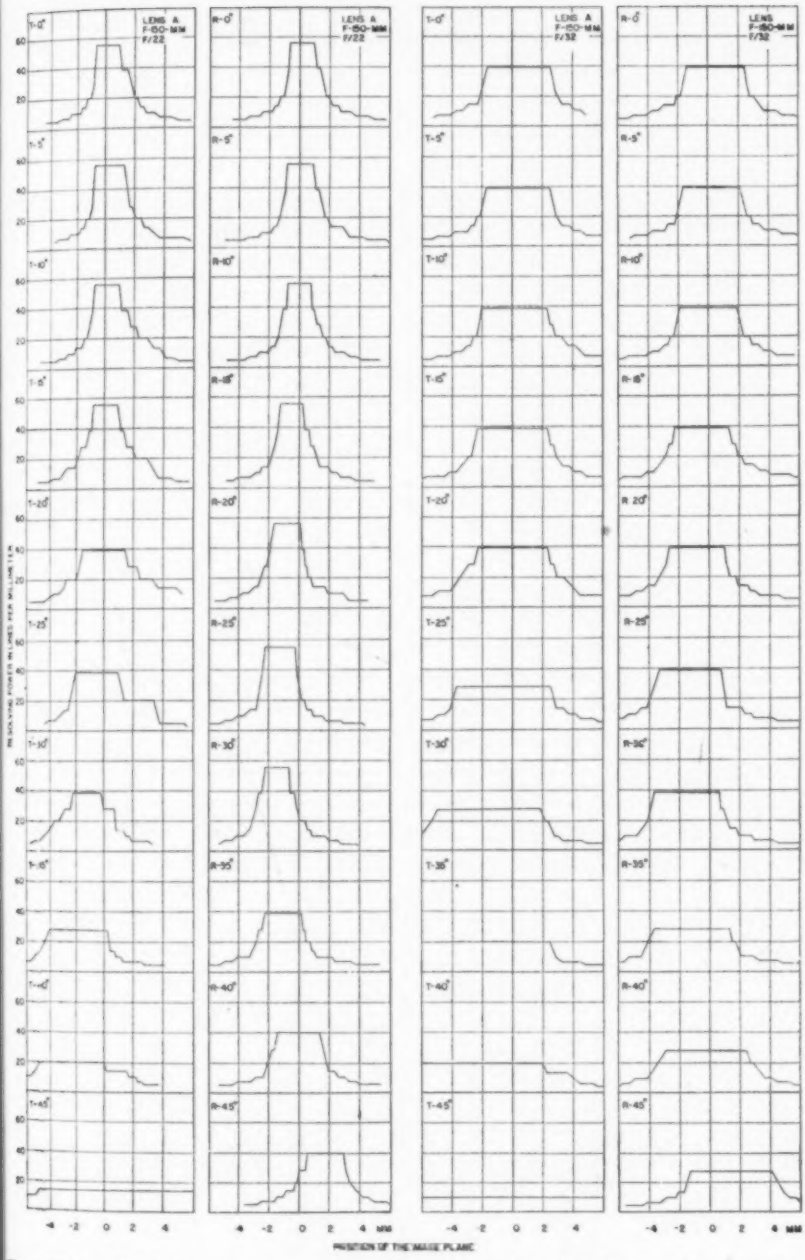

FIGURE 4.—*Resolving power versus position of the image plane for lens A at apertures f/22 and f/32.*

The resolving power throughout the region of useful imagery is shown for tangential (*T*) and radial (*R*) lines at 5° intervals from 0° to 45°. The zero of abscissas marks the position of best visual focus on the axis at 0°, and positive values of abscissas indicate positions farther from the lens.

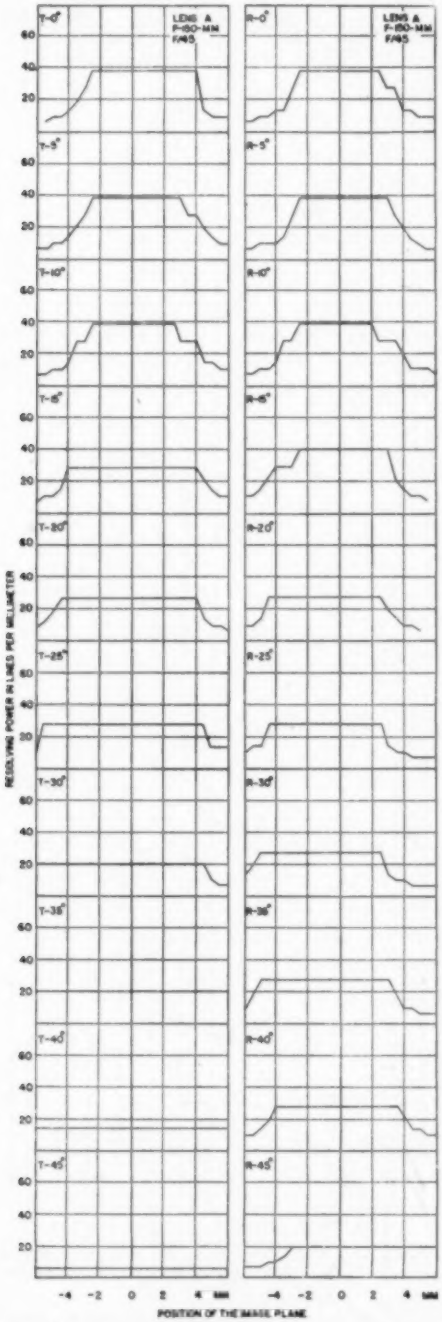

FIGURE 5.—*Resolving power versus position of the image plane for lens A at aperture f/45.*

The resolving power throughout the region of useful imagery is shown for tangential (*T*) and radial (*R*) lines at 5° intervals from 0° to 45°. The zero of abscissas marks the position of best visual focus on the axis at *f*/6, and positive values of abscissas indicate positions farther from the lens.

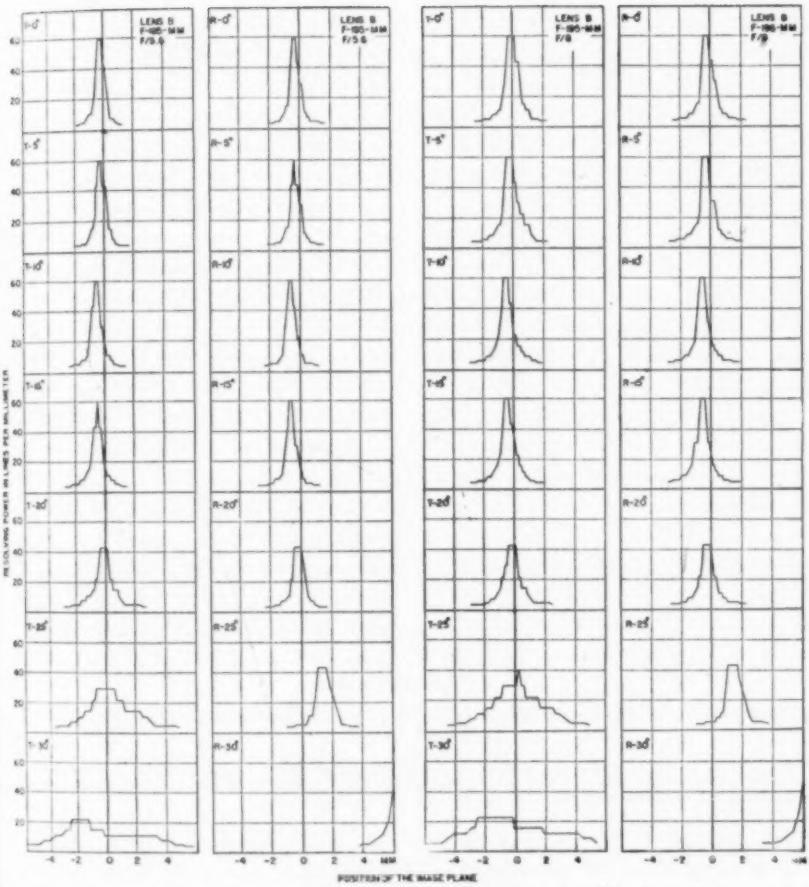

FIGURE 6.—*Resolving power versus position of the image plane for lens B at apertures f/5.6 and f/8.*

The resolving power throughout the region of useful imagery is shown for tangential (*T*) and radial (*R*) lines at 5° intervals from 0° to 30°. The zero of abscissas marks the position of best visual focus on the axis at f/5.6, and positive values of abscissas indicate positions farther from the lens.

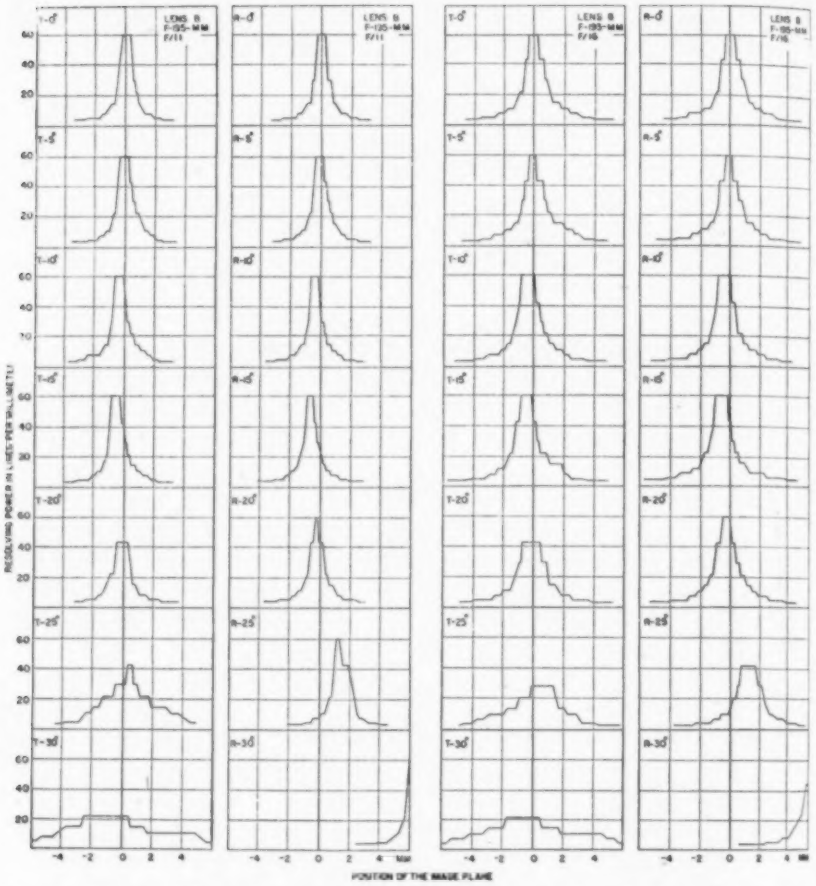

FIGURE 7.—*Resolving power versus position of the image plane for lens B at apertures f/11 and f/16.*

The resolving power throughout the region of useful imagery is shown for tangential (*T*) and radial (*R*) lines at 5° intervals for 0° to 30°. The zero of abscissas marks the position of best focus on the axis at *f*/5.6, and positive values of abscissas indicate positions farther from the lens.

Thoughtful examination of the curves in figures 2 to 8 yields a wealth of qualitative information on particular phases of lens performance and on the manner in which these separate phases form one coherent whole. However, in view of the complexity of the configuration when viewed as a whole, it is desirable to discuss in separate sections the various aspects of lens performance that are here shown in the integrated form. Chief among these aspects are depth of focus, effect of stop opening, variation with angular separation from the axis, and field curvature. In these sections data derived for lenses *C* and *D* from sets of curves similar to those in figures 2 to 8 (but not shown to conserve space) are presented and discussed in conjunction with the derived data for lenses *A* and *B*. In these discussions, the experimental results are also compared with those predicted from theory.

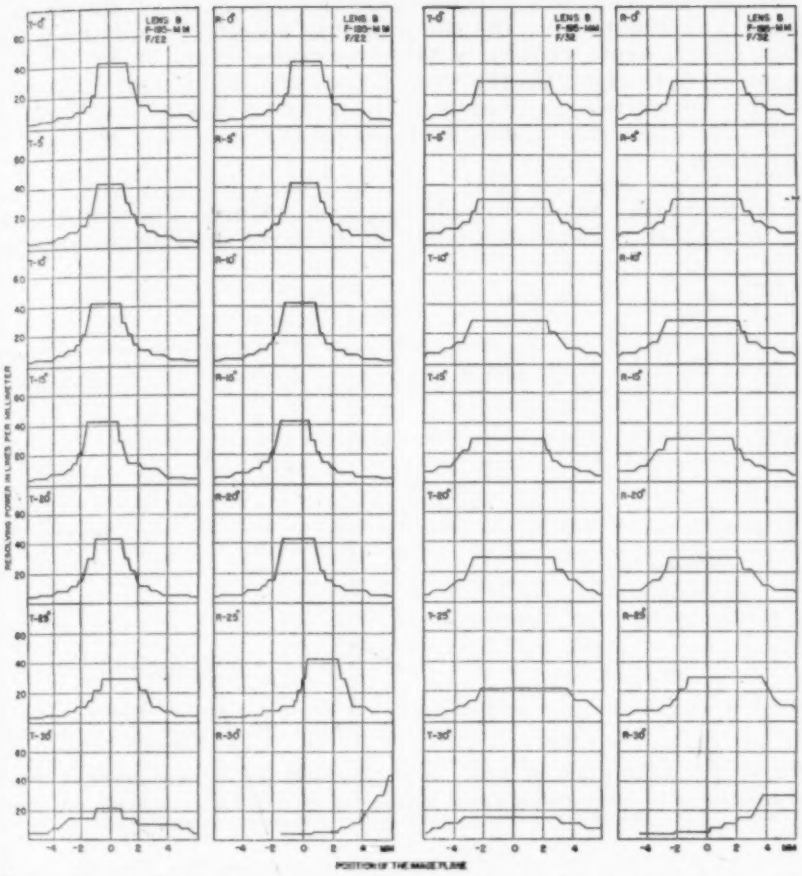

FIGURE 8.—*Resolving power versus position of the image plane for lens B at apertures f/22 and f/32.*

The resolving power throughout the region of useful imagery is shown for tangential (T) and radial (R) lines at 5° intervals from 0° to 30°. The zero of abscissas marks the position of best focus on the axis at $f/5.6$, and positive values of abscissas indicate positions farther from the lens.

1. VARIATION IN DEPTH OF FOCUS ON THE AXIS WITH STOP OPENING

When an infinitely distant object is imaged by a lens, the depth of focus is a measure of the range of positions along the optic axis that may be assumed by the image plane without reduction of the resolving power below a specified value. In figures 2 to 8 the depths of focus for any observed resolving power is simply the length of the segment of a straight line parallel to the axis of abscissas cut off by the curve at the selected value of resolving power. Thus the length of this segment for the maximum observed resolving power gives directly the depth of focus in millimeters. However, for comparison purposes, it is preferable to select some value of the resolving power that is attained at each stop opening for the lens considered.

The least axial resolving power allowable under most federal specifications dealing with lens performance is 20 lines per millimeter. It is

therefore pertinent to study the range throughout which this value is found and also to note the effect of stop opening. In figure 9, the variation of depth of focus with stop opening is shown for the four lenses *A*, *B*, *C*, and *D* for the resolving power of 20 lines per millimeter, or as near thereto as feasible. The actual value of the resolving power for which the measurements are made is indicated on curve 1 in each frame.

The values used for plotting curve 1 are computed with the aid of eq 6 for the indicated resolving power. Curve 2 is plotted from the experimental data, each circle on the curve showing the observed

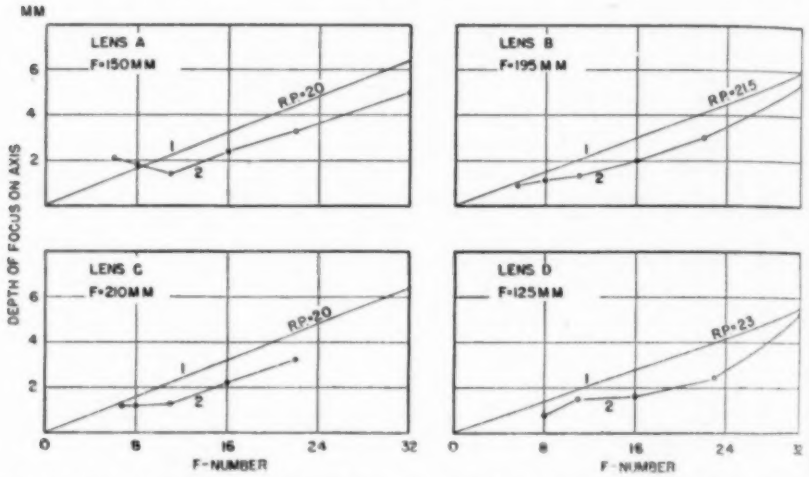

FIGURE 9.—*Axial depth of focus versus f-number for a fixed resolving power.*

Curve 1 shows the computed relation for an ideal lens, and curve 2 shows the observed relation for an actual lens. The value of the fixed resolving power in lines per millimeter is indicated on curve 1 for each lens.

value of d for the given f-number. It is noteworthy that the depth of focus for an actual lens does not always increase with diminishing aperture. In fact in some instances it may decrease, as is seen in the curve for lens *A*. Here the depth of focus decreases from $f/6$ to $f/11$, and then begins to increase and continues to increase in a linear fashion but at a slope less than that of curve 1. Thus at $f/6$ and $f/8$ the depth of focus is greater than that predicted, whereas at all smaller f-numbers it is substantially less than predicted. The predicted values are not exceeded for lenses *B*, *C*, and *D*. However, the increase with diminishing aperture appears to become more uniform at $f/11$ for *B* and *C*, and at $f/16$ for *D*.

It is clear from these four examples that the increase of depth of focus with diminishing aperture does not proceed in regular fashion until an aperture appreciably smaller than the maximum is reached. The value of the aperture ratio that marks the beginning of regular increase is usually $f/11$, although in some instances it begins as early as $f/8$ and in other instances as late as $f/16$. However, on the basis of many other examples not reported here, $f/11$ is the transition point in the majority of cases studied. In this region of uniform increase, the depth of focus, while increasing steadily with diminishing aperture, is nonetheless lower than that predicted by eq 6 and in most

cases 15 percent or more lower. The anomalous behavoir at large aperture ratios, such as is shown by lens *A* at *f*/6 and *f*/8, can only be accounted for by the presence of lens aberrations, which in some instances may so broaden the base of the resolving power curve that values of the depth of focus greater than predicted are found. If the

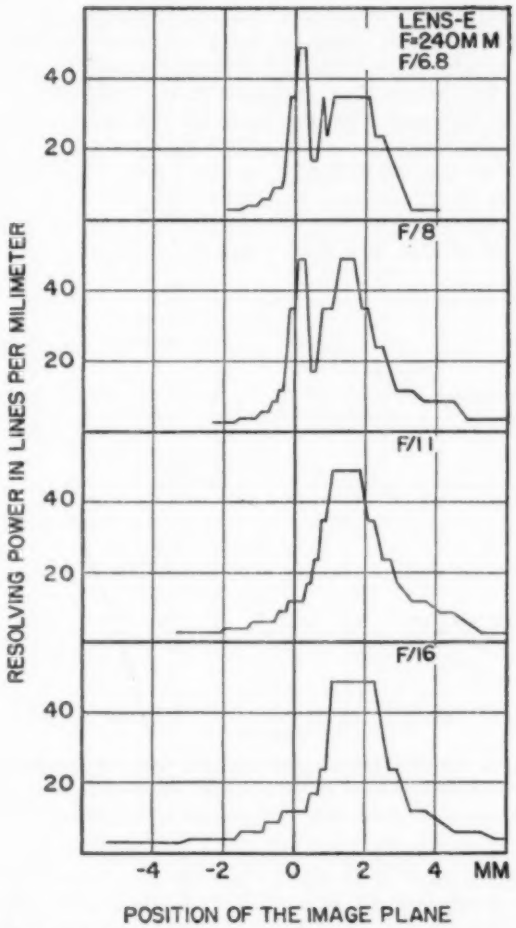

FIGURE 10.—*Axial resolving power versus position of the image plane for a lens possessing multiple foci at several stop openings.*

The zero of abscissas marks the position of best visual focus on the axis at *f*/6.8, and positive values of abscissas indicate positions farther from the lens.

axial imagery of such a lens as *A* be examined either visually with a microscope or photographically with finer test charts, then it is probable that two or more foci will be seen at full aperture. The axial separation of these foci may vary from a few tenths of a millimeter to more than a millimeter.

This phenomenon has been observed on other lenses and in figure 10, resolving-power curves for lens *E* at *f*/6.8, *f*/8, *f*/11, and *f*/16 show the effect in a striking manner. This lens shows three foci on the axis at

$f/6.8$, drops to two foci at $f/8$ and to a single focus at $f/11$ and $f/16$. It is evident that the outer zones are focused at a point nearer to the lens than the inner zones, the separation of foci in this instance amounting to nearly a millimeter. It is clear from the curves that, if the depth of focus is measured, say at 17 lines per millimeter, the depth of focus will decrease with diminishing aperture so long as conditions contributing to a multiple focus effect are present. Although only this one example is given, it is by no means unusual to find two or more foci on the axis with either visual or photographic means of observation. In the present instance it is evident that the principal focus is the one farthest from the lens, for it remains fixed with respect to the zero of abscissas for all aperture ratios shown. This effect may also account for the lowering of central definition with diminishing aperture which is sometimes observed. If the focal plane is located by the maximum nearest to the lens, the resolving power will be markedly lower at $f/11$ and $f/16$ than at $f/6.8$ and $f/8$.

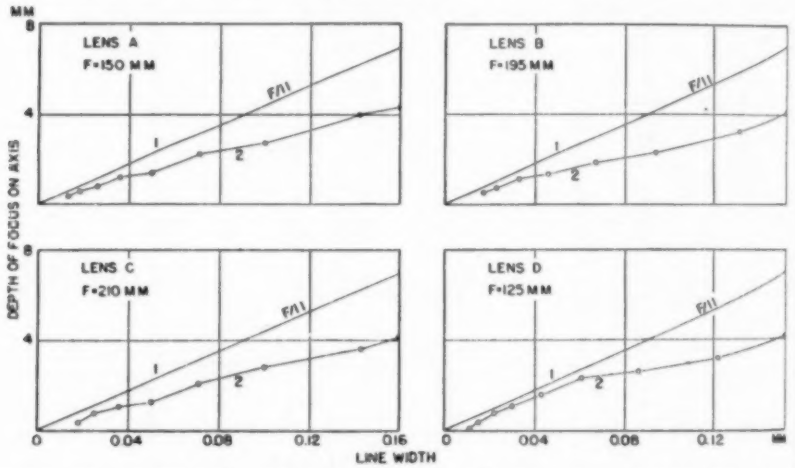

FIGURE 11.—*Axial depth of focus versus line width (or reciprocal of resolving power in lines per millimeter) for aperture f/11.*

Curve 1 shows the computed relation for an ideal lens, and curve 2 shows the observed relation for an actual lens.

From curves 2 to 8 it is clear that the depth of focus diminishes with increasing resolving power. To provide a more clear cut picture of this effect, the curves in figure 11 show the manner in which the depth of focus varies with resolving power for a given f-number, in this instance $f/11$. The reciprocals of resolving power, or line spacings, rather than values of resolving power are plotted as abscissas in order that the theoretical curve computed from eq 6 appear as a straight line instead of a rectangular hyperbola. Curve 1 shows the variation predicted and curve 2 shows that actually found. Aside from the observed values of depth of focus being lower than the predicted, there are no important deviations from theory. The curves do show the greater freedom in selection of a focal plane that exists for the lower resolving powers.

2. VARIATION IN RESOLVING POWER ON THE AXIS WITH STOP OPENING

The upper limit of resolving power, expressed in lines per millimeter, is determined by aperture ratio and wavelength of the image forming light. The capacity of a lens to yield this maximum resolving power is in practice impaired by lens aberrations. In the present instance, the patterns of the test chart are not sufficiently fine to show variations in the maximum resolving power at the larger stop openings. This is evident when it is noted that the maximum resolving power on the test chart for lens *A* is 78 lines per millimeter, which is higher than can be expected for *f*/22 and lower than predicted for *f*/16. For lens *B*, the test-chart maximum is 56, which is greater than the predicted value at *f*/32 and less than predicted at *f*/22.

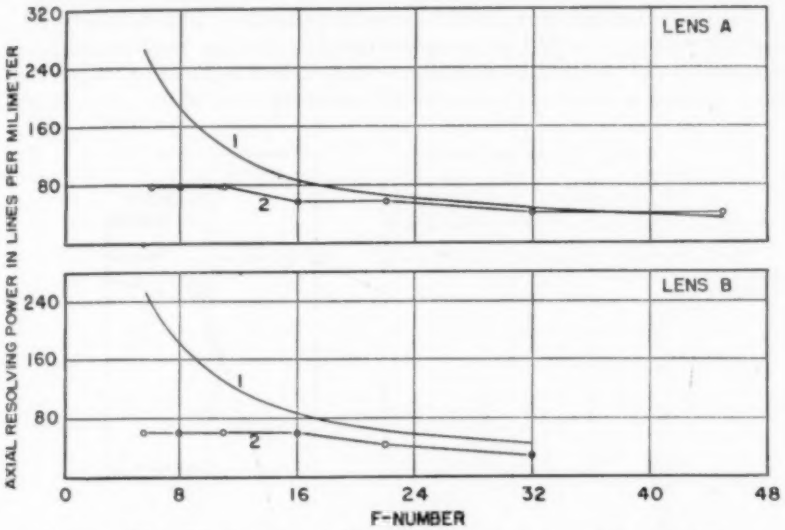

FIGURE 12.—*Maximum axial resolving power versus stop opening.*

Curve 1 shows the computed relation for an ideal lens for a wavelength of 575 millimicrons. Curve 2 shows the observed relation for an actual lens.

However, despite these limitation in the test-chart scale, some information on the change in resolving power with stop opening can be obtained from the curves in figures 2 to 8. To facilitate study, the maximum observed resolving power is plotted against *f*-number as curve 2 in figure 12 for lens *A* and *B*. Curve 1 in each frame shows the maximum theoretical resolving power.

For lens *A*, it is evident that the maximum fixed by the test chart is obtained for *f*/6, *f*/8, and *f*/11. However, the resolving power drops to 56 at *f*/16, which drop can be attributed to lens aberrations. The value of 56 is still maintained at *f*/22, and since the theoretical is only 65, it can be stated that the lens aberrations definitely affect the resolving power less at *f*/22 than at *f*/16. The two curves are nearly in coincidence at *f*/32 and *f*/45, thus clearly showing the drop in resolving power with diminishing aperture as well as demonstrating that the drop in resolving power at small apertures results from

theoretical limitations based on aperture rather than on the effect of lens aberrations.

In the case of lens *B*, the limitations imposed by the test chart preclude any effect becoming noticeable for most of the range; however, it is clear that lens aberrations are effective at *f*/22 and *f*/32 in preventing the lens from performing as predicted by theory.

3. EFFECT OF FIELD CURVATURE

It is apparent on examination of a given series of curves at a specified stop opening, for either tangential or radial imagery, that the position of maximum resolving power occurs at different distances from the position of best axial definition for the various angular separations from the axis. This effect is a result of curvature of the image field. The curves of primary and secondary curvature can readily be visualized if, while examining figures 2 to 8, one holds the page at an angle of 20° to 30° with the line of sight and looks along the page from the bottom to the top. The central regions of the tangential curves then describe the curve of primary curvature, and similarly

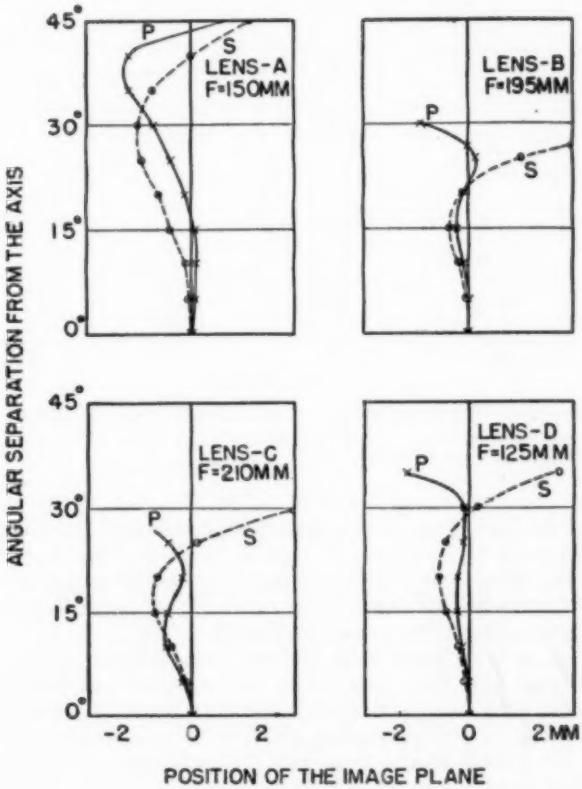

FIGURE 13.—*Field curvature.*

Curve *P* shows the primary curvature and is the locus of the positions of maximum resolving power for tangential lines at the indicated angular separations from the axis. Curve *S* shows the secondary curvature and is the locus of the positions of maximum resolving power for radial lines at the indicated angular separations from the axis. The zero of abscissas marks the position of best axial focus and positive values of abscissas indicate positions farther from the lens.

the central regions of the radial curves show the curve of secondary curvature.

The primary and secondary curvatures for lenses *A*, *B*, *C*, and *D* are shown in conventional form in figure 13. The curves, as drawn, represent an average value of the field curvature for several apertures and consequently do not portray precisely the observed field curvature at any single aperture. It was noted in the course of this investigation that the shape of the field curves changes appreciably when going from the largest stop opening to the smallest. However, it was not considered worthwhile to show this change in detail.

It is this effect produced by field curvature that makes it pointless to search out an image plane that yields say 200 lines per millimeter on the axis, because so placing the image plane automatically fixes the resolving power obtainable for the 30° region at 14 lines per millimeter or less. It is clear from the curves in figures 2 to 8, and 13 that no single image plane can include the position of maximum resolving power for all angular separations from the axis for either type of imagery. Consequently, selection of an image plane that will yield values of the resolving power sufficient for good usable photography in all parts of the image plane for both types of imagery is preferable to selection of the plane of best axial imagery. It may also be noted that this shift of the maxima of resolving power for the various angular separations from the axis justified setting the upper limit of the test-chart patterns to exceed that of the average emulsion but not necessarily to exceed the theoretical resolving power of the lens at the larger stop opening.

4. CHANGE IN DEPTH OF FOCUS WITH ANGULAR SEPARATION FROM THE AXIS

Examination of the curves in figures 2 to 8 shows that for a given *f*-number and specified resolving power the depth of focus is not generally constant. This behavior is markedly different from that which would be manifested by an ideal lens for which the depth of focus is constant under these conditions. Accordingly, curves illustrating this lack of constancy in depth of focus for the lenses studied are shown in figure 14. The resolving power in each case is 20 lines per millimeter or as near thereto as feasible, the actual value being indicated. The variation of depth of focus with angular separation from the axis is shown for a series of *f*-numbers for each of the lenses *A*, *B*, *C*, and *D*. The theoretical depth of focus on the axis is marked by a short line projecting from the axis of ordinates. It must be borne in mind that the ordinates for any value of the abscissas represent only the range throughout which the particular resolving power for that type of imagery is observed, and the curves do not show the space relationship of these ranges with respect to one another. It is possible to draw curves, showing the depth of focus, that preserve the space relationships but since this would involve the effect of field curvature, the change in depth of focus with angle would be somewhat obscured.

It is noteworthy that of these four examples only lens *B* preserves a near constancy of depth of focus for tangential and radial lines with angular separation from the axis, and that even here there is an abrupt change between 20° and 25°. Since this change is more pronounced at the larger stop opening, it is probable that the increase

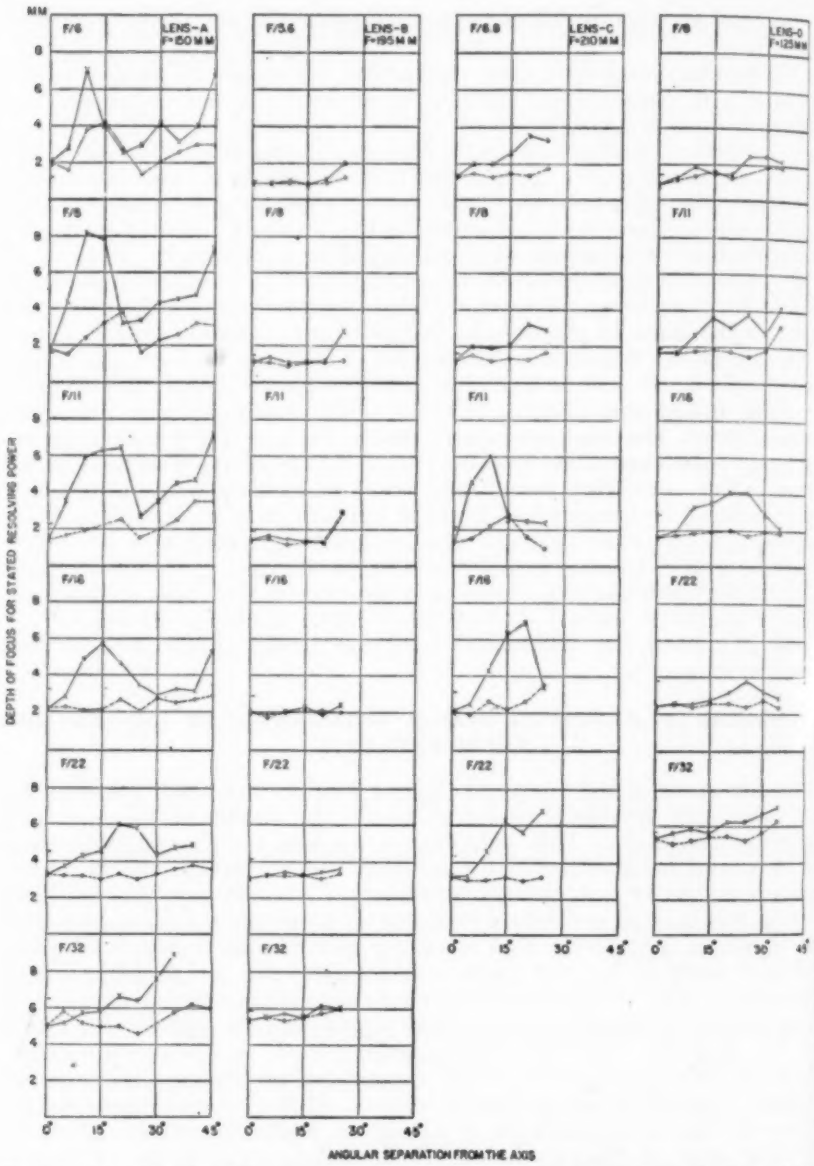

FIGURE 14.—*Depth of focus versus angular separation from the axis for a fixed resolving power for a series of stop openings.*

The value of the resolving power is 20 lines per millimeter for lenses *A* and *C*, 21.5 for lens *B*, and 23 for lens *D*. The solid curve shows the depth of focus for tangential imagery, and the dotted curve shows the depth of focus for radial imagery. The short line projecting from the axis of ordinates shows the computed depth of focus for an ideal lens.

in depth of focus is a consequence of vignetting by the lens boundaries which produces a sharp reduction in effective aperture between 20° and 25°. Too, it may be noted that in the region of 0° to 20° the theoretical maximum is not exceeded. Wide variations in the depth of focus with angle are shown by lenses *A*, *C*, and *D*, and the variations for tangential lines make the greater changes. Since these changes in many instances carry the depth of focus above the theoretical maximum it is reasonable to suppose that this is another manifestation of the multiple focus effect discussed in section 1.

The fact that the depth of focus for tangential lines is usually greater than that for radial lines is probably a consequence of the asymmetric use of aperture for tangential imagery, thus permitting the aberrations to increase the depth of focus at the expense of a lowered maximum observable resolving power.

5. CHANGE IN MAXIMUM RESOLVING POWER WITH ANGULAR SEPARATION FROM THE AXIS

Examination of the curves shown in figures 2 to 8 shows that the maximum resolving power decreases with increasing angular separation from the axis. This effect is more pronounced for tangential than for radial lines, although definitely present in the latter. This effect is compounded from lens aberrations and limitations set by aperture ratio. For the larger stop openings the decrease evident from the curves arises mainly from aberrations because the upper limit set by the stop opening is well above the upper limit set by the test charts. The variation in the maximum value of resolving power with angular separation from the axis is shown graphically in figure

The solid line curves represent the variation in maximum resolving power with angle as computed with the aid of eqs 4 and 5. The broken curves are the results of observation.

It is interesting to note that, save for one exception, the resolving power decreases monotonically from a maximum on the axis to the last observed value for both tangential and radial lines. However, the resolving power for tangential lines decreases more rapidly than does the resolving power for radial lines. This behavior is of course predicted by theory, but it is interesting to note that this behavior is present for those stop openings where the least resolving power predicted for any angle is nonetheless higher than the upper limit of the test chart, as can be seen from the curves for *f*/6 and *f*/8. At *f*/11, the effect of diminishing aperture is evident, particularly for tangential values, although even here it is clear that aberrations are chiefly responsible for the failure of the lens to yield full theoretical resolving power. At *f*/16, the limits imposed by stop opening become more evident, the theoretical and observed curves are closer together and their similarity becomes more pronounced. At *f*/22, the effects of aberrations are practically nil and the two curves nearly coincide. This close coincidence of the two curves continues through *f*/32 and *f*/45.

From the study of these curves it is evident that lens aberrations are of primary importance in limiting the maximum resolving power of lens *A* for the aperture ratios from *f*/6 to *f*/11. From *f*/16 on, the maximum values of the observed resolving power conform more and more closely to the values predicted by theory; thus these observations tend to validate the accuracy of eqs 4 and 5.

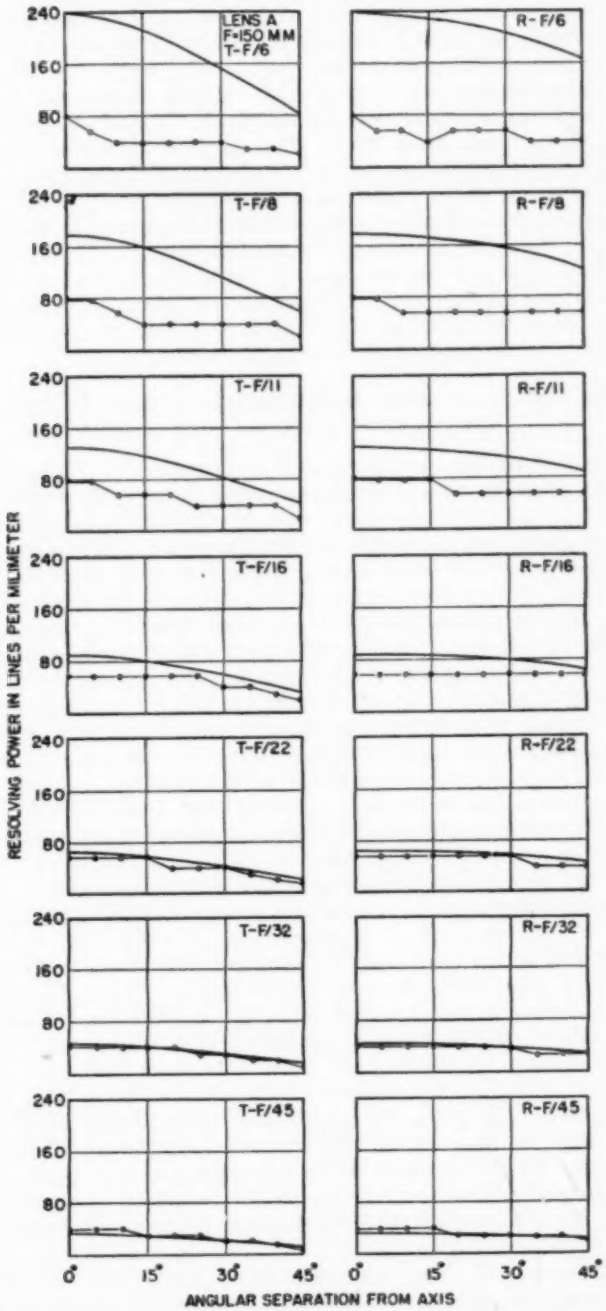

FIGURE 15.—*Maximum resolving power versus angular separation from the axis for a series of stop openings.*

The solid curve shows the computed relation for an ideal lens, and the broken curve shows the observed relation for an actual lens. *T* signifies tangential imagery and *R* radial imagery.

6. VARIATION OF RESOLVING POWER IN A GIVEN IMAGE PLANE WITH STOP OPENING

A general improvement in definition throughout the image plane is frequently encountered when the imagery obtained with a lens set at a small stop opening is compared with that obtained with the same lens set at a larger stop opening. At first thought, this behavior appears to be at variance with the fact that the resolving power of a lens for any given part of the image plane is a maximum at the largest stop opening. However, because of curvature of the image field (discussed in section 3) the image plane for an actual lens cannot usually be so placed as to contain all the resolving power maxima for all angular separations from the axis. On the contrary, a given image plane can include only a few of the resolving-power maxima for a lens set at maximum stop opening; and, as is evident from examination of the master curves shown for lens *A* at *f*/6 in figure 2, the small depth of focus present for maximum resolving power at the various angular separations from the axis further serves to limit the number of resolving-power maxima obtainable in the image plane.

If, as is the case for airplane cameras, the image plane is maintained at a fixed distance from the lens, which distance is established as yielding best average definition at full stop opening, it is clear that when a smaller stop opening is used the depth of focus for each maximum increases. Consequently, there is greater likelihood of the given image plane including more resolving-power maxima than it did at the full stop opening and, as a result, the definition considered throughout the image plane will show improvement. As a matter of fact, some improvement is likely even if more maxima are not included because the increased depth of focus for any observed resolving power makes it probable that some regions will be benefited by an increase in resolving power even if the maximum is not reached. The manner in which this effect is operative can be seen from the curves shown in figures 2 to 8. For lens *A*, if one selects an image plane 0.20 mm nearer the lens than the plane of best axial focus, the resolving power for tangential lines at 5° from the axis increases from 28 to 56 lines per millimeter when the aperture is reduced from *f*/6 to *f*/11. Similar gains can be noted in other parts of the field.

This improvement does not continue indefinitely with diminishing stop opening. For lens *A*, reducing the *f*-number below *f*/22 causes a general decrease in resolving power throughout the image plane. This arises from the fact that the limitations set by aperture radio (described in section 2) becomes noticeable. For apertures between *f*/6 and *f*/22, the upper limit of the resolving power for the various regions of the image plane is set preponderantly by lens aberrations; but for *f*/32 and *f*/45, the upper limit is set by aperture ratio.

It must be mentioned that there are additional reasons for the betterment of photographic quality with diminishing stop opening. Chief of these is the reduction of the large variation in effective exposure over the photographic plate which otherwise would be produced by vignetting. The difference in relative illumination is of course much less when the diaphragm stop is the only limiting aperture.[3]

WASHINGTON, November 14, 1944.

[3] J. Research NBS **29**, 233 (1912) RP1498.

U. S. DEPARTMENT OF COMMERCE NATIONAL BUREAU OF STANDARDS

RESEARCH PAPER RP1637

Part of Journal of Research of the National Bureau of Standards, Volume 34, February 1945

RELAXATION OF STRESSES IN ANNEALING GLASS

By Arthur Q. Tool

ABSTRACT

An empirical equation representing relaxation of stresses in annealing glass is derived. Although the derivation is based on Maxwell's equation for viscous flow, consideration is also given to the changing viscosity as a glass anneals at a constant temperature. This new equation has been applied to data that were obtained by Adams and Williamson on the relaxation of stresses in annealing glass at various temperatures. It is shown that this equation applies very satisfactorily to their data. Also, it appears to be much more suitable than the reciprocal relation which these authors proposed as a substitute for the wholly unsatisfactory exponential relation that is derived directly from Maxwell's equation. This exponential relation is unsatisfactory simply because it does not take into account the changing viscosity of annealing glass. Finally, the new equation leads to a clearer understanding of the nature and behavior of glass because it does not neglect the change in viscosity.

CONTENTS

		Page
I.	Introduction	199
II.	Changing viscosity of annealing glass	200
III.	Equation for the relaxation of stresses in unannealed glass	202
IV.	Application of the equation to experimental data	204
V.	Remarks concerning the values obtained for A, K_T, and k	207
VI.	Conclusion	210

I. INTRODUCTION

In procuring data for a previous publication [1],[1] it was noted that the relaxation time [2] of the strains in glass during an annealing at a constant temperature was generally much less when the relative retardations exceeded a thousand millimicrons than when they were under fifty. This should not be the case if the viscosity remains constant as long as the temperature is constant and if the stresses relax according to Maxwell's law. At the time, it was thought possible that the observed results might indicate that glass, even at relatively high annealing temperatures, is appreciably plastic. On further consideration, the degree of plasticity indicated by the results seemed unreasonable, although glass is undoubtedly plastic to a certain degree at very low annealing temperatures. It also seemed improbable that the indicated increase in the relaxation time with decreasing load was the result of observational errors, although the method of measuring

[1] Figures in brackets indicate the literature references at the end of this paper.

[2] In a case in which the stress, F, relaxes according to the relation, $F=F_0e^{-t/\vartheta}$, the constant, ϑ, is the relaxation time and F_0 is the stress when the time $t=0$.

the large relative retardations was comparatively inaccurate. Moreover, a more extensive set of data showing practically the same conditions was obtained by Adams and Williamson [2] at about the same time.

These results show either that Maxwell's law does not apply to the relaxation of stresses in annealing glass, possibly because the glass is plastic, or that the viscosity of an annealing glass at a constant temperature changes and thus causes the factor representing the relaxation time in Maxwell's equation for inelastic flow to be a variable. On finding that Maxwell's equation was inadequate, Adams and Williamson used a reciprocal relation to express the decay of the relative retardation. That this subject is still a matter of some interest is shown by the fact that Weyl and Pincus [3] have recently mentioned the results of Adams and Williamson and their use of the reciprocal relation. For this reason a recently presented theory [4, 5] of the behavior of annealing glass has been applied to their data and the results are presented in this paper.

II. CHANGING VISCOSITY OF ANNEALING GLASS

In any thorough study of annealing glass, it will soon be found that all of the properties of the glass are changed by the annealing, even though the temperature is unchanged. Moreover, it will be found that the properties are a function of the annealing temperature as well as of the actual temperature at which the glass is tested. That is, if the annealing is continued until the equilibrium condition is reached at any annealing temperature, this temperature as well as the standard temperature at which the glass is tested should always be given consideration. Also during an annealing at a constant temperature and before equilibrium is reached, the condition of the glass [3] at any time is always that which approximates an equilibrium condition at a higher or lower temperature which, as the annealing proceeds, continually approaches that of the annealing [6]. This equilibrium, or fictive, temperature, which continually changes while the glass is annealing at an actual temperature, T, will be designated by τ. Furthermore, the time rate of change in τ is always roughly proportional to $T-\tau$ if the annealing is accomplished while T is constant.

If the coefficient of a property of a glass, when τ is constant, can be related reasonably well to the temperature by some expression, such as $D=D_0(1-a(T-T_0)-. \ . \ .)$ in the case of density, for example, it will usually be found that a similar expression with different constants relates the coefficient equally well to the fictive temperature, τ, when T is constant. Thus, in the above relation for the change in density with T, the variation in the initial density because of any change in τ is expressed equally well by the relation $D_0=D'_0(1-\alpha(\tau-\tau_0)-. \ . \ .)$. As a result of his studies of annealing glass, Twyman [7] concluded that the inelastic deformability (reciprocal of viscosity) of the average glass doubled approximately with each increment of about 8° C in the actual temperature. Consequently, the relaxation time, ϑ, which is closely related to the coefficient of viscosity, should vary approximately according to the expression, $\vartheta=\vartheta_0 e^{-T/k}$ as the temperature changes, if $k=11.5°$ C. That is, although the modulus of elasticity, E, also changes with temperature, its variation is doubtless insignifi-

[3] Certain glasses behave in an unusual manner, but these are excluded from the present discussion.

cant when compared to the very rapid change in the coefficient of viscosity, $\eta = E\vartheta$. If the changes in the relaxation time with T and τ can be expressed reasonably well by similar relations, it follows that $K = 1/\vartheta = K_0 e^{T/g} e^{\tau/h}$ should express approximately the value of the reciprocal of the relaxation time for different values of T and τ. If a glass is cooled or heated so slowly that it never departs materially from the equilibrium condition, $T = \tau$, it follows that $k = gh/(g+h)$, provided it is assumed that Twyman's empirical relation was based on measurements on deformations that developed almost entirely while the glass was never far from equilibrium. A study of his experiments suggests that this assumption is applicable, since the deformations which he observed almost certainly were developed mainly at comparatively high annealing temperatures at which τ never departs materially from T unless the cooling rate is quite high. That is, the deformations were developed mainly before the glass departed from the equilibrium curve of its liquid form.

If the expression for $1/\vartheta$ is introduced into Maxwell's equation for inelastic flow [1, 2], a modification, $dF/dt = EdS/dt - K_0 F e^{T/g} e^{\tau/h}$, is obtained that should apply reasonably well to the development of inelastic deformation in stressed glass, provided the variations in E with T and τ are not too great.

As it has been observed [8] that the manner in which temperature affects the velocity of approach by any coefficient (density, refractivity, etc.) to its equilibrium value is roughly the same (provided the coefficient has a given displacement from its equilibrium value regardless of the temperature) as the manner in which temperature affects the mobility of the glass, it seems that the viscosity governs the rate of these approaches. Consequently, it appears that

$$d\tau/dt = K_0(T-\tau)e^{T/g}e^{\tau/h} \qquad (1)$$

should represent approximately the velocity of the change in τ as both T and τ change. In part at least, this differential equation allows for the lack of strict proportionality between $d\tau/dt$ and $T-\tau$ in an annealing glass at a constant temperature. Its solution (in terms of exponential integrals)

$$Ei(y) - Ei(y_0) = -K_0 e^{T/k} t \qquad (2)$$

(if T is constant and if $y = (T-\tau)/h$ and y_0 is its value when $t=0$) applies rather satisfactorily to data on the changes in τ as they are derived from experimental results on the varying coefficients of an annealing glass.

If a glass is cooled very rapidly from temperatures well above the annealing range, τ is very high when atmospheric temperatures are reached, and if the cooling is particularly severe, it may be more than 50° C above the temperatures at which the rapid expansion and endothermic effects become appreciable; whereas, if a glass is cooled very slowly so that it can follow its equilibrium curve as a liquid throughout the annealing range and possibly to even lower temperatures, τ may be reduced as much as 70° to 90° C below the beginning points of the heat effects mentioned. Somewhere in the range 10° to 40° C below these points, the relaxation time is approximately 1 hour, and the point at which $K=1$ is, therefore, roughly the midpoint of the

range of possible values of τ in glass at ordinary temperatures. That is, without exceptional treatments, the possible range of τ-values in the average glass is about 140° C, and when the glass is in equilibrium ($T=\tau$) at a temperature near the midpoint of this range, the viscosity coefficient, $\eta=E\vartheta$, (ϑ expressed in seconds) should be approximately 2.2×10^{15} if $E=6\times10^{11}$ at such temperatures. This assumed value for E is only slightly less than the average value for a number of glasses [9] at ordinary temperatures. Consequently, the above estimate of the value of η is presumably rather high, since E undoubtedly decreases appreciably as the temperature approaches the annealing range. Although η has been determined experimentally [10, 11] at temperatures that are so low that they probably were near the upper limits of, or were well within, the annealing ranges of the glasses tested, the results cannot safely be compared with the above estimate because no auxiliary determinations on the locations of the rapid expansion ranges were made. However, the η-values for the lowest temperatures used in these experimental determinations ranged from 10^{13} to 10^{16}.

If a slowly cooling glass follows its equilibrium curve throughout the range of temperatures corresponding to the range of τ-values that may exist even after ordinary temperatures are reached and also if $k=10°$ C, the η-values for this interval of cooling will range, according to the above estimate for the midpoint value, from 2×10^{12} to 2×10^{18} approximately. However, if the glass is cooled so rapidly through this temperature interval that τ does not change, and if $g=h=20°$ C, the initial η-value on reaching the lower limit of the temperature interval will be about 2×10^{15}, and any stresses in the glass will begin to relax almost as rapidly as they would have relaxed if the glass were in equilibrium at the midpoint. However, the decrements in the relaxations as time progresses will be greatly different in the two cases. Moreover, if the glass after being brought to equilibrium at the lower limit of the temperature interval is heated so rapidly to the upper limit that τ does not change, the initial η-value will again be that of the glass in equilibrium at the midpoint of the interval. (These values for g, h, and the resulting η, although they are not improbable, were introduced merely as aids in conceiving the effects of a varying or unvarying τ.) Effects of this nature, which are the result of the previous history of the glass, were noted and studied by the authors of the reports cited.

III. EQUATION FOR THE RELAXATION OF STRESSES IN UNANNEALED GLASS

In a severely chilled piece of glass, the value of τ may be very high, and the residual stresses, which comprise a balanced system and which are the result of the temperature gradients that existed as the glass passed through the annealing range, may approach the breaking limit of the glass. The high value of τ and of these stresses are maintained without appreciable decay at ordinary temperatures because the viscosity is so extremely high; but, when the glass is reheated, the viscosity is so reduced, as the annealing range is approached, that τ and the average absolute magnitudes, F, of the stresses immediately begin to decrease at an appreciable rate.

Usually, stressed glasses are double refracting unless the stresses are the same at all points and in all directions. Except in certain

limited portions, this uniformity of the stresses is never met in glass strained by chilling. If the strained piece of glass has some simple geometrical form, such as a rectangular prism, it is usually possible to pass a beam of plane polarized light through it along a path which makes it possible to bisect, throughout most of the path at least, the angle between the directions of principal stresses with that of the plane of polarization. Because of the photoelastic action of most glasses, the component oscillation in the direction of one principal stress is retarded (or accelerated) in its velocity of propagation relative to the component in the other direction. This relative retardation, δ, (usually measured in millimicrons, mμ, per centimeter of path) is proportional to the average difference between the principal stresses, which usually vary both in sign and magnitude along the path. That is, it does not measure the maximum difference nor does it give a certain indication of the average magnitude of the stresses, particularly, if those seldom used paths along which one principal stress is always practically zero are excepted. Moreover, as the stresses decay in an annealing glass, δ will not be a certain indicator of the rate of decay unless care is taken to preserve the pattern of the stress distribution throughout the time required for the test.

Under suitable conditions it may be assumed [4] that δ and F are proportional throughout an annealing test. That is, as in the case of the elastic modulus E, it will be assumed that the changes in the photoelastic constant with τ and T are insignificant compared to the changes in η with τ and T. Moreover, experience indicates that δ may also be considered as proportional to the average absolute value of $\tau - T$, which is usually large and positive in a severely chilled glass if T is not too high. That is, $x=\delta/\delta_0=F/F_0=(\tau-T)/(\tau-T)_0$ if the conditions at any time t are compared to the conditions at the time from which t is measured. On writing $A=(\tau-T)_0/h$ and substituting hAx for $\tau-T$ in eq 1, the relation, $d(Ax)/dt=-(K_0e^{T/k})\ Axe^{Ax}$, is obtained for annealing at a constant temperature. The solution of this differential equation is

$$Ei(-Ax)-Ei(-A)=-K_0e^{T/k}t=-K_Tt, \tag{3}$$

since $x=1$ when $t=0$. Clearly, K_T is the value of the reciprocal of the relaxation time that will be reached provided the annealing is continued until $\tau=T$. In certain cases this condition exists from the beginning and Maxwell's equation, $dF/dt=-K_TF$, applies. (In the case of a balanced system $dS/dt=0$, since the sum of the elastic and inelastic strains remains constant.) That is, in view of the assumed proportionality of F and δ,

$$\ln(\delta/\delta_0)=K_Tt. \tag{4}$$

Moreover, in exceptional cases, T exceeds the average value of τ In such cases A is negative.

[4] No doubt this assumption merely approximates the actual relation between the relaxing stresses and the changing fictive temperature. In regard to this relation, it will be noted that the density changes that accompany the changes in τ will react on the stresses if τ-gradients exist in the glass. That is, appreciable τ-gradients doubtless are present in any severely strained glass, and the accompanying differential density changes should as a rule hasten the relaxation. This follows because the highest values of τ and the consequent highest rate in its decrease are presumably near the surface where the compressive stresses approach a maximum. The comparatively large increase caused in the density by the decrease in τ in the region of these stresses should reduce them to a greater extent than the tractions in the interior are enhanced by lesser increases in density.

IV. APPLICATION OF THE EQUATION TO EXPERIMENTAL DATA

To procure data that have the required accuracy for thoroughly testing eq 3 or any other proposed expression concerning the decay of the double refraction in annealing glass is not an easy matter. In the first place, sizeable pieces of glass are usually considered necessary for the tests. Consequently, temperature gradients of considerable magnitude are likely to be present at the time of testing unless exceptional care is taken. These gradients make the effective temperature of the glass rather uncertain. Also, they cause the stresses to relax more quickly in some parts of the glass than in others. Through this differential action, the double refraction pattern is gradually changed, and, as a result, δ may actually increase for a time if the observations are made along some possible paths through the glass. In the second place, K changes so rapidly with temperature that the temperature range available for the tests is rather limited. That is, the decay is so rapid at the upper limit of the range that much of the double refraction effect has disappeared before the glass can be heated to that point; while it is so slow at the lower limit that the tests are extremely tedious unless the strains are large. As a result, the observations obtained in a test at high temperatures are usually few in number and made when δ is small, whereas those obtained at low temperatures, although comparatively numerous, are made when δ is very much larger. In view of the dependence of K on τ, data of this sort will yield values for k that are too large by varying degrees if the simple Maxwellian equation is used. Moreover, because of the limited range available, the temperature intervals between tests designed for the determination of k are often scarcely more than double the possible errors in the temperature determinations.

Presumably, because of the effect of a changing fictive temperature, τ, Adams and Williamson found that eq 4 was inapplicable to their data and, therefore, proposed the reciprocal relation

$$1/\delta - 1/\delta_0 = A't. \tag{5}$$

Consequently, to test the relative applicability of eq 3, 4, and 5 to the decay of double refraction in annealing glass, they were applied to the data obtained by Adams and Williamson (page 622, reference 2) on a light flint while it was being annealed at 300° C. The experimental data and resulting computed curves are shown in figure 1.

In fitting these data, eq 3 has the obvious advantage of an additional constant. In arriving at tentative values for the three constants, δ_0, A, and K_T, required in using this equation, the method followed was essentially, (a) the drawing of a smooth curve that seemingly approximated the trend of the experimental data, (b) the choosing of three trial points on this curve in order to obtain two equations for the purpose of eliminating K_T, and finally (c) the search for a value of A that would satisfy the equation resulting after the elimination. A few trials will yield such a value if an adequate table of exponential integrals is used. In the case of the above-mentioned data for a light flint, the first and third trial points coincided, respectively, with the first and eleventh experimental points, while the second was near the third experimental point. These trial points yielded the values

5.56 and 6.97×10^{-5} for A and K_T, respectively, and the computed curve resulting from the use of these constants is that designated by A in figure 1. Since this curve fits the experimental data reasonably well, a betterment was not attempted.

As Adams and Williamson pointed out, eq 5 does not yield a reasonable fit for these particular experimental data, and eq 4 is even less satisfactory as curves B and C, respectively, indicate. In computing these curves, only two trial points are required to determine tentative values for δ_0 and A' in one case and δ_0 and K_T in the other.

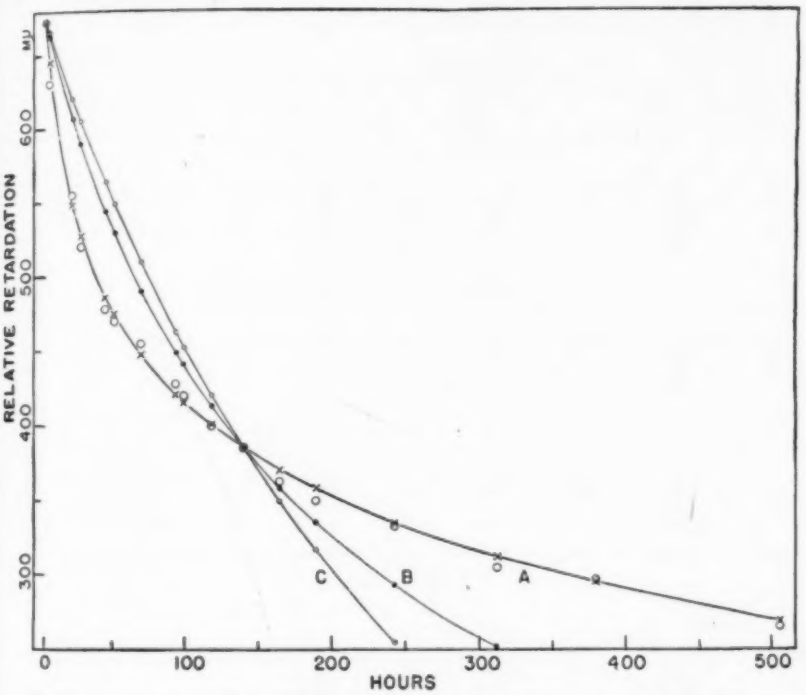

FIGURE 1.—*Decay of double refraction in light flint annealing at 300° C.*

Curve *A*: Circles, experimental data by Adams and Williamson; crosses, points computed by equation 3.
Curve *B*: Points computed by equation 5.
Curve *C*: Points computed by equation 4.

The trial points used in these cases were the first and third of those used previously.

In addition to this test at 300° C, Adams and Williamson determined the decay of double refraction in a light flint at three higher temperatures that are within the upper half of the annealing range. Table 1 presents the residuals (R_3) obtained through the use of eq 3 and also those (R_5) obtained by Adams and Williamson through the use of eq 5. In applying the first of these equations to their data, it usually was endeavored to balance approximately the positive and negative residuals both in magnitude and distribution, also to make those residuals as few as possible which exceeded an assumed maximum probable error of $\pm5m\mu$ in the δ-determinations. In only a few cases was it necessary to depart markedly from these aims, provided the results on ordinary crown are excepted.

For simplicity in applying eq 3, the observed initial relative retardation was chosen as the value of δ_0. The ratios $x=\delta/\delta_0$ for the remaining observations were then multiplied by various trial values for A and corresponding sets of values for $K_T t$ and K_T were computed. The A-value that yielded a spread that seemingly approximated the minimum possible in the K_T-values and the average of its set of K_T-values were then used to compute values of δ and the residuals $(\delta_e - \delta_c)$ for the various times of observation. Usually it was necessary to adjust these A- and K_T-values a few times in order to procure more satisfactory sets of differences between the experimental (δ_e) and computed (δ_c) retardations.

TABLE 1.—*Comparison of residuals obtained*

LIGHT FLINT

$T=385°C$, $\delta_0=415$, $K_T=0.21$, $A=2.93$

t (hr)	0.000	0.183	0.367	0.567	0.800	1.200	1.600	2.333
δ (mμ)	415	280	223	188	155	118	100	80
R_1 (mμ)	−15	+16	+12	+4	+3	+3	−5	−7
R_2 (mμ)	0	−4	−2	−1	+3	+8	−1	−2

$T=400°C$, $\delta_0=280$, $K_T=0.60$, $A=1.53$

t (hr)	0.000	0.167	0.433	0.733	1.000	1.500	2.317	
δ (mμ)	280	195	135	97	72	47	27	
R_1 (mμ)	+9	−1	−8	−6	+1	+6	+10	
R_2 (mμ)	0	+1	−2	−2	+2	+2	0	

$T=415°C$, $\delta_0=293$, $K_T=1.74$, $A=1.5$

t (hr)	0.000	0.083	0.167	0.333	0.467	0.667		
δ (mμ)	293	185	130	80	58	40		
R_1 (mμ)	+6	−8	−4	0	+4	+6		
R_2 (mμ)	0	−2	+2	+1	0	−3		

MEDIUM FLINT

$T=306°C$, $\delta_0=356$, $K_T=0.87\times10^{-4}$, $A=4.3$

t (hr)	0	267	483	1004				
δ (mμ)	356	205	170	130				
R_1 (mμ)	−5	+18	+3	−18				
R_2 (mμ)	0	0	+1	0				

$T=374°C$, $\delta_0=594$, $K_T=0.042$, $A=2.75$

t (hr)	0.000	0.533	0.950	1.533	3.017	4.500	6.083	
δ (mμ)	594	465	409	349	261	228	192	
R_1 (mμ)	−16	+18	+19	+21	+13	−10	−10	
R_2 (mμ)	0	−3	−3	+3	+11	−4	−4	

$T=390°C$, $\delta_0=573$, $K_T=0.24$, $A=2.00$

t (hr)	0.000	0.333	0.917	1.417	2.000	2.333		
δ (mμ)	573	378	253	190	160	139		
R_1 (mμ)	−5	+13	0	+4	−7	+6		
R_2 (mμ)	0	+4	−1	+5	−9	+2		

$T=406°C$, $\delta_0=350$, $K_T=0.53$, $A=2.27$

t (hr)	0.000	0.167	0.333	0.667	1.000	1.500		
δ (mμ)	350	205	160	103	80	52		
R_1 (mμ)	−5	+12	−1	0	−4	−3		
R_2 (mμ)	0	+6	−2	+2	−3	−1		

In particular, the results obtained on ordinary crown at 450° C offered exceptional difficulties, since there is evidence of a serious temperature change after the eleventh hour of this test. As a matter of fact, the authors state that most of the measurements on this glass were of a preliminary nature and, from their remarks, it may be assumed that some of the results possibly are affected by considerable errors in the temperature determinations. Furthermore, most of the relative retardations were determined by an inferior method in the case of this glass.

In addition to the light flint, Adams and Williamson also tested a medium flint not only at points restricted mainly to the upper half of the annealing range but also at a temperature, 306° C, which is far below that range as it is limited by normal practice. For this reason, the results obtained by applying eq 3 to the data on medium flint also are included in table 1. In the case of both of these glasses it will be noted that the averages of the residuals resulting from the use of eq 3 usually are less than one-half the averages of the residuals obtained

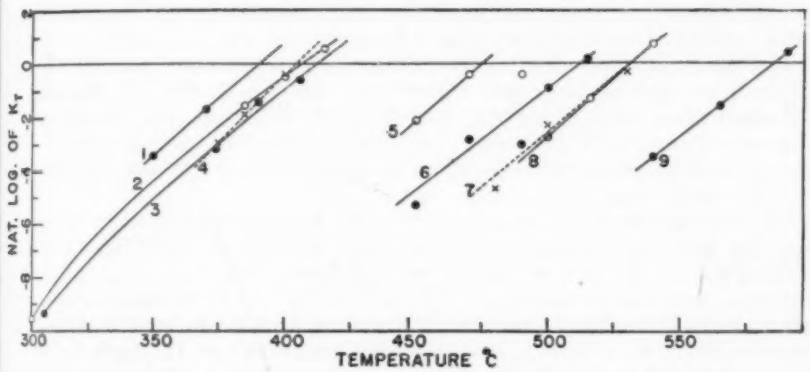

FIGURE 2.—*Natural logarithms of K_T for various glasses at various temperatures.*

The values of K_T were computed by equation 3 from data obtained by Adams and Williamson for various glasses annealing at various temperatures.

Curve 1, extra-heavy flint; 2, light flint; 3, medium flint; 4, heavy flint; 5, barium flint; 6, ordinary crown; 7, borosilicate crown; 8, light barium crown; 9, dense barium crown.

by Adams and Williamson from the use of eq 5. Usually, this experience was repeated when eq 3 was applied to data for the seven other glasses which these authors tested. Consequently, the residuals for these remaining glasses are not presented. However, the natural logarithms of the values for K_T are indicated in all cases in figure 2.

V. REMARKS CONCERNING THE VALUES OBTAINED FOR A, K_T, AND k

When δ_0 was large and the testing temperature was comparatively low, the values found for A ranged from 5.6 to 3, whereas, when δ_0 was relatively low and the testing temperature was high, they ranged from 1.5 to −0.6. Otherwise the A-values were intermediate and came in the order anticipated except in a few cases, such as the values obtained from the tests on medium flint at 390° and 406° C (see table 1). However, such reversals should not be uncommon, since a glass in

equilibrium at any point in the upper half of the annealing range can be cooled sharply enough to be as severely strained as a glass that has been cooled less sharply from a higher temperature but still sharply enough to prevent a too great recession in τ.

With regard to small values of A, two minor points observed while applying eq 3 to these data deserve mention. The first is concerned with the paucity of data on light barium crown in the test at 540° C. Two observations are sufficient to yield a value for K_T or A' if eq 4 or 5 is used, but are inadequate for the determination of A and K_T of eq 3. Since 162 mμ is not a very large value for δ_0 (in view of the 7.5-cm path in this case), it seemed possible that eq 4 might be adequate, but its use yielded the result $K_T=1.38$, which is somewhat out of line with the values of K_T (0.066 and 0.264) that were obtained from the results of the tests at 500° and 516° C, respectively. That is, these results indicate that a better value for K_T at 540° C is 2.1, although the introduction of this value yields the result $A=-0.565$ when eq 3 is applied to the data obtained at 540° C. Since this temperature is not particularly high, a negative value for A, in this case, seems somewhat improbable, but it calls attention to the fact that such values should be common whenever the stresses are relaxing at an annealing temperature that is higher than others at which the glass just previously was annealing. For instance, in heating a strained glass at a moderate rate through the annealing range, $\tau-T$ decreases not only because τ is decreasing but also because T is rising, and it, consequently, often becomes negative while the stresses are still rather large.

The second point concerns the results $A=0.2$ and $K_T=0.4$ obtained for the test on ordinary crown at 500° C and in which $\delta_0=120$ mμ. When these values were used, the residuals were 0, 0, −2, and +1, in the order of decreasing δ. The low value of A indicates that eq 4 should apply almost equally well, and that this is the case is shown by the residuals 0, +2, −1, and 0, which are obtained through its use if K_T is given the value 0.45. The corresponding residuals obtained by Adams and Williamson are +3, −6, −2, and +10. In this case also, the number of observations is unsatisfactory and the testing temperature, 500° C, is scarcely high enough to cause a close approach to the condition, $(\tau-T)_0=0$, ordinarily; but the result calls attention to the fact that eq 4 alone applies if A approximates zero.

Although it would be quite difficult, if the testing temperatures were in the upper half of the annealing range, it is still possible to so manipulate the chilling treatments and the reheating to the annealing temperatures that the values of $(\tau-T)_0$ are known, at least approximately, in tests such as these that are being discussed. In that case, when A is determined, h becomes known. Unfortunately, it is impossible to determine the h-values for any of the glasses tested by Adams and Williamson because there is nothing in their data to indicate the values of τ_0.

When the natural logarithms of the values found for K_T are plotted as ordinates against the temperatures of the tests, as in figure 2, the result is much the same as that shown by Adams and Williamson in a similar presentation of the relation that their A'-values bore to the same temperatures. Since the lines representing the trend of the plotted points in figure 2 were located graphically, judgment played a considerable role in their positions, curvature and slopes. Since

they are all approximately straight, these lines indicate that the k-values of the glasses do not change materially within the annealing ranges. Consequently, since the relaxation time, $\vartheta = 1/K_T$, has been expressed in hours, $k = (T - T_1)/\ln K_T$ approximately if the relaxation time is 1 hour at T_1. In preparing these curves and computing the following values of k, only two determinations of $\ln K_T$ were ignored. These were the results derived from the data on barium flint and on ordinary crown at the temperature 490° C in both cases. These results were ignored because it seemed possible that errors of 20° were made in recording the temperatures.

The values obtained for k are as follows: 11.8° C, extra heavy flint; 12.6°, light flint; 10.2°, heavy flint; 12.8°, medium flint; 11.6°, barium flint; 13.4°, ordinary crown; 10.5°, borosilicate crown; 10.6°, light barium crown; and 12.9°, dense barium crown. Although the probable errors in these determinations are undoubtedly large, the average of the k-values is 11.8° C, which agrees closely with Twyman's experience. From the change in the constant A', Adams and Williamson obtained an average value for their constant, $M_1 = (\log_{10} e)/k$, that approximates 0.33. This corresponds to a k-value approximating 13.2°. However, presumably for the purpose of simplifying the computations in preparing their sample annealing schedules, they gave $p = (\log_{10} 2)/M_1$ the value 10°, in a relation which is essentially $A' = A'_0 2^{(T-T_0)/p}$, rather than 9.1°, which their average value for M_1 indicates or the value, 8°, which was found by Twyman. Comparatively few if any of the optical glasses ordinarily produced have a k-value as high as 14.4°, which corresponds to $p = 10°$. This rather high value for p suggests that the annealing times computed by Adams and Williamson are too short and particularly so for the comparatively low annealing temperatures. However, it must be considered that they were merely demonstrating a method of preparing annealing schedules and were not recommending schedules that could be used for all of the glasses that may be included in the types tested. This is obvious, since it is well known that the upper limits of the ranges of suitable annealing temperatures for the various glasses that may be included within a single type often cover a range of 50° C or more.

Dimensionally, both K and $A'L$, when L represents the length of the light path in glass, are time reciprocals and are directly related to the fluidity of the glass. The minute was the time unit used by Adams and Williamson in making their observations. Consequently, at the temperature T at which $1/A'L$ becomes 1 minute, $M_2 = M_1 T = (T \log_{10} e)/k$. Such temperatures, T, are far above the annealing range and are high enough to cause considerable deformation in a short time. Within the annealing range, the hour is a suitable unit for measuring the relaxation time, $\vartheta = 1/K$. In that case, the temperatures, T_1, at which $K = 1$ and $\ln K = 0$, are suitable for annealing optical blanks that are not too large. These temperatures can be determined from figure 2 and are as follows: 390° C, extra-heavy flint; 407°, light flint; 405°, heavy flint; 413°, medium flint; 475°, barium flint; 513°, ordinary crown; 532°, borosilicate crown; 532°, light barium crown; and 585°, heavy barium crown. As the annealing temperatures of pieces of glass with a thickness of 2 cm, Adams and Williamson recommended the following corresponding temperatures: 382° C, 408°, 407°, 418°, 494°, 514°, 541°, 552°, and 592° C.

Finally, the results obtained for K at very low temperatures, in the cases of the light and medium flints, indicate that k decreases appre-

ciably from its magnitude at ordinary annealing temperatures whenever a glass is cooled to temperatures near or below the lower limit of its practical annealing range. That is, the K-values obtained for these glasses indicate that curves representing $\ln K$, as in figure 2, should become appreciably steeper at very low annealing temperatures. Such a decrease is to be expected, since it seems probable that there is a continual decrease in the available flow planes as a glass cools through these low temperatures and gradually changes from a highly viscous liquid condition to an elastic solid condition in which it shows no more viscous and plastic deformability than many crystalline solids. It will be noted, however, that glasses that have been cooled very rapidly from high temperatures should show, because of their high τ-values, a much greater inelastic deformability than well annealed glasses. In fact, it should be possible to chill fine threads of glasses or plastics, especially those with very low annealing ranges, so severely that they will anneal at atmospheric temperatures until τ decreases sufficiently to raise the viscosity and plasticity beyond that possibility.

VI. CONCLUSION

When a glass is cooled very slowly from high temperatures, it continues to behave as a liquid throughout the annealing range and apparently to even lower temperatures if the cooling rate is extremely low. Naturally, its properties, including viscosity, all change accordingly, that is, their temperature coefficients are generally much higher than when the glass or plastic behaves as a solid at temperatures far below the annealing range.

When the cooling rate is comparatively high, the glass departs from the equilibrium curve of its liquid condition at temperatures that are determined by the rate and nature of the glass. These temperatures of departure will be above the usual annealing range if the rate is exceptionally high. If the rapid cooling is continued after such departures, the glass begins to behave as a solid even before the annealing range is left behind. That is, even within the annealing range, a glass, although greatly undercooled, will react temporarily as a solid to comparatively sudden temperature changes.

Far below their annealing ranges, glasses and many of the so-called plastics behave as solids; but, when they are reheated, they drift toward the equilibrium curves of their liquid conditions as soon as the annealing range is reached. When the undercooling is considerable and the rate of reheating is comparatively low, this drift is very marked and often begins 50° C or more below the lowest annealing temperatures. Drifts of this kind are accompanied by large contraction and exothermic effects, which practically cease as soon as the equilibrium curve of the liquid condition is neared.

If the heating is continued after the equilibrium curve is reached, the glass becomes superheated, and this superheating will be quite large if the heating rate is high enough and the prior cooling rate was comparatively low. However, the rising temperature ultimately reduces the viscosity so greatly that the glass or plastic returns rapidly to the equilibrium curve, and this return is accompanied by large "rapid expansion" and endothermic effects.

When the rate of reheating is much higher than the prior rate of cooling, the drift while the glass is in an undercooled condition is

quite negligible, and the curve followed by a glass or plastic while in its solid condition at comparatively low temperatures continues beyond the point at which it intersects the curve of the equilibrium condition. This point or temperature of intersection has been referred to in previous papers by such terms as the "effective annealing," "equilibrium," or "fictive" temperature of the glass while it is in the particular solid condition corresponding to a particular intersection point. This temperature, which can be varied at will over a wide range by reheating the glass, was termed the fictive temperature because it is, in most cases, at least as effective in determining the properties of a glass as the actual temperature.

Although most of the properties of glass are affected considerably by any large change in the fictive temperature, any rise or fall in it causes an exceptionally marked decrease or increase, respectively, in the viscosity and, consequently, greatly affects the relaxation of any stresses that may be in the glass. This leads to an interesting situation, since the fictive temperature is usually changing continually even when the stresses are relaxing at a constant real temperature.

Based on experience, an empirical expression was proposed previously for the relation between the time rate of change in this temperature and the magnitudes of it and the real temperature. In this report, this expression has been used in connection with Maxwell's equation for the development of inelastic deformation (that is, for the flow in stressed visco-elastic materials) in order to obtain an expression for the relaxation of stresses in an annealing glass. The resultant expression has been applied to the data obtained by Adams and Williamson on the stress relaxation at different annealing temperatures and for different kinds of glasses, and it has been found to fit experimental data better than previously suggested expressions fit them.

VII. REFERENCES

[1] A. Q. Tool and J. Valasek, Sci. Pap. BS **15,** 537 (1920) S358.
[2] L. H. Adams and E. D. Williamson, J. Franklin Inst. **190,** 597, 835 (1920).
[3] W. A. Weyl and A. G. Pincus, J. Applied Phys. **14,** 37 (1943).
[4] A. Q. Tool, Bul. Am. Ceramic Soc. **21,** 13 (Apr. 15, 1942).
[5] A. Q. Tool, Bul. Am. Ceramic Soc. **22,** 92 (Apr. 15, 1943).
[6] A. Q. Tool and C. G. Eichlin, J. Am. Opt. Soc. **8,** 419 (1924).
[7] F. Twyman, J. Soc. Glass Techn. **1,** 61 (1917).
[8] A. Q. Tool and C. G. Eichlin, BS J. Research **6,** 523 (1931) RP292; J. Am. Ceramic Soc. **14,** 276 (1931).
[9] H. Hovestadt, Jena Glass, English Ed., p. 158 (The Macmillan Co., New York, N. Y., 1902).
[10] V. H. Stott, E. Irvine, and D. Turner, Proc. Roy. Soc. [A] **108,** 154 (1925); J. Soc. Glass Techn. **9,** 207 (1925).
[11] H. R. Lillie, J. Am. Ceramic Soc. **14,** 502 (1931); J. Am. Ceramic Soc. **16,** 619 (1933).

WASHINGTON, November 28, 1944.

○